University of South Bohemia in České Budějovice
Faculty of Science

Excited state processes in linear conjugated systems

Ph.D. Thesis

Mgr. Václav Šebelík

Supervisor: prof. RNDr. Tomáš Polívka, Ph.D.

Faculty of Science, University of South Bohemia in České Budějovice

České Budějovice 2020

This thesis should be cited as:

Šebelík, V., 2020: Excited state processes in linear conjugated systems. Ph.D. Thesis Series, No. 16. University of South Bohemia, Faculty of Science, České Budějovice, Czech Republic, 171 pp.

Annotation

The main topics of this thesis are the excited states of carotenoids in solvents and in light-harvesting antennas. The first two chapters provide an introduction into the topic, while the later ones are the research chapters, based on published papers. In the research section, the different methods of ultrafast spectroscopy were used. Transient absorption spectroscopy, two-photon excitation, and pump-dump-probe experiments were used to explore the so-called dark states of carotenoids in solvents. The femtosecond dynamics of long polyenes was also studied by the transient absorption spectroscopy. In addition to the exploration of the nature of carotenoids and polyenes in solvents, the energy transfer in the CAC antenna of *Rhodomonas salina* was studied by transient absorption spectroscopy.

Declaration [in Czech]

Prohlašuji, že svoji disertační práci jsem vypracoval samostatně pouze s použitím pramenů a literatury uvedených v seznamu citované literatury.

Prohlašuji, že v souladu s § 47b zákona č. 111/1998 Sb. v platném znění souhlasím se zveřejněním své disertační práce, a to v úpravě vzniklé vypuštěním vyznačených částí archivovaných Přírodovědeckou fakultou elektronickou cestou ve veřejně přístupné části databáze STAG provozované Jihočeskou univerzitou v Českých Budějovicích na jejích internetových stránkách, a to se zachováním mého autorského práva k odevzdanému textu této kvalifikační práce. Souhlasím dále s tím, aby toutéž elektronickou cestou byly v souladu s uvedeným ustanovením zákona č. 111/1998 Sb. zveřejněny posudky školitele a oponentů práce i záznam o průběhu a výsledku obhajoby kvalifikační práce. Rovněž souhlasím s porovnáním textu mé kvalifikační práce s databází kvalifikačních prací Theses.cz provozovanou Národním registrem vysokoškolských kvalifikačních prací a systémem na odhalování plagiátů.

České Budějovice, 16.7.2020 .....

Václav Šebelík

Přírodovědecká
fakulta
Faculty
of Science

Financial support

The research presented in this thesis was supported by grants from the Czech Science Foundation (16-10417S, 19-28323X), and by grant (021/2017/P) provided by the Grant Agency of the University of South Bohemia.

Acknowledgement

Tomáši, thank you so much for introducing me into the fascinating world of carotenoids! It was a great journey full of discoveries under your guidance. Thank you for you support, patience, and trust.

Mami, tati, bez Vás by nic v mém životě, včetně téhle dizertce, nebylo. Nikdy nebudu moct vyjádřit slovy, jak moc jsem vděčný za všechno, co jste pro mě v udělali. Jediné, co můžu říct – děkuju!

Lenko, Tobě děkuju za skvělých posledních víc jak osm let a už se těším na další léta prožitá s Tebou a s Vašíkem.

Valja, Robert – I can not describe in a few sentences all the fun we had in the office, in the lab and elswhere. These memories will always stay in my heart. I will never forget Valja's crazy ideas, Robert's singing in the lab and the great times during conferences. You both always had words of understanding and encouragement when something went wrong. Thank you!

Gürkan, Denys, thank you for nice chats in the office, during lunch and everywhere else. And even though Denys was not a member of our spectroscopic group, he was definitelly the member of my doctoral student life. Hristina, thank you for the first lessons learned in the femtosecond lab, I wish you only the best with your nice big family. Marceli, you did a great job in educating me further after Hristina left the lab, thank you for a great explanation of plenty of things in the lab and in the theory. Tuhin, thank you for showing me the scientific passion and showing me many details, which I overlooked before. Emrah, Ivča, I wish to both of you good luck on your way to get the PhD. Vašku, Franto, Milane, Radku, Davide, I would like to thank you guys for the willing help anytime, it was needed by me.

Human subtlety will never devise an invention more beautiful, more simple or more direct than does nature, because in her inventions nothing is lacking, and nothing issuperfluous.

Leonardo da Vinci

List of papers and Author's contribution

The thesis is based on the following papers (listed in the order of their presentation in the Research Section):

Paper I. **V. Šebelík**, M. Fuciman, R. G. West, T. Polívka Time-resolved two-photon spectroscopy of carotenoids. Chem. Phys., 522 (2019), pp. 171–177, https://doi.org/10.1016/j.chemphys.2019.02.023 (IF = 1.77)
VŠ built the setup, performed two-photon time-resolved transient absorption measurements; analysed the data; participated in writing and revision of the manuscript.

Paper II. **V. Šebelík**, M. Kloz, M. Rebarz, M. Přeček, E.-H. Kang, T.-L. Choi, R. L. Christensen, T. Polívka Spectroscopy and excited state dynamics of nearly infinite polyenes. *In preparation.*
VŠ performed time-resolved transient absorption measurements; analysed the data; participated in writing and revision of the manuscript.

Paper III. **V. Šebelík**, R. G. West, E. Kuthanová Trsková, R. Kaňa, T. Polívka Energy transfer pathways in the CAC light-harvesting complex of *Rhodomonas salina*. *BBA-Bioenergetics, in press.* (IF = 3.47)
VŠ performed time-resolved transient absorption measurements; analysed the data; participated in writing and revision of the manuscript.

Paper IV. R. G. West, M. Fuciman, H. Staleva-Musto, **V. Šebelík**, D. Bína, M. Durchan, V. Kuznetsova, T. Polívka Equilibration dependence of fucoxanthin S_1 and ICT signatures on polarity, proticity, and temperature by multi-pulse femtosecond absorption spectroscopy. J. Phys. Chem. B 122 (2018), pp. 7264–7276, https://doi.org/ 10.1021/acs.jpcb.8b04217 (IF = 2.92)
VŠ assisted in developing the population dynamic model scripts.

Contents

1 INTRODUCTION

1.1 OVERVIEW

The conjugated systems consist of covalently bonded carbon atoms, with alternating single and multiple bonds. This arrangement leads to the delocalization of the electrons across the molecule, which means the electron does not belong to the particular carbon atom, but rather to a group of atoms. The length of the conjugated system affects the unique electronic properties, e.g., the energies and dynamics of their excited electronic states, and as a result also their color. The bright yellow to red colors are the most visible feature of the important example of linear conjugated system - carotenoids.

1.1.1 A BRIEF HISTORY OF CAROTENOIDS

The first chapter of a carotenoid story was written most probably 2 billion years ago, in the Proterozoic.[1] Back then, cyanobacteria (or their progenitors) started to perform one of the most important processes on Earth – photosynthesis. It launched enormous changes in hydrosphere, atmosphere, and geosphere. One of the major consequences was the release of oxygen as a byproduct. Its combination with photosynthetic pigments and light can be fatal for living organisms if it is not under control. And this was the point when carotenoids were coming to the scene, protecting against destruction by photooxidation. But how far back in time can we trace the real relicts of carotenoids?

When looking for the oldest preserved carotenoids, it is advisable to turn to an environment that preserves them. The oxygen- and light-free places are most suitable.[2] One of these places is the Blake-Bahama Basin in the western North Atlantic Ocean where the oldest intact carotenoids were found. These carotenoids were dated 20 million years ago and were not specified.[3] The oldest specified carotenoid is isorenieratene, which was found in marl from Vena del Gesso basin (Italy).[4] These findings can help reveal life composition in old times since some species produce carotenoids that are unique for them.[5]

A long time after the first carotenoids appeared, evolution has endowed humans with a carotenoid-containing eyes and let them to be fascinated by the colors of autumn leaves, marigold flowers, or flamingo’s feathers. A lot of scientists tried to find out, what substance is responsible for a hue ranging from

yellow to orange to red. The first one, who isolated a carotenoid (currently known as β-carotene), was H. W. F. Wackenroder in 1831.[6] He made his discovery while searching for a medical agent, which would serve as a treatment against parasitic worms, so we can call his finding a lucky accident. The second scientist successful in isolation of carotenoid was six years later Berzelius, who named the substance xanthophyll[7] (it got the name from Greek *xanthos*, meaning yellow, and *phyllon*, meaning leaf, and is today known as lutein). The hydrocarbon nature of carotenoids was correctly determined already in 1847 by W. C. Zeise,[8] although the absolute values of atoms in the molecule were incorrect, most probably because of low purity of a sample he used. The correct formula of β-carotene ($C_{40}H_{56}$) was published more than a half-century later in 1907 by R. Willstätter and W. Mieg.[9] At this point, it is necessary to point out the determination and diligence of the scientist working before the introduction of chromatography when to get a few milligrams of pure carotenoid, dozens of kilograms of initial substance (carrot, eggs, leaves, etc.) had to be used.[1] After these first small steps, the fascinating journey of exploring other carotenoids could be started.

The so-called „Golden age" of the carotenoid chemistry is dated from the 1930s to 1940s and it is associated with names Paul Carrer and Richard Kuhn. Between the years 1933 and 1948, the number of isolated carotenoids increased from about 15 to nearly 80.[1] This could happen mostly because of new methods and developing of the known ones, e.g. chromatography and spectroscopy. The next goal after isolating carotenoids was an exploration of their functions and features.

The ability of carotenoids to serve as light-harvesting molecules was first reported in 1943 by Dutton et al.[10] The next important step in this research field happened in 1972 when Schulten and Karplus showed that the lowest absorbing state of longer polyenes is not the lowest excited state; instead there is a „dark" S_1 state between the ground state and the absorbing state, which is since that discovery denoted as S_2.[11] Since the late 1980s it was possible to measure the dynamics of excited states on (sub)picosecond time scales, which enabled the first measurement of β-carotene S_1 lifetime.[12] Since then a large number of successive experiments targeting the excited-state dynamics of carotenoids were carried out, resulting for example in the discovery of other dark states.[13–15]

Since the first isolation of β-carotene, more than 750 different carotenoids were reported,[16,17] and a lot of effort has been made to examine their properties and functions in nature. A small portion of carotenoids appearing in nature is shown on the cover of this thesis, described in more detail in Table 1-1, where the organism (or its part) and the most common carotenoid(s) in this part are listed. Despite the progress in the field in the last century, a lot of unanswered questions about carotenoids and their excited states remain.

1.1.2 SPECTROSCOPY OF CAROTENOIDS

The optical features of carotenoids are tightly bound with their structure. They typically consist of 40 carbon atoms and have π-electron conjugated backbone, which is built of alternating single and double carbon bonds. The key property determining spectroscopic properties is the conjugation length, which relies on the partial overlap of π-orbitals on adjacent double bonds. The majority of carotenoids found in nature have conjugated length N between 7 and 13. Linear carotenoids (i.e carotenoids without terminal rings or methyl substituents along the chain) show a $1/N$ dependence of their spectroscopic properties on the conjugation length. For a carotenoid of a more complicated structure one can determine the effective conjugation length (N_{eff}). It is obtained after comparison of e.g. the lowest excited state lifetime of a carotenoid with the $1/N$ dependence of linear carotenoids. N_{eff} then shows how conjugation extended to terminal rings affects the total conjugation length of a carotenoid.[18–22] For example the N_{eff} of β-carotene (in Figure 1-1 $N = 9β2$, which means the conjugation extends to two terminal β-ionylidene rings) was estimated to be ~10.[19] The spectroscopic properties of carotenoids can be also affected by e.g. the solvent, or atoms included in conjugation (the carotenoids containing only carbon and hydrogen are denoted as carotenes while the oxygenated carotenoids are denoted as xanthophylls). The carotenoids frequently used for spectroscopic studies are shown in Figure 1-1.

In theoretical studies, carotenoids are frequently approximated by polyenes, allowing to use the idealized C_{2h} point symmetry. The C_{2h} symmetry is specified by the identity, the two-fold rotational axis, the plane of symmetry, and the center of inversion. The usual way to describe energy levels of carotenoids is a three-

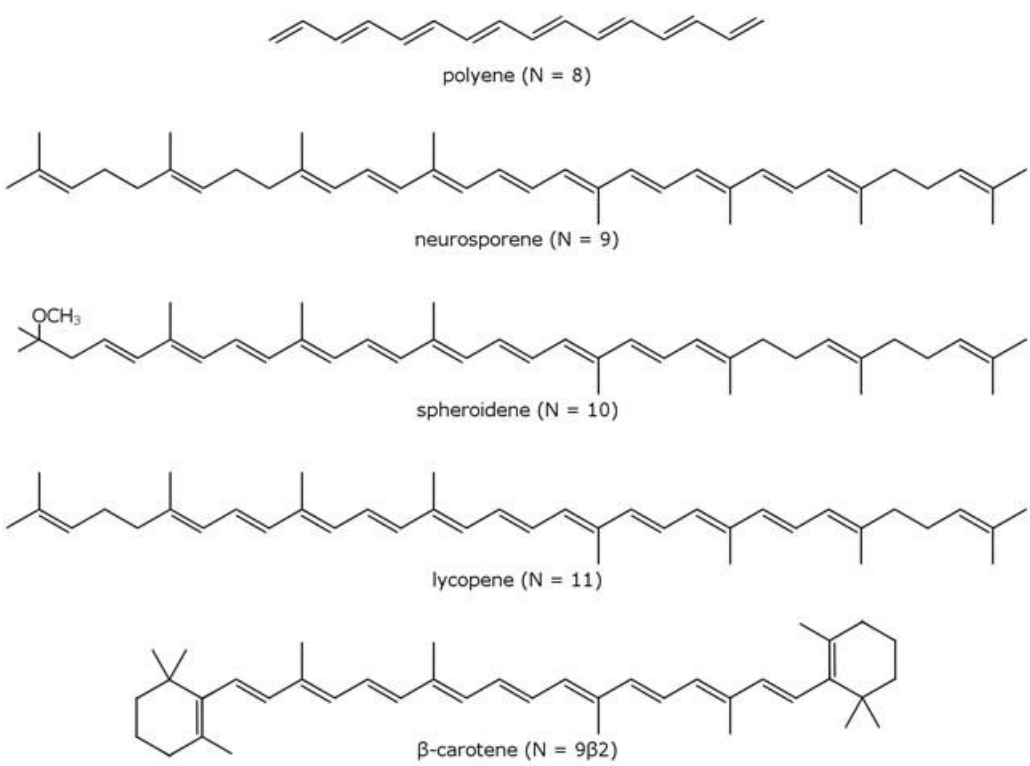

Figure 1-1: Chemical structures of polyene and commonly studied carotenoids with their conjugation length shown in brackets.

state system. This model consists of the ground state S_0 (in terms of C_{2h} symmetry labels denoted as $1^1A_g^-$), and two singlet excited states denoted S_1 ($2^1A_g^-$) and S_2 ($1^1B_u^+$). The question which of the transitions are allowed and which are forbidden can be answered via the equation for the transition dipole moment

$$\boldsymbol{\mu_{nm}} = \int \psi_n \hat{\boldsymbol{\mu}} \psi_m dV \qquad (1.1)$$

where ψ_m and ψ_n are wavefunctions of the initial and final states, respectively, and $\hat{\boldsymbol{\mu}}$ is the electric dipole moment operator. If this integral is nonzero, the transition is allowed. This is accomplished if the overall function in the integral is totally symmetric with respect to all symmetry operations of the point symmetry group. For carotenoids, it means the $S_0 \rightarrow S_1$ transition is one-photon forbidden, while the $S_0 \rightarrow S_2$ transition is strongly allowed.

One has to have in mind that the theory described above is directly applicable only for molecules having ideal C_{2h} symmetry. Most of the carotenoids, of course, do not have exactly the C_{2h} symmetry so some deviations from these rules occur (e.g. slightly allowed S_1-S_0 transition which makes observable a weak emission from the S_1 state for some carotenoids[23]). Moreover, recent studies suggest that other mechanisms will have to be included when explaining the excited-state properties of carotenoids.[24–26]

The energy scheme diagram for a general carotenoid is depicted in Figure 1-2 (bottom right), with all different possible transitions indicated, including S_0-S_2 excitation, S_1-S_N transition, etc. Some states in the scheme are common for all carotenoids, while others appear only for specific type of carotenoids. The transient absorption and steady-state absorption spectra, resulting from this scheme, are shown in the same figure. All the states mentioned there are described below in greater detail.

1.1.3 S_1 STATE

The presence of the forbidden lowest excited state in carotenoids and polyenes, the S_1 state, was theoretically predicted and experimentally demonstrated for a polyene in 1972.[11,27] The first measurements of the S_1 state energy and lifetime of a carotenoid were performed in the 1990s.[12] The S_1 energy depends mainly on the carotenoid conjugation length and in some cases also on the solvent, which is used. For example, the S_1 energy of spirilloxanthin ($N = 13$) in *n*-hexane is 11 900 cm^{-1} [28] while the S_1 state energy of the shorter heptaene ($N = 7$) in the same solvent is 18 160 ± 40 cm^{-1}.[29] The S_1 state has crucial importance for understanding the relaxation pathways in carotenoids since the molecule excited to the S_2 state undergoes fast relaxation to the S_1 state in 50 – 300 fs.[30] Therefore, significant effort was given to developing new experimental methods to study ultrafast relaxation pathways and to determine energies of the forbidden excited state(s) of carotenoids.

There are numerous spectroscopic methods that can assess the energies of excited states and some of these methods, with specific modifications, were used to determine the S_1 energy. In this thesis, only the most important methods will be mentioned. These methods may be divided into two separate subgroups:

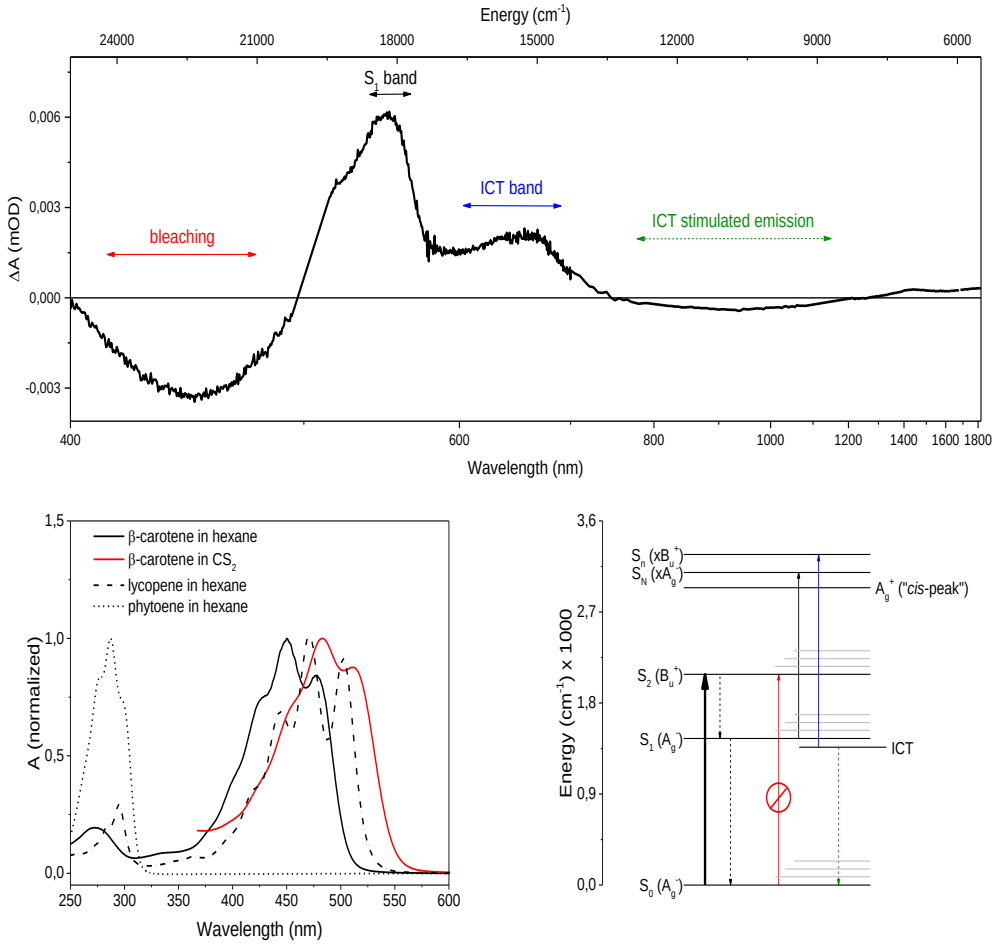

Figure 1-2: The signal from transient absorption spectroscopy experiment typical for a carbonyl carotenoid (top), showing ground state bleaching (negative signal between 400 and 500 nm), $S_1 \rightarrow S_N$ transition (highest peak around 550 nm), S* state signal (blue shoulder of $S_1 \rightarrow S_N$ transition), ICT state (red shoulder of $S_1 \rightarrow S_N$ transition), and stimulated emission of ICT state (negative signal in NIR). Steady state absorption spectra revealing dependence of peak position and resolution of peaks on carotenoid and solvent (bottom left). Energy level scheme of carbonyl carotenoid with the typical transitions (bottom right), where the thick arrow is excitation.

the ones relying on a steady-state spectroscopy (fluorescence or Raman spectroscopy) and the ones employing femtosecond time-resolved spectroscopy (method based on measurements of the S_1-S_2 transition or two-photon spectroscopy). Each of these methods has its own advantages and disadvantages.

For the best result of measurement, the most appropriate method depending on the studied system has to be chosen.

The first method used to determine the S_1 energy was fluorescence. For getting relevant results, standard fluorescence spectroscopy had to be upgraded to allow an extremely precise detection of the fluorescence signal, because the S_1 state emission of carotenoids with $N > 9$ is very weak (quantum yield of fluorescence is typically less than 10^{-6}).[29,31] Due to this weak emission, the first measurements of β-carotene S_1 emission done by Bondarev and Knyukshto in 1994 were influenced by a poor signal/noise ratio.[32] After this first study, a lot of subsequent experiments were carried out, which found out for instance, that the S_1 energy is much less sensitive to solvent polarizability than the S_2 state.

The next method used for getting the S_1 energies of carotenoids is resonance Raman spectroscopy.[33–36] The values obtained by this technique fit into the range of the S_1 energies calculated by energy-gap law. They are also very similar to those reported by fluorescence (despite the fact the energies obtained from fluorescence were slightly larger for longer carotenoids). The Raman spectroscopy of carotenoids suffers for the same problem as fluorescence detection. The intensity of Raman lines is much higher for excitation in resonance with the strongly allowed $S_0 – S_2$ transition than for the excitation in resonance with the forbidden $S_0 – S_1$ transition. [30]

The ultrafast time-resolved methods are based on detecting allowed transitions. Since the capability of tuning the femtosecond pulses in the 1 – 2 μm spectral range where the allowed $S_1 – S_2$ transition is expected, it was possible to obtain the S_1 energies of carotenoids based on measurements of the spectral profile of the S_1-S_2 transition. If one knows the energy of the $S_1 – S_2$ and $S_0 – S_2$ transitions, the S_1 energy can be obtained by subtraction of these two.[37]

Another ultrafast time-resolved method, two-photon spectroscopy, was used in Paper 1. A big advantage of this method is the reduction of parasitic events because there is no relaxation from other excited states to S_1 state while the S_1 state is directly excited. Quantum physics tells us that if a transition in a molecule with C_{2h} symmetry is forbidden for a one-photon process, then this transition should be allowed for two-photon processes. This is exploited by two-photon spectroscopy that is also used to explore excited states of carotenoids. The

quantity expressing the probability of a particular transition between two states i and f is the transition dipole moment (Eq. 1.1). The transition dipole moment M_{gf} from the initial state i to final state f for a single beam two-photon experiment is given by:[23,38,39]

$$M_{gf} = \sum_{i \neq g, i \neq f} \left\{ \frac{2}{\hbar} \frac{(\vec{\mu}_{gi} \cdot \vec{e})(\vec{\mu}_{if} \cdot \vec{e})}{(\omega - \omega_{ig})} \right\} - \frac{2(\Delta\vec{p}_{gf} \cdot \vec{e})(\vec{\mu}_{gf} \cdot \vec{e})}{\omega} \qquad (1.2)$$

where g, i, and f are the ground, intermediate, and final states of the two-photon transition, $h\omega_{ig}$ is the energy difference between i and g, $\vec{e}$ is the electric field vector, ω is the frequency of the excitation light, $\vec{\mu}_{gi}$ is the transition dipole moment from state g to state i, and $\Delta\vec{p}_{gf}$ is the change in static dipole moment between the ground and final states. In agreement with Eq. 1.2, there are two possibilities when two-photon transition can arise. The first one is via (virtual) intermediate states while the other one is due to a change in static dipole moment between the ground and final states. At this point, it is necessary to distinguish between nonpolar (e.g. β-cryptoxanthin, β-carotene) and polar (e.g. astaxanthin, cis-astaxanthin) carotenoids. For nonpolar carotenoids, the two-photon excitation is connected only with the first term of Eq. 1.2. For this type of carotenoids, the states of the same symmetry as the ground state are populated via two-photon excitation. The ground state, as well as the S_1 state, is of A_g^- symmetry. Therefore, the S_1 state of nonpolar carotenoids can be selectively populated by this mechanism. On the other hand, the transition dipole moment of polar carotenoids is affected by both terms of Eq. 1.2. The two-photon absorption facilitated by the second term thus occurs also for the states, which can be excited by the one-photon process (e.g. S_2 state).[23] The two-photon excitation is not a linear process thus the power dependence of the signal should be quadratic. This feature is usually exploited to test whether the signal originating from the S_1 state is achieved via two-photon excitation.

A graphical way to understand two-photon excitation is shown in Figure 1-3.[40] Here the approximation of carotenoids by polyenes shows the spins of ground state S_0 and the first excited state S_1. Looking closer, one can see that

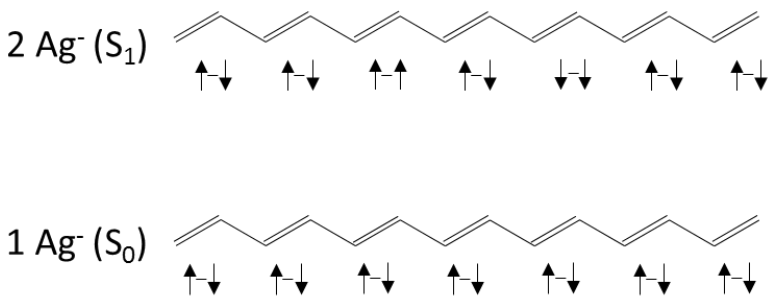

Figure 1-3: The electronic structure of the first excited state (top) and the ground state (bottom) of the polyenes. In the ground-state structure there are singlet spin pairings within each ethylic units, while in the first excited state the simultaneous spin flips in two ethylene units result in the overall singlet.

two singlet pairing of S_0 have to convert to triplet pairing in order to achieve S_1 state (the position of the pair is not fixed and they can move over the whole polyene). Thus, two photons are needed to excite the S_1 state directly.

A few two-photon experiments on carotenoids and carotenoid-containing protein complexes have been carried out in the last two decades. Here, these studies will be summarized in chronological order. The fluorescence from chlorophyll-a after two-photon excitation of carotenoid was first observed in 1990 in thylakoid membranes from the algae *Phaeodactylum tricornutum*.[41] This technique, which uses coupling of carotenoids and (bacterio)chlorophyll via singlet energy transfer has been employed in other experiments too. It was also the case of observation of the S_1 state of spheroidene in LH2 in 1999.[42] They also estimated of the *in situ* spheroidene S_1 transition energy to be 13 900 ±150 cm^{-1}. One year later, Walla et al. investigated light-harvesting complexes of purple bacteria *Rhodopseudomonas acidophila*. They reported the lifetimes of the carotenoid S_1 states after two-photon excitation in the B800-B850 complex and B800-B820 complex as 7 ± 0.5 ps and 6 ± 0.5 ps, respectively. The lifetime of the S_1 state in the light-harvesting complex II of *Rhodobacter sphaeroides* was determined to be approximately 1.9 ± 0.5 ps. These authors calculated the carotenoid to bacteriochlorophyll energy transfer efficiency after two-photon excitation of the S_1 state and explained differences in the energy transfer efficiency after the S_2 state is populated via one-photon excitation.[43] The same year, Walla et al. measured the two-photon excitation spectrum of light-

harvesting complex II in the spectral region of 1000 – 1600 nm.[44] They reported a band with an origin at ca. 2 × 660 nm (ca. 15 100 ± 300 cm^{-1}, which is in good agreement with estimates for the S_1 energy of the carotenoids isolated from LHC II measured in solution)[37,45,46] and a maximum at ca. 2 × 600 nm.

The next part of their study dealt with the fluorescence of the chlorophyll after two-photon excitation. The two-photon excitation wavelength was set to excite the maximum of the band observed in the two-photon excitation spectrum. They reported Chl-a fluorescence characterized by a fast rise of 250 ± 50 fs followed by a multiexponential decay on the picosecond time scale.[44] Later, Walla et al. (2002) expanded the study by measuring the two-photon excitation spectra of lutein and β-carotene in solution. The authors also compared these spectra with the two-photon excitation spectra of light-harvesting complex II. The results suggested that the shape of the S_1 spectrum is significantly influenced by the solvent.[47]

Zimmermann et al. 2002 measured the two-photon fluorescence excitation spectra of peridinin in benzene and in the peridinin chlorophyll a-protein.[23] The authors excited the samples in the 920 – 1320 nm spectral region. Excited peridinin in the peridinin chlorophyll a-protein (PCP) transfers the energy to chlorophyll. For peridinin in benzene, the faint fluorescence of peridinin was measured, while at for PCP the two-photon excitation was characterized via chlorophyll fluorescence. The measured signal was much higher for the peridinin chlorophyll *a*-protein because of the higher fluorescence quantum yield of chlorophyll compared to peridinin. Zimmermann et al. 2002 concluded that a two-photon absorption for peridinin in benzene starts at 600 nm with a shoulder peaking at 505 nm, while for PCP the edge of two-photon absorption begins at 655 nm and reaches the maximum at 527 nm.[23]

Another two-photon excitation spectra of peridinin and PCP were measured by Linden et al. (2004). In this case, peridinin was dissolved in methanol. The authors observed a two-photon transition just to the red tail of one-photon allowed $S_0 – S_2$ band. This transition was ascribed to the S_1 state.[48] Wehling & Walla (2005) measured two-photon pump-probe data of photosystem I of *Thermosynechococcus elongatus* (a thermophilic unicellular cyanobacterium)[49]. They used excitation wavelength 2 × 575 nm. The S_1 state of carotenoid in this

protein gave rise to 800 fs and 9 ps decay components. Wehling & Walla (2005) also measured a solution of a pure β-carotene under the same conditions and they found only a 9 ps decay component. The 800 fs component was thus interpreted as due to energy transfer from β-carotene to chlorophyll via the S_1 state.[50]

In contrast, long-lived species were observed after two-photon excitation of 8'-apo-β-caroten-8'-al and 7',7'-dicyano-7'-apo-β-carotene. These long-lived species were not found when the carotenoids were excited to S_2 state and underwent the internal conversion to S_1 state. The authors suggest these features are associated with a charge-transfer complex involving a solvent molecule.[51] Buckup et al. 2010 excited β-carotene with NIR pulses and then detected the dynamics for several wavelengths in the visible (510 – 590 nm) as well as in the NIR region (870 – 1000 nm). They observed the characteristic internal conversion to S_0 state and additional slow dynamics in the blue-wing of excited-state absorption and in the NIR. The authors also reported 340 – 400 fs relaxation component in NIR.[52] Kosumi et al. 2009 and Kosumi et al. 2011 carried out femtosecond two-photon spectroscopy of fucoxanthin in polar (methanol) and non-polar (cyclohexane) solvents. They also compared one- and two-photon excitation spectra and concluded that the ICT state (for details see Section 1.1.5) decays independently from the S_1 state.[53,54]

Recently, Betke & Lokstein studied two-photon excitation of LHCII samples with different carotenoid composition and isolated chlorophylls *a* and *b* in solution. Their findings suggest that two-photon absorption of chlorophylls is the major part of observed excitation and it dominates over the carotenoid excitation.[55] This would mean the experiments carried out previously on two-photon excitation of carotenoids and observing fluorescence from chlorophyll, could have been interpreted in a wrong way. Even though it changes a view on the pioneering experiments proving the two-photon nature of the S_1 state of carotenoid, it does not change the fact it is possible to populate the carotenoid S_1 state directly by two-photon excitation, which was shown in other experiments (e.g. in Paper 1 of this thesis).

1.1.4 S_2 STATE

The typical coloration of carotenoids is due to the strongly allowed S_0 - S_2 transition, which absorbs between 400 and 550 nm (ca 25 000 – 18 200 cm^{-1}) for naturally occurring carotenoids with conjugation length between 7 and 13. This transition exhibits a typical three-peak structure, resulting from the lowest three vibronic levels of the S_2 state. This vibrational structure can be readily observed in linear carotenoids, whereas the carotenoids with conjugation extended to various groups usually lose the resolution of vibrational bands due to conformational disorder of the terminal groups.[56]

There are some structural features of carotenoids, which can affect the S_0 – S_2 transition. It is known that the conjugation length almost does not influence the vibrational structure, but it significantly affects the energy of the S_0 – S_2 transition – the longer the conjugation length the smaller is the energy of the S_0-S_2 transition. The dependence of the S_2 energy on conjugation length N can be approximated as $E = A + B/N$, where A and B are free parameters.[29,31,57] Another circumstance affecting mainly the carotenoids possessing the conjugated carbonyl group in their structure is the solvent polarity. If such a carbonyl carotenoid is dissolved in a polar solvent the vibrational structure of the S_0 – S_2 band is lost and the absorption spectrum is broadened toward longer wavelengths.[30,58–61]

Why the middle peak in steady-state absorption of all carotenoids is the highest? *According to the Frank-Condon principle, the nucleus is much heavier in comparison to an electron. It implies that electronic transition occurs without a change in the position of the nuclei. The potentials of the ground and excited states are shifted and the vibrational level whose vibrational wave function overlap more significantly with the ground state wave function is favored. In the case of carotenoids, it is the first vibrational level.*

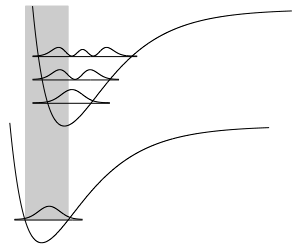

Another important property of the S_2 state is its lifetime. There were made experiments on a lot of carotenoids, which set the S_2 lifetime to the range of 100

– 300 fs. It was also reported that the lifetime of the S_2 state can be influenced by conjugation length and solvent parameters.[29,57,62–65]

1.1.5 OTHER SINGLET STATES

Besides the S_1 and S_2 there exist at least two more singlet states that are of interest to scientists. These states are bound to specific conditions in both solvent and protein. The first one is called Intramolecular Charge-Transfer (ICT) and the other one is called S*. Both of them are heavily discussed since their origin is still not clearly understood.[66–70]

The ICT state appears exclusively in carbonyl carotenoids, thus carotenoids containing carbonyl group in a conjugation (although there is an exception for carotenoids with the symmetrically placed C=O groups, where ICT state is not observed – e.g. astaxanthin, crocin), and it is strongly polarity dependent. The ICT band (Fig. 1-2) becomes more pronounced with the higher polarity of the solvent. This is caused by the large dipole moment of ICT state, which is stabilized in polar solvents. The ICT state manifests itself in transient absorption spectra in two ways, namely by a new peak which is redshifted to the S_1-S_n transition (550-700 nm), and by stimulated emission in NIR (Fig. 1-2). Despite efforts to clarify the origin of ICT state, it is still a matter of debate and three main scenarios are involved in the attempts of its explanation:

a) ICT is an independent state,[60,71,72] or
b) strongly coupled to the S_1 state,[48,58,59,73] or
c) the S_1 state with a large charge-transfer character.[61,74]

This state is of interest of this thesis since it is the main topic in Paper 4, in which we try to shed some light on the ICT state origin.

The S* state promotes itself as a long decaying feature appearing on the blue shoulder of the S_1-S_N peak in the transient absorption spectrum.[69,75,76] It is more enhanced in long carotenoids and in carotenoids with conjugation extended to terminal rings.[77] The S* lifetime changes with conjugation length. While in shorter carotenoids its lifetime is indistinguishable from the S_1 lifetime, for carotenoids with N_{eff} >12 the S* lifetime is longer than the S_1 lifetime.[78–80] No clear dependence of the S* lifetime on N has been found so far. It is also interesting that the S* is more pronounced after the two-photon excitation (Paper

1). The origin of S* state remains unknown and the theories made a few big twists during a history. After the first observation in a long analogue of β-carotene, the explanation pointed to a hot ground state.[81] Later it was though S* is a separated excited state, which is caused by a specific conformation of some part of carotenoid molecules.[78] Nowadays the explanation is turning back to the hot ground state for carotenoids with N >12, while for carotenoids with N<12 it seems the signal comes mostly from the S_1 state.[70,78,82,83]

1.1.6 FUNCTIONS OF CAROTENOIDS

Carotenoids can be found in all sorts of organisms, but their origin is linked to the beginnings of oxygenic photosynthesis.[1] Photosynthetic organisms include algae, cyanobacteria, and plants, which are the most familiar to humans. Although the most obvious sign of carotenoids presence in plants – color – is usually exposed in blooms or fruits, they hold the most important role in plant's leaves, where chlorophylls cover their brightness. The connection of chlorophylls and carotenoids in proteins is crucial for oxidative photosynthesis, in which carotenoids fulfill several functions. The first of them, light-harvesting, exploits the fact that carotenoids absorb light mainly in the blue-green region. These wavelengths are only poorly accessible to chlorophylls, so carotenoids serve as energy donors in photosynthetic antenna; they absorb light in this spectral region and transfer energy to chlorophylls.

***Justification of light-harvesting in an example**: The photosynthetically active radiation (PAR) in tropical regions is around 1800 μmol photons m^{-2} s^{-1}(this value decreases to only 4 to 10 % for understory plants). Taking into account the maximal PAR and the optical cross-section of chlorophyll (Chl) ≈ 0.01 nm^2, one molecule of Chl absorbs photon once per 100 ms. The rate is too slow for photosynthesis, with typical times in ms, and reveals the reason for employing light-harvesting machinery in photosynthetic organisms.*

The carotenoid-to-chlorophyll energy transfer can occur from the S_2 (Car) state to the Q_x (Chl) state, or from the S_1 (Car) state to the Q_y (Chl) state. These transitions between molecules can be described by more mechanisms, for

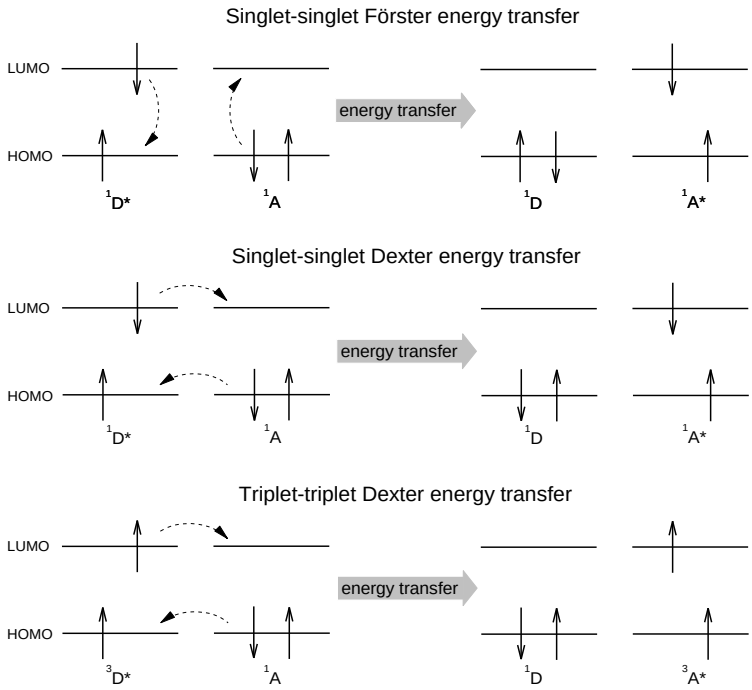

Figure 1-4: Schematic diagram for mechanism of Förster and Dexter energy transfer.

example via Dexter or Förster energy transfer (Figure 1-4). The first one is specified by an electron exchange and thus it proceeds over a shorter distance (< 10 Å). The second one proceeds at distances up to 100 Å and its mechanism is driven by a virtual photon exchange. In this case, electrons remain within the same molecule during the energy transfer.[84,85]

Carotenoids also provide photoprotection to the photosynthetic organisms.[86,87] If there is too much light, it can promote the conversion of excited chlorophyll into a triplet state, which can further react with a ground-state oxygen eventually leading to the creation of singlet oxygen.[88] The singlet oxygen is extremely reactive and can cause damage to biomolecules.[89,90] Carotenoids prevent this damage on different levels: by quenching both singlet[91] and triplet[92] excited states of chlorophyll molecules, and also directly by scavenging singlet oxygen.[90,93,94]

The last two mentioned functions (light-harvesting and photoprotection) can be achieved via a change of the conjugation length of a carotenoid molecule. An

adjustment of the carotenoid molecule by epoxidation or deepoxydation may optimize the carotenoid for light-harvesting (carotenoid with shorter conjugation length able to transmit energy to chlorophyll) or photoprotection (carotenoid with longer conjugation length able to quench). Examples of these so-called cycles are e.g. violaxanthin cycle in higher plants, ferns, or mosses (employed carotenoids are violaxanthin, antheraxanthin, and zeaxanthin),[95,96] siphonaxanthin cycle in *Chlorophyta* (siphonaxanthin and lutein)[97] or diadinoxanthin cycle in diatoms, and brown algae (diadinoxanthin and diatoxanthin).[98,99]

The last function of carotenoids in photosynthetic organisms is the structural function. Experiments performed on different green algae and cyanobacterial mutants showed the genetically modified organisms lacking certain carotenoids are not able to properly assemble photosystem I, photosystem II, light-harvesting complexes or thylakoid membrane.[100–104] Not only the carotenoid-lacking mutants but also the ones with an alternated composition of carotenoids were affected.[105]

Carotenoids are widely represented also in animals (as it can be seen on feathers of flamingos, shells of shrimps, or in the meat of tuna fish), including humans. Approximately 40 carotenoids are present in the human diet from which ca 20 are found in blood and tissues, fulfilling several till today known functions, from which one of best known is serving as antioxidants. In humans, one can clearly see the presence of carotenoids in a yellow spot on the retina, where lutein, zeaxanthin, and meso-zeaxantin are found in large concentrations,[106] serving as photoprotective agents and protecting against the age-related macular degeneration.[107] A lot of studies were also carried out to clarify the role of carotenoids in cancer prevention and modulation of the pathogenesis of coronary heart disease.[108–111] Last but not least is the provitamin A activity of some carotenoids. The dietary deficiency of vitamin A can lead to blindness and especially in developing countries, it is nowadays still a problem.

Despite great importance for animals, carotenoids can be only synthesized by plants and microorganisms. The two exceptions that actually demonstrate synthesis of carotenoids by animals are aphids and spider mites, which received this ability due to a transfer of genes from fungi.[112–114]

REFERENCES

1. G. Britton, S. Liaaen-Jensen, H. Pfander, Carotenoids: A colorful history, 1st ed., CaroteNature, Norway, 2017.

2. P.R. Leavitt, D.A. Hodgson, Sedimentary pigments, in: J.P. Smol, H.J.B. Birks, W.M. Last, R.S. Bradley, K. Alverson (Eds.), Track. environ. chang. using lake sediments, Springer, Dordrecht, 2002: pp. 295–325. https://doi.org/10.1007/0-306-47668-1_15.

3. J.N. Cardoso, A.M.K. Wardroper, C.D. Watts, P.J. Barnes, J.R. Maxwell, G. Eglinton, D.G. Mound, G.C. Speers, Site 391: Blake-Bahama Basin, in: Initial reports deep sea drill. proj., 1978: pp. 617–623. https://doi.org/10.2973/dsdp.proc.44.105.1978.

4. B.J. Keely, S.R. Blake, P. Schaeffer, J.R. Maxwell, Distributions of pigments in the organic matter of marls from the Vena del Gesso evaporitic sequence, Org. Geochem. 23 (1995) 527–539. https://doi.org/10.1016/0146-6380(95)00046-H.

5. E.C. Hopmans, S. Schouten, W.I.C. Rijpstra, J.S. Sinninghe Damsté, Identification of carotenals in sediments, Org. Geochem. 36 (2005) 485–495. https://doi.org/10.1016/j.orggeochem.2004.10.001.

6. H. Wackenroder, Ueber das Oleum radicis Dauci aetherum, das Carotin, den Carotenzucker und den officinellen succus Dauci; so wie auch über das Mannit, welches in dem Möhrensafte durch eine besondere Art der Gährung gebildet wird, Geigers Mag. Der Pharm. 33 (1831) 144–172.

7. Berzelius, Ueber die gelbe Farbe der Blätter im Herbste, Ann. Der Pharm. 21 (1837) 257–262. https://doi.org/10.1002/jlac.18370210303.

8. W.C. Zeise, Ueber das Carotin, Ann. Der Chemie Und Pharm. 62 (1847) 380–382. https://doi.org/10.1002/jlac.18470620305.

9. R. Willstätter, W. Mieg, Untersuchungen über Chlorophyll; IV. Ueber die gelben Begleiter des Chlorophylls, Justus Liebig's Ann. Der Chemie. 355 (1907) 1–28. https://doi.org/10.1002/jlac.19073550102.

10. H.J. Dutton, W.M. Manning, B.M. Duggar, Chlorophyll fluorescence and energy transfer in the diatom *Nitzschia closterium*, J. Phys. Chem. 47 (1943) 308–313. https://doi.org/10.1021/j150427a002.

11. K. Schulten, M. Karplus, On the origin of a low-lying forbidden transition in polyenes and related molecules, Chem. Phys. Lett. 14 (1972) 305–309. https://doi.org/10.1016/0009-2614(72)80120-9.

12. M.R. Wasielewski, L.D. Kispert, Direct measurement of the lowest excited singlet state lifetime of all-trans-β-carotene and related carotenoids, Chem. Phys. Lett. 128 (1986) 238–243. https://doi.org/10.1016/0009-2614(86)80332-3.

13. T. Sashima, Y. Koyama, T. Yamada, H. Hashimoto, The $1B_u^+$, $1B_u^-$, and $2A_g$ energies of crystalline lycopene, β-carotene, and mini-9-β-carotene as determined by resonance-Raman excitation profiles: Dependence of the $1B_u^-$ state energy on the conjugation length, J. Phys. Chem. B. 104 (2000) 5011–5019. https://doi.org/10.1021/jp994185b.

14. K. Furuichi, T. Sashima, Y. Koyama, The first detection of the $3A_g^-$ state in carotenoids using resonance-Raman excitation profiles, Chem. Phys. Lett. 356 (2002) 547–555. https://doi.org/10.1016/S0009-2614(02)00412-8.

15. T. Polívka, V. Sundström, Dark excited states of carotenoids: Consensus and controversy, Chem. Phys. Lett. 477 (2009) 1–11. https://doi.org/10.1016/j.cplett.2009.06.011.

16. K. Shindo, N. Misawa, New and rare carotenoids isolated from marine bacteria and their antioxidant activities, Mar. Drugs. 12 (2014) 1690–1698. https://doi.org/10.3390/md12031690.

17. G. Britton, S. Liaaen-Jensen, H. Pfander, Carotenoids - Handbook, Birkhäuser Basel, Springer Basel AG, 2004. https://doi.org/10.1007/978-3-0348-7836-4.

18. M. Fuciman, P. Chábera, A. Župčanová, P. Hříbek, J.B. Arellano, F. Vácha, J. Pšenčík, T. Polívka, Excited state properties of aryl carotenoids, Phys. Chem. Chem. Phys. 12 (2010) 3112–3120. https://doi.org/10.1039/b921384h.

19. M. Fuciman, G. Keşan, A.M. LaFountain, H.A. Frank, T. Polívka, Tuning the spectroscopic properties of aryl carotenoids by slight changes in structure, J. Phys. Chem. B. 119 (2015) 1457–1467. https://doi.org/10.1021/jp512354r.

20. M.M. Mendes-Pinto, E. Sansiaume, H. Hashimoto, A.A. Pascal, A. Gall, B. Robert, Electronic absorption and ground state structure of carotenoid molecules, J. Phys. Chem. B. 117 (2013) 11015–11021. https://doi.org/10.1021/jp309908r.

21. R. Withnall, B.Z. Chowdhry, J. Silver, H.G.M. Edwards, L.F.C. De Oliveira, Raman spectra of carotenoids in natural products, Spectrochim. Acta - Part A Mol. Biomol. Spectrosc. 59 (2003) 2207–2212. https://doi.org/10.1016/S1386-1425(03)00064-7.

22. M.J. Llansola-Portoles, A.A. Pascal, B. Robert, Electronic and vibrational properties of carotenoids: From in vitro to in vivo, J. R. Soc. Interface. 14 (2017) 20170504. https://doi.org/10.1098/rsif.2017.0504.

23. J. Zimmermann, P.A. Linden, H.M. Vaswani, R.G. Hiller, G.R. Fleming, Two-photon excitation study of peridinin in benzene and in the peridinin chlorophyll a-protein (PCP), J. Phys. Chem. B. 106 (2002) 9418–9423. https://doi.org/10.1021/jp020565c.

24. L. Fiedor, Heriyanto, J. Fiedor, M. Pilch, Effects of molecular symmetry on the electronic transitions in carotenoids, J. Phys. Chem. Lett. 7 (2016) 1821–1829. https://doi.org/10.1021/acs.jpclett.6b00637.

25. E.J. Taffet, B.G. Lee, Z.S.D. Toa, N. Pace, G. Rumbles, J. Southall, R.J. Cogdell, G.D.

Scholes, Carotenoid nuclear reorganization and interplay of bright and dark excited states, J. Phys. Chem. B. 123 (2019) 8628–8643. https://doi.org/10.1021/acs.jpcb.9b04027.

26. T. Wei, V. Balevičius, T. Polívka, A. V. Ruban, C.D.P. Duffy, How carotenoid distortions may determine optical properties: Lessons from the orange carotenoid protein, Phys. Chem. Chem. Phys. 21 (2019) 23187–23197. https://doi.org/10.1039/c9cp03574e.

27. B.S. Hudson, B.E. Kohler, A low-lying weak transition in the polyene α,ω-diphenyloctatetraene, Chem. Phys. Lett. 14 (1972) 299–304. https://doi.org/10.1016/0009-2614(72)80119-2.

28. R. Fujii, T. Ishikawa, Y. Koyama, M. Taguchi, Y. Isobe, H. Nagae, Y. Watanabe, Fluorescence spectroscopy of all-trans-anhydrorhodovibrin and spirilloxanthin: Detection of the $1B_u^-$ fluorescence, J. Phys. Chem. A. 105 (2001) 5348–5355. https://doi.org/10.1021/jp010150b.

29. H.A. Frank, J.S. Josue, J.A. Bautista, I. Van der Hoef, F.J. Jansen, J. Lugtenburg, G. Wiederrecht, R.L. Christensen, Spectroscopic and photochemical properties of open-chain carotenoids, J. Phys. Chem. B. 106 (2002) 2083–2092. https://doi.org/10.1021/jp013321l.

30. T. Polívka, V. Sundström, Ultrafast dynamics of carotenoid excited states-from solution to natural and artificial systems, Chem. Rev. 104 (2004) 2021–2071. https://doi.org/10.1021/cr020674n.

31. H.A. Frank, R.Z.B. Desamero, V. Chynwat, R. Gebhard, I. Van Der Hoef, F.J. Jansen, J. Lugtenburg, D. Gosztola, M.R. Wasielewski, Spectroscopic properties of spheroidene analogs having different extents of π-electron conjugation, J. Phys. Chem. A. 101 (1997) 149–157. https://doi.org/10.1021/jp962373l.

32. S.L. Bondarev, V.N. Knyukshto, Fluorescence from the $S_1(2\ ^1A_g)$ state of all-trans-β-carotene, Chem. Phys. Lett. 225 (1994) 346–350. https://doi.org/10.1016/0009-2614(94)87092-6.

33. K. Gaier, A. Angerhofer, H.C. Wolf, The lowest excited electronic singlet states of all-trans β-carotene single crystals, Chem. Phys. Lett. 187 (1991) 103–109. https://doi.org/10.1016/0009-2614(91)90492-R.

34. T. Sashima, M. Shiba, H. Hashimoto, H. Nagae, Y. Koyama, The $2A_g^-$ energy of crystalline all-trans-spheroidene as determined by resonance-Raman excitation profiles, Chem. Phys. Lett. 290 (1998) 36–42. https://doi.org/10.1016/S0009-2614(98)00481-3.

35. T. Noguchi, H. Hayashi, M. Tasumi, G.H. Atkinson, Solvent effects on the ag C=C stretching mode in the $2^1A_g^-$ excited state of β-carotene and two derivatives: Picosecond time-resolved resonance Raman spectroscopy, J. Phys. Chem. 95 (1991) 3167–3172. https://doi.org/10.1021/j100161a040.

36. H. Hashimoto, Y. Koyama, Y. Mori, Mechanism activating the 2^1A_g state in all-trans-β-carotene crystal to resonance Raman scattering, Jpn. J. Appl. Phys. 36 (1997) L916–L918. https://doi.org/10.1143/jjap.36.l916.

37. T. Polívka, J.L. Herek, D. Zigmantas, H.E. Åkerlund, V. Sundström, Direct observation of the (forbidden) S_1 state in carotenoids, Proc. Natl. Acad. Sci. U. S. A. 96 (1999) 4914–4917. https://doi.org/10.1073/pnas.96.9.4914.

38. B. Dick, G. Hohlneicher, Importance of initial and final states as intermediate states in two-photon spectroscopy of polar molecules, J. Chem. Phys. 76 (1982) 5755–5760. https://doi.org/10.1063/1.442971.

39. S. Abe, Two-photon probe of forbidden exciton states in symmetric aggregates of asymmetric molecules, Chem. Phys. 264 (2001) 355–363. https://doi.org/10.1016/S0301-0104(01)00258-0.

40. P. Tavan, K. Schulten, Electronic excitations in finite and infinite polyenes, Phys. Rev. B. 36 (1987) 4337–4358. https://doi.org/10.1103/PhysRevB.36.4337.

41. A.P. Shreve, J.K. Trautman, T.G. Owens, A.C. Albrecht, Two-photon excitation spectroscopy of thylakoid membranes from *Phaeodactylum tricornutum*: Evidence for an in vivo two-photon-allowed carotenoid state, Chem. Phys. Lett. 170 (1990) 51–56. https://doi.org/10.1016/0009-2614(90)87088-9.

42. B.P. Krueger, J. Yom, P.J. Walla, G.R. Fleming, Observation of the S_1 state of spheroidene in LH2 by two-photon fluorescence excitation, Chem. Phys. Lett. 310 (1999) 57–64. https://doi.org/10.1016/S0009-2614(99)00729-0.

43. P.J. Walla, P.A. Linden, C.P. Hsu, G.D. Scholes, G.R. Fleming, Femtosecond dynamics of the forbidden carotenoid S_1 state in light-harvesting complexes of purple bacteria observed after two-photon excitation, Proc. Natl. Acad. Sci. U. S. A. 97 (2000) 10808–10813. https://doi.org/10.1073/pnas.190230097.

44. P.J. Walla, J. Yom, B.P. Krueger, G.R. Fleming, Two-photon excitation spectrum of light-harvesting complex II and fluorescence upconversion after one- and two-photon excitation of the carotenoids, J. Phys. Chem. B. 104 (2000) 4799–4806. https://doi.org/10.1021/jp9943023.

45. V. Chynwat, H.A. Frank, The application of the energy gap law to the S_1 energies and dynamics of carotenoids, Chem. Phys. 194 (1995) 237–244. https://doi.org/10.1016/0301-0104(95)00017-I.

46. H.A. Frank, A. Cua, V. Chynwat, A. Young, D. Gosztola, M.R. Wasielewski, Photophysics of the carotenoids associated with the xanthophyll cycle in photosynthesis, Photosynth. Res. 41 (1994) 389–395. https://doi.org/10.1007/BF02183041.

47. P.J. Walla, P.A. Linden, K. Ohta, G.R. Fleming, Excited-state kinetics of the carotenoid S_1 state in LHC II and two-photon excitation spectra of lutein and β-carotene in solution:

Efficient Car S_1→Chl electronic energy transfer via hot S_1 states?, J. Phys. Chem. A. 106 (2002) 1909–1916. https://doi.org/10.1021/jp011495x.

48. P.A. Linden, J. Zimmermann, T. Brixner, N.E. Holt, H.M. Vaswani, R.G. Hiller, G.R. Fleming, Transient absorption study of peridinin and peridinin-chlorophyll a-protein after two-photon excitation, J. Phys. Chem. B. 108 (2004) 10340–10345. https://doi.org/10.1021/jp031331b.

49. Y. Nakamura, T. Kaneko, S. Sato, M. Ikeuchi, H. Katoh, S. Sasamoto, A. Watanabe, M. Iriguchi, K. Kawashima, T. Kimura, Y. Kishida, C. Kiyokawa, M. Kohara, M. Matsumoto, A. Matsuno, N. Nakazaki, S. Shimpo, M. Sugimoto, C. Takeuchi, M. Yamada, S. Tabata, Complete genome structure of the thermophilic cyanobacterium *Thermosynechococcus elongatus* BP-1, DNA Res. 9 (2002) 123–130. https://doi.org/10.1093/dnares/9.4.123.

50. A. Wehling, P.J. Walla, Time-resolved two-photon spectroscopy of photosystem I determines hidden carotenoid dark-state dynamics, J. Phys. Chem. B. 109 (2005) 24510–24516. https://doi.org/10.1021/jp053890j.

51. Y. Pang, G.A. Jones, M.A. Prantil, G.R. Fleming, Unusual relaxation pathway from the two-photon excited first singlet state of carotenoids, J. Am. Chem. Soc. 132 (2010) 2264–2273. https://doi.org/10.1021/ja908472y.

52. T. Buckup, A. Weigel, J. Hauer, M. Motzkus, Ultrafast multiphoton transient absorption of β-carotene, Chem. Phys. 373 (2010) 38–44. https://doi.org/10.1016/j.chemphys.2009.12.020.

53. D. Kosumi, T. Kusumoto, R. Fujii, M. Sugisaki, Y. Iinuma, N. Oka, Y. Takaesu, T. Taira, M. Iha, H.A. Frank, H. Hashimoto, One- and two-photon pump-probe optical spectroscopic measurements reveal the S_1 and intramolecular charge transfer states are distinct in fucoxanthin, Chem. Phys. Lett. 483 (2009) 95–100. https://doi.org/10.1016/j.cplett.2009.10.077.

54. D. Kosumi, T. Kusumoto, R. Fujii, M. Sugisaki, Y. Iinuma, N. Oka, Y. Takaesu, T. Taira, M. Iha, H.A. Frank, H. Hashimoto, Ultrafast S_1 and ICT state dynamics of a marine carotenoid probed by femtosecond one- and two-photon pump-probe spectroscopy, J. Lumin. 131 (2011) 515–518. https://doi.org/10.1016/j.jlumin.2010.09.018.

55. A. Betke, H. Lokstein, Two-photon excitation spectroscopy of photosynthetic light-harvesting complexes and pigments, Faraday Discuss. 216 (2019) 494–506. https://doi.org/10.1039/c8fd00198g.

56. R.L. Christensen, M. Goyette, L. Gallagher, J. Duncan, B. DeCoster, J. Lugtenburg, F.J. Jansen, I. van der Hoef, S_1 and S_2 states of apo- and diapocarotenes, J. Phys. Chem. A. 103 (1999) 2399–2407. https://doi.org/10.1021/jp983946s.

57. P.O. Andersson, S.M. Bachilo, R.-L. Chen, T. Gillbro, Solvent and temperature effects on dual fluorescence in a series of carotenes. Energy gap dependence of the internal

conversion rate, J. Phys. Chem. 99 (1995) 16199–16209. https://doi.org/10.1021/j100044a002.

58. D. Zigmantas, R.G. Hiller, A. Yartsev, V. Sundström, T. Polívka, Dynamics of excited states of the carotenoid peridinin in polar solvents: Dependence on excitation wavelength, viscosity, and temperature, J. Phys. Chem. B. 107 (2003) 5339–5348. https://doi.org/10.1021/jp0272318.

59. H.A. Frank, J.A. Bautista, J. Josue, Z. Pendon, R.G. Hiller, F.P. Sharples, D. Gosztola, M.R. Wasielewski, Effect of the solvent environment on the spectroscopic properties and dynamics of the lowest excited states of carotenoids, J. Phys. Chem. B. 104 (2000) 4569–4577. https://doi.org/10.1021/jp000079u.

60. J.A. Bautista, R.E. Connors, B.B. Raju, R.G. Hiller, F.P. Sharples, D. Gosztola, M.R. Wasielewski, H.A. Frank, Excited state properties of peridinin: Observation of a solvent dependence of the lowest excited singlet state lifetime and spectral behavior unique among carotenoids, J. Phys. Chem. B. 103 (1999) 8751–8758. https://doi.org/10.1021/jp9916135.

61. S. Shima, R.P. Ilagan, N. Gillespie, B.J. Sommer, R.G. Hiller, F.P. Sharples, H.A. Frank, R.R. Birge, Two-photon and fluorescence spectroscopy and the effect of environment on the photochemical properties of peridinin in solution and in the peridinin-chlorophyll-protein from *Amphidinium carterae*, J. Phys. Chem. A. 107 (2003) 8052–8066. https://doi.org/10.1021/jp022648z.

62. A.N. Macpherson, T. Gillbro, Solvent dependence of the ultrafast S_2-S_1 internal conversion rate of β-carotene, J. Phys. Chem. A. 102 (1998) 5049–5058. https://doi.org/10.1021/jp980979z.

63. M. Ricci, S.E. Bradforth, R. Jimenez, G.R. Fleming, Internal conversion and energy transfer dynamics of spheroidene in solution and in the LH-1 and LH-2 light-harvesting complexes, Chem. Phys. Lett. 259 (1996) 381–390. https://doi.org/10.1016/0009-2614(96)00832-9.

64. S. Akimoto, I. Yamazaki, S. Takaichi, M. Mimuro, Excitation relaxation of carotenoids within the S_2 state probed by the femtosecond fluorescence up-conversion method, Chem. Phys. Lett. 313 (1999) 63–68. https://doi.org/10.1016/S0009-2614(99)01015-5.

65. S. Akimoto, I. Yamazaki, T. Sakawa, M. Mimuro, Temperature effects on excitation relaxation dynamics of the carotenoid β-carotene and its analogue β-apo-8′-carotenal, probed by femtosecond fluorescence spectroscopy, J. Phys. Chem. A. 106 (2002) 2237–2243. https://doi.org/10.1021/jp0125653.

66. N.L. Wagner, J.A. Greco, M.M. Enriquez, H.A. Frank, R.R. Birge, The nature of the intramolecular charge transfer state in peridinin, Biophys. J. 104 (2013) 1314–1325. https://doi.org/10.1016/j.bpj.2013.01.045.

67. D.M. Niedzwiedzki, T. Kajikawa, K. Aoki, S. Katsumura, H.A. Frank, Excited states

energies and dynamics of peridinin analogues and the nature of the intramolecular charge transfer state in carbonyl-containing carotenoids, J. Phys. Chem. B. 117 (2013) 6874–6887. https://doi.org/10.1021/jp400038k.

68. M.M. Enriquez, M. Fuciman, A.M. Lafountain, N.L. Wagner, R.R. Birge, H.A. Frank, The intramolecular charge transfer state in carbonyl-containing polyenes and carotenoids, J. Phys. Chem. B. 114 (2010) 12416–12426. https://doi.org/10.1021/jp106113h.

69. F. Ehlers, M. Scholz, J. Schimpfhauser, J. Bienert, K. Oum, T. Lenzer, Collisional relaxation of apocarotenals: Identifying the S* state with vibrationally excited molecules in the ground electronic state S_0*, Phys. Chem. Chem. Phys. 17 (2015) 10478–10488. https://doi.org/10.1039/c4cp05600k.

70. V. Balevičius, A.G. Pour, J. Savolainen, C.N. Lincoln, V. Lukeš, E. Riedle, L. Valkunas, D. Abramavicius, J. Hauer, Vibronic energy relaxation approach highlighting deactivation pathways in carotenoids, Phys. Chem. Chem. Phys. 17 (2015) 19491–19499. https://doi.org/10.1039/c5cp00856e.

71. H.M. Vaswani, C.P. Hsu, M. Head-Gordon, G.R. Fleming, Quantum chemical evidence for an intramolecular charge-transfer state in the carotenoid peridinin of peridinin-chlorophyll-protein, J. Phys. Chem. B. 107 (2003) 7940–7946. https://doi.org/10.1021/jp030086t.

72. E. Papagiannakis, D.S. Larsen, I.H.M. Van Stokkum, M. Vengris, R.G. Hiller, R. Van Grondelle, Resolving the excited state equilibrium of peridinin in solution, Biochemistry. 43 (2004) 15303–15309. https://doi.org/10.1021/bi047977r.

73. T. Polívka, I.H.M. Van Stokkum, D. Zigmantas, R. Van Grondelle, V. Sundström, R.G. Hiller, Energy transfer in the major intrinsic light-harvesting complex from *Amphidinium carterae*, Biochemistry. 45 (2006) 8516–8526. https://doi.org/10.1021/bi060265b.

74. M. Durchan, M. Fuciman, V. Šlouf, G. Keşan, T. Polívka, Excited-state dynamics of monomeric and aggregated carotenoid 8′-apo-β-carotenal, J. Phys. Chem. A. 116 (2012) 12330–12338. https://doi.org/10.1021/jp310140k.

75. V. Balevičius Jr., D. Abramavicius, T. Polívka, A. Galestian Pour, J. Hauer, A unified picture of S* in carotenoids, J. Phys. Chem. Lett. 7 (2016) 3347–3352. https://doi.org/10.1021/acs.jpclett.6b01455.

76. F. Ehlers, M. Scholz, K. Oum, T. Lenzer, Excited-state dynamics of 3,3′-dihydroxyisorenieratene and (3R,3′R)-zeaxanthin: Observation of vibrationally hot S_0 species, Arch. Biochem. Biophys. 646 (2018) 137–144. https://doi.org/10.1016/j.abb.2018.03.035.

77. D.M. Niedzwiedzki, J.O. Sullivan, T. Polívka, R.R. Birge, H.A. Frank, Femtosecond time-resolved transient absorption spectroscopy of xanthophylls, J. Phys. Chem. B. 110 (2006) 22872–22885. https://doi.org/10.1021/jp0622738.

78. C.C. Gradinaru, J.T.M. Kennis, E. Papagiannakis, I.H.M. Van Stokkum, R.J. Cogdell, G.R. Fleming, R.A. Niederman, R. Van Grondelle, An unusual pathway of excitation energy deactivation in carotenoids: Singlet-to-triplet conversion on an ultrafast timescale in a photosynthetic antenna, Proc. Natl. Acad. Sci. U. S. A. 98 (2001) 2364–2369. https://doi.org/10.1073/pnas.051501298.

79. H. Staleva, M. Zeeshan, P. Chábera, V. Partali, H.R. Sliwka, T. Polívka, Ultrafast dynamics of long homologues of carotenoid zeaxanthin, J. Phys. Chem. A. 119 (2015) 11304–11312. https://doi.org/10.1021/acs.jpca.5b08460.

80. P. Chábera, M. Fuciman, P. Hříbek, T. Polívka, Effect of carotenoid structure on excited-state dynamics of carbonyl carotenoids, Phys. Chem. Chem. Phys. 11 (2009) 8795–8803. https://doi.org/10.1039/b909924g.

81. P.O. Andersson, T. Gillbro, Photophysics and dynamics of the lowest excited singlet state in long substituted polyenes with implications to the very long-chain limit, J. Chem. Phys. 103 (1995) 2509–2519. https://doi.org/10.1063/1.469672.

82. W. Wohlleben, T. Buckup, H. Hashimoto, R.J. Cogdell, J.L. Herek, M. Motzkus, Pump-deplete-probe spectroscopy and the puzzle of carotenoid dark states, J. Phys. Chem. B. 108 (2004) 3320–3325. https://doi.org/10.1021/jp036145k.

83. E.E. Ostroumov, G.M. Müller, M. Reus, A.R. Holzwarth, On the nature of the "dark S*" excited state of β-carotene, J. Phys. Chem. A. 115 (2011) 3698–3712. https://doi.org/10.1021/jp105385c.

84. A. Gilbert, J. Baggott, Essentials of molecular photochemistry, CRC Press, London, UK, 1991. https://doi.org/10.5860/choice.29-0309.

85. G.D. Scholes, Long-range resonance energy transfer in molecular systems, Annu. Rev. Phys. Chem. 54 (2003) 57–87. https://doi.org/10.1146/annurev.physchem.54.011002.103746.

86. B. Demmig-Adams, W.W. Adams, The role of xanthophyll cycle carotenoids in the protection of photosynthesis, Trends Plant Sci. 1 (1996) 21–26. https://doi.org/10.1016/S1360-1385(96)80019-7.

87. B. Demmig-Adams, Carotenoids and photoprotection in plants: A role for the xanthophyll zeaxanthin, BBA - Bioenerg. 1020 (1990) 1–24. https://doi.org/10.1016/0005-2728(90)90088-L.

88. A. Krieger-Liszkay, Singlet oxygen production in photosynthesis, J. Exp. Bot. 56 (2005) 337–346. https://doi.org/10.1093/jxb/erh237.

89. K.K. Niyogi, Photoprotection revisited: Genetic and molecular approaches, Annu. Rev. Plant Physiol. Plant Mol. Biol. 50 (1999) 333–359. https://doi.org/10.1146/annurev.arplant.50.1.333.

90. N.I. Krinsky, Carotenoid protection against oxidation, Pure Appl. Chem. 51 (1979) 649–660. https://doi.org/10.1351/pac197951030649.

91. H.A. Frank, R.J. Cogdell, Carotenoids in photosynthesis, Photochem. Photobiol. 63 (1996) 257–264. https://doi.org/10.1111/j.1751-1097.1996.tb03022.x.

92. A. Gall, R. Berera, M.T.A. Alexandre, A.A. Pascal, L. Bordes, M.M. Mendes-Pinto, S. Andrianambinintsoa, K. V. Stoitchkova, A. Marin, L. Valkunas, P. Horton, J.T.M. Kennis, R. Van Grondelle, A. Ruban, B. Robert, Molecular adaptation of photoprotection: Triplet states in light-harvesting proteins, Biophys. J. 101 (2011) 934–942. https://doi.org/10.1016/j.bpj.2011.05.057.

93. C.S. Foote, Y.C. Chang, R.W. Denny, Chemistry of singlet oxygen. XI. Cis–trans isomerization of carotenoids by singlet oxygen and a probable quenching mechanism, J. Am. Chem. Soc. 92 (1970) 5218–5219. https://doi.org/10.1021/ja00720a037.

94. F. Ramel, S. Birtic, S. Cuiné, C. Triantaphylidès, J.-L. Ravanat, M. Havaux, Chemical quenching of singlet oxygen by carotenoids in plants, Plant Physiol. 158 (2012) 1267–1278. https://doi.org/10.1104/pp.111.182394.

95. E. Pfündel, W. Bilger, Regulation and possible function of the violaxanthin cycle, Photosynth. Res. 42 (1994) 89–109. https://doi.org/10.1007/BF02187121.

96. M. Havaux, K.K. Niyogi, The violaxanthin cycle protects plants from photooxidative damage by more than one mechanism, Proc. Natl. Acad. Sci. U. S. A. 96 (1999) 8762–8767. https://doi.org/10.1073/pnas.96.15.8762.

97. R. Raniello, M. Lorenti, C. Brunet, M.C. Buia, Photoacclimation of the invasive alga *Caulerpa racemosa* var. *cylindracea* to depth and daylight patterns and a putative new role for siphonaxanthin, Mar. Ecol. 27 (2006) 20–30. https://doi.org/10.1111/j.1439-0485.2006.00080.x.

98. M. Olaizola, J. La Roche, Z. Kolber, P.G. Falkowski, Non-photochemical fluorescence quenching and the diadinoxanthin cycle in a marine diatom, Photosynth. Res. 41 (1994) 357–370. https://doi.org/10.1007/BF00019413.

99. M. Lohr, C. Wilhelm, Algae displaying the diadinoxanthin cycle also possess the violaxanthin cycle, Proc. Natl. Acad. Sci. U. S. A. 96 (1999) 8784–8789. https://doi.org/10.1073/pnas.96.15.8784.

100. F.G. Plumley, G.W. Schmidt, Reconstitution of chlorophyll a/b light-harvesting complexes: Xanthophyll-dependent assembly and energy transfer, Proc. Natl. Acad. Sci. 84 (1987) 146–150. https://doi.org/10.1073/pnas.84.1.146.

101. I.W. Ng, P.G. Adams, D.J. Mothersole, C. Vasilev, E.C. Martin, H.P. Lang, J.D. Tucker, C. Neil Hunter, Carotenoids are essential for normal levels of dimerisation of the RC-LH1-PufX core complex of *Rhodobacter sphaeroides*: Characterisation of R-26 as a crtB (phytoene synthase) mutant, Biochim. Biophys. Acta - Bioenerg. 1807 (2011) 1056–

1063. https://doi.org/10.1016/j.bbabio.2011.05.020.

102. T. Zakar, H. Laczko-Dobos, T.N. Toth, Z. Gombos, Carotenoids assist in cyanobacterial photosystem II assembly and function, Front. Plant Sci. 7 (2016) 1–7. https://doi.org/10.3389/fpls.2016.00295.

103. S. Santabarbara, A.P. Casazza, K. Ali, C.K. Economou, T. Wannathong, F. Zito, K.E. Redding, F. Rappaport, S. Purton, The requirement for carotenoids in the assembly and function of the photosynthetic complexes in *Chlamydomonas reinhardtii*, Plant Physiol. 161 (2013) 535–546. https://doi.org/10.1104/pp.112.205260.

104. T.N. Tóth, V. Chukhutsina, I. Domonkos, J. Knoppová, J. Komenda, M. Kis, Z. Lénárt, G. Garab, L. Kovács, Z. Gombos, H. Van Amerongen, Carotenoids are essential for the assembly of cyanobacterial photosynthetic complexes, Biochim. Biophys. Acta - Bioenerg. 1847 (2015) 1153–1165. https://doi.org/10.1016/j.bbabio.2015.05.020.

105. J.E.W. Polle, K.K. Niyogi, A. Melis, Absence of lutein, violaxanthin and neoxanthin affects the functional chlorophyll antenna size of photosystem-II but not that of photosystem-I in the green alga *Chlamydomonas reinhardtii*, Plant Cell Physiol. 42 (2001) 482–491. https://doi.org/10.1093/pcp/pce058.

106. J.T. Landrum, R.A. Bone, Lutein, zeaxanthin, and the macular pigment, Arch. Biochem. Biophys. 385 (2001) 28–40. https://doi.org/10.1006/abbi.2000.2171.

107. J.A. Mares, Carotenoids and eye disease: Epidemiological evidence, in: N.I. Krinsky, S.T. Mayne, H. Sies (Eds.), Carotenoids Heal. Dis., CRC Press, 2004: pp. 427–444.

108. H. Nishino, Cancer prevention by natural carotenoids, in: Antioxid. food suppl. hum. heal., 1999: pp. 231–238. https://doi.org/10.1016/b978-012543590-1/50016-0.

109. G. Van Poppel, R.A. Goldbohm, Epidemiologic evidence for β-carotene and cancer prevention, Am. J. Clin. Nutr. 62 (1995) 1393S-1402S. https://doi.org/10.1093/ajcn/62.6.1393s.

110. E. Giovannucci, Tomatoes, tomato-based products, lycopene, and cancer: Review of the epidemiologic literature, J. Natl. Cancer Inst. 91 (1999) 317–331. https://doi.org/10.1093/jnci/91.4.317.

111. G. Block, B. Patterson, A. Subar, Fruit, vegetables, and cancer prevention: A review of the epidemiological evidence, Nutr. Cancer. 18 (1992) 1–29. https://doi.org/10.1080/01635589209514201.

112. N.A. Moran, T. Jarvik, Lateral transfer of genes from fungi underlies carotenoid production in aphids, Science. 328 (2010) 624–627. https://doi.org/10.1126/science.1187113.

113. B. Altincicek, J.L. Kovacs, N.M. Gerardo, Horizontally transferred fungal carotenoid genes in the two-spotted spider mite *Tetranychus urticae*, Biol. Lett. 8 (2012) 253–257.

https://doi.org/10.1098/rsbl.2011.0704.

114. E. Nováková, N.A. Moran, Diversification of genes for carotenoid biosynthesis in aphids following an ancient transfer from a fungus, Mol. Biol. Evol. 29 (2012) 313–323. https://doi.org/10.1093/molbev/msr206.

2 EXPERIMENTAL METHODS AND DATA ANALYSIS

2.1 STEADY-STATE ABSORPTION SPECTROSCOPY

The interaction of light with matter wondered humans throughout history because this interaction enables us to see. In the 17th century, a great scientist Isaac Newton used the word *spectrum* for the first time in the description of the rainbow he obtained after white light passed through a prism. The instruments and the materials were improved and at the beginning of the 20th century, the method called steady-state absorption spectroscopy settled permanently in the laboratories.

In steady-state absorption spectroscopy, the white light goes continuously through the sample. This causes a repeated creation and elimination of excited states, leading to absorption of photons with certain energy (or wavelength) equal to the energy of excited states. When the concentration of both excited and nonexcited states remains constant, a steady-state is reached. After passing the sample, the white light is dispersed on prism or grating and continues to the detector, where the light intensity as a function of wavelength is recorded. The light intensity is typically measured with the sample $\left(I(\lambda)\right)$ but also without a sample or on a reference sample $\left(I_0(\lambda)\right)$. The final sample absorbance is given by

$$A = log\frac{I_0}{I} \tag{2.1}$$

where the inverted fraction (I/I_0) is called transmittance T. The important property of absorbance is its direct proportionality to the concentration c of the sample, which is expressed in the Beer-Lambert law

$$A = c\varepsilon(\lambda)l \tag{2.2}$$

where $\varepsilon(\lambda)$ is the molar extinction coefficient and l is the path length of the cuvette containing the measured sample. Steady-state absorption spectroscopy is typically used in two variants. The first one is called single beam measurement and as the name suggests, $I_0(\lambda)$ is measured by the same beam as $I(\lambda)$, and two separate measurements, with and without the sample, must be carried out. The

second technique measures both $I_0(\lambda)$ and $I(\lambda)$ simultaneously using separate pathways for the sample and reference beams.

The steady-state absorption spectroscopy is a powerful tool in revealing some of the crucial properties of carotenoids. After taking spectra, one notices usually the characteristic three-peak structure, which is caused by the transition from the ground state S_0 to the first three vibrational levels of the S_2 state. The resolution of the peaks is most clear for linear carotenoids, while addition of various end groups to the conjugation leads to loss of a fine structure (see Figure 1-2 for comparison of lycopene and β-carotene). Another information about the structure of carotenoid, based on the absorption spectra, is the presence of *cis*-isomers in a sample. The *cis*-isomers manifest themselves by introducing the so-called *cis*-peak in the ultraviolet region of the spectrum and by shifting the main peak by ~ 4 nm to shorter wavelengths.[1] Next, the conjugation length of carotenoid can be estimated since the addition of a double bond to conjugation moves the position of the main peak towards the red part of the spectra (Figure 1-2). A tremendous influence on the optical properties of carotenoids has an environment which surrounds them (in case of this thesis solvent or buffer). It affects the intensity of absorption and also the position of the main peak.[2] For example, the difference between the position of the main peak of β-carotene dissolved in hexane and carbon disulfide is 31 nm.[3]

What is the origin of cis-peak? *The cis-peak in the steady-state absorption spectrum is the consequence of the lowest state of A_g^+ symmetry. Since the ground state is of A_g^- symmetry, the transition to A_g^+ state is forbidden for the all-trans carotenoids, but it becomes allowed for the cis-isomers. For different cis-isomers of the same carotenoid, the intensity and position of the cis-peak and S_2 state vary,*[4] *so one can track which isomers are in a particular sample.*

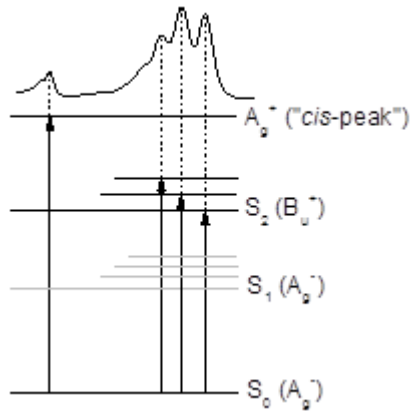

2.1.1 TRANSIENT ABSORPTION SPECTROSCOPY

The key subject of this thesis are carotenoids, their optical properties, and role during photosynthesis. If one wants to obtain information about processes taking place during photosynthesis (e.g. energy transfers, lifetimes, …), steady-state absorption spectroscopy is no longer a sufficient tool. Since the usual lifetimes in photosynthesis are on the time scale of nanoseconds, or even picoseconds, the time resolution of a used method has to be higher than this. In our case, this is achieved by employing a subpicosecond laser system in a method called transient absorption spectroscopy and its modifications.

Let us first consider the basic transient absorption spectroscopy (for the arrangement of setup in our laboratory see Figure 2-1). At the beginning there is the primary pulse generated by the Spitfire Ace regenerative amplifier system (Spectra Physics), producing ~ 4.2 mJ pulses at 800 nm at 1 kHz repetition rate by chirped pulse amplification of a mode-locked Ti:Saphire laser (MaiTai, Spectra Physics) pumped by a Nd:YLF pump laser (Empower, Spectra Physics). The important step of the method lies in splitting the primary pulse into two pulses, called pump and probe.

The pump pulse serves to excite the sample and to ensure population of only the spectral region of interest, it has to be spectrally narrow. For this purpose serves the optical parametric amplifier (OPA) (Topas, Light Conversion), in which the desired wavelength in the range between 240 and 2500 nm can be set. As the name suggests, the OPA also serves to amplify the pump beam via the parametric amplification. After leaving OPA the pump beam is led through a chopper working at 500 Hz, thus blocking every second pulse. This procedure enables an increase of the signal/noise ratio by introducing the correction to laser power fluctuations. Before reaching the sample, the polarization of the pump beam is changed so the angle between the polarization of pump and probe pulses is set to 54.7°. This is done by the Berek variable wave plate to prevent the occurrence of polarization and photoselection effects in the sample.[5] Then the pump pulse is focused to the sample and after it excites the sample it is eventually blocked.

The probe beam, still with the wavelength 800 nm, is first directed into the retroreflective mirror placed on a translation stage (delay line), which enables to

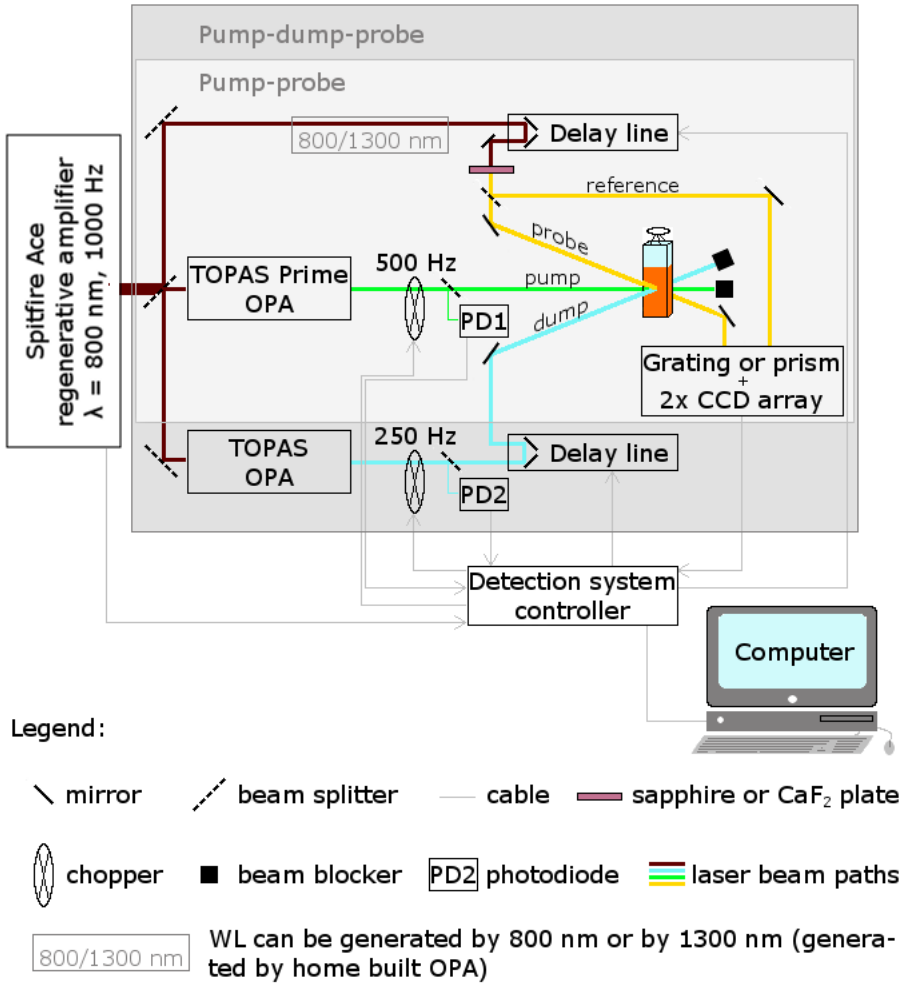

Figure 2-1: A simplified scheme of experimental setup. The area framed by light gray indicates pump-probe setup, while the darker gray area frames pump-dump-probe setup.

set the required delay between pump and probe pulses. Probe beam then continues to a sapphire or calcium fluoride plate, where the white light continuum (WLC) is generated. The WLC is then split into the so-called probe and reference beams. The probe beam is focused to the sample by a spherical mirror. The spot size of the probe beam on the sample should be smaller than the spot size of the pump beam to ensure all studied molecules are excited. The reference beam may or may not pass through the sample, depending on the experimentalist's choice.

Both probe and reference beams are detected using a double-diode array detection system (Pascher Instruments) with a 300-groove grating spectrometer. The final ΔA spectrum can be then calculated as

$$\Delta A(\Delta t, \lambda) = log\frac{I_{ref}}{I_{pp}} - log\frac{I_{ref}}{I_{np}} \tag{2.3}$$

where I_{ref} is the intensity of the reference beam, $I_{pp}$the intensity of the probe when the excitation beam is present, and I_{np} the intensity of the probe with no excitation.

From the description of the experimental setup, it is obvious that pump and probe beams should have specific properties to enable the best accomplishment of the experiment. The pump beam has to be spectrally as narrow as possible, so it is guaranteed the sample is excited to the desired state. At first sight, the best option would be the pulse with a spectral width of few nanometers. But here comes into play the quantum theory with its famous uncertainty principle that can be written in the form of $\Delta E \Delta t \geq \hbar/2$. For a Gaussian pulse, the equation changes to $\tau \Delta \upsilon \geq 0.441$, where τ represents the pulse duration and $\Delta \upsilon$ the consequent bandwidth. In other words, the narrower the spectral width of the pulse we choose, the longer the pulse must be (and thereby making it impossible to observe the ultrafast features) and *vice versa*. Thus, it is always necessary to compromise between time and spectral resolution. On the other hand, the probe beam should be spectrally broad to cover all the possible spectral features, which can appear after the excitation of the sample. There are usually three dominating processes, which can be observed: ground-state bleaching, stimulated emission, and excited-state absorption.

Ground-state bleaching arises because the pump pulse promotes a fraction of the molecules to the excited state and so there are fewer molecules in the ground state. It causes fewer photons are absorbed from the excited sample than from the reference sample and consequently, the ground state absorption in the excited sample is less than that in the non-excited sample. It follows that a negative signal is observed.

Stimulated emission is a mirror process of absorption. It is a result of the fact that in a two-level system the Einstein coefficients for absorption from the

ground to excited state (B_{12}) and stimulated emission from the excited to the ground state (B_{21}) are equal. The incoming photon from the probe pulse can trigger off the stimulated emission. This returns the molecule to the ground state. During this process, a photon in the same direction as the probe photon is produced, causing the stimulated emission. Both these photons are detected, so the detected intensity of the excited sample will be larger than the unexcited one, again leading to a negative signal. Stimulated emission is observed only for allowed transitions.

The third contribution is excited-state absorption. When molecules are in the excited state, there may exist optically allowed transitions from this excited state to higher excited states for photons in certain wavelength regions. More photons are consequently absorbed in this spectral region, resulting in a positive signal in the ΔA spectrum.

There are other possible processes affecting the final ΔA spectrum. One of them is for example a product absorption. Transient or long-lived molecular states (charge-separated states, isomer formation…) may occur after the excitation of a molecule. The absorption of this product decreases the intensity of excited state and it will appear as a positive signal in the ΔA spectrum.

A specific variant of ultrafast transient absorption spectroscopy, used in Paper 1, uses two-photon excitation to excite the sample. The two-photon excitation is based on the fact that the states forbidden for one-photon transition should be allowed for two-photon transition in molecules with a certain symmetry.[6] This approach to study the forbidden S_1 state of carotenoids can bring new information and it may help to solve for example the problem stated in Staleva et al. 2015[7], namely that approaching the S_1 state either from S_2 state or from S_0 state may result in the population of different minima at the S_1 potential surface. The core of this technique lies in the fact that instead of populating a state by one photon of energy E, two photons, each of energy E/2, are absorbed simultaneously in the two-photon process. Since from other methods we know approximately the energy of the S_1 state,[8–11] the photons used for two-photon excitation must be in the near-IR region in the wavelength range of 1100 – 1500 nm. Two-photon excitation is a non-linear process thus the power dependence of the signal is quadratic. This feature is often exploited to test whether the S_1 state is indeed excited via a two-photon process.[12–15]

The major advantage of the two-photon excitation is the reduction of the number of other processes because there is no relaxation from other excited states to the S_1 state when this state is directly excited. Thus, it will allow studying properties of the S_1 state without interfering signals from other states, which is a typical situation when the S_1 state is populated via relaxation from the S_2 state as it is done in the vast majority of experiments aiming to elucidate properties of the S_1 state.

However, with the advantages come disadvantages too. Leaving aside the problems with alignment that stems from the fact the pump is in the near-infrared region, other troubles arise. First, one has to prove a signal has an S_1 origin. To ensure this, we used several approaches. The first one already mentioned is the quadratic power dependence of the signal. We also checked the NIR part of the transient absorption spectrum to see whether we excite S_2 state or even create radicals. This procedure helped us a lot with tuning the excitation power we used in the experiments. To be sure, we do not have any fraction of visible light in the pump, we also tried to excite the dyes with strong absorption in the visible region. Since we did not excite these dyes, it proved there was no visible light in the pump beam.

Another multipulse transient absorption spectroscopy technique is called pump-dump-probe (PDP). It uses three beams, in order to excite the sample, manipulate the excited state population, and probe it. The dump beam is used here to depopulate the excited state prematurely and populate the state of interest by the laser pulse in resonance with the transition. This can help to observe states otherwise hidden in a standard pump-probe experiment. The experiment itself is very similar to pump-probe, only the dump beam is added. To ensure that a significant fraction of the excited molecules are dumped, the dump spot size at the sample should be always bigger than the pump spot size. The polarization of the dump pulse is usually set to be the same as the pump beam polarization, so it can affect as many pump-excited molecules as possible. The whole measurement of pump-dump-probe consists of four datasets; probe, pump-probe (PP), dump-probe (DP), and pump-dump-probe (PDP). This is achieved by choppers working at different frequencies, which is 500 Hz for the pump, and 250 Hz for the dump. Every 4 ms is thus recorded the whole set of data, containing probe, PP, DP, and PDP.

2.1.2 ANALYSIS OF TIME-RESOLVED SPECTRA

After collecting data in a pump-probe experiment one is facing a task of how to process the relatively large amount of data. Let us look first at the form of data; they are represented by a matrix in which the first row and the first column correspond to measured wavelengths (λ) and times(t), respectively. The rest of the matrix contains information about differential absorbance $\Delta A(t, \lambda)$ and can be written as

$$\mathbb{A} = \begin{pmatrix} \Delta A(t_0, \lambda_0) & \cdots & \Delta A(t_0, \lambda_n) \\ \vdots & \ddots & \vdots \\ \Delta A(t_n, \lambda_0) & \cdots & \Delta A(t_n, \lambda_n) \end{pmatrix} \tag{2.4}$$

and is showed as a 2D graph in Figure 2-2. In this 2D graph, one can see some of the typical features of transient absorption data of an antenna complex containing carotenoid and chlorophyll after carotenoid excitation. Some of them are connected to the time evolution of the sample after excitation (e.g. $S_1 \rightarrow S_n$ transition, chlorophyll bleaching), but some are unwanted features associated with the experiment, such as noise, chirp, or scattering, which have to be removed from the data prior to the fitting procedure. First, one has to subtract the background. This is achieved by subtracting the average of several spectra before the time zero. Next, the scattering caused by the pump beam must be removed. In the case of not excessive scattering of the pump light, it was already done with background subtraction. If the background subtraction is not enough, the best option is to remove the spectral region of the data, which contains it. The last part of preparing data for fitting is the chirp correction. Chirp arises because the group velocity dispersion of light in the optical components preceding the sample. In other words, the light of different wavelengths travels through optical elements with different velocity. Therefore, the pulse of the probe beam travels with the photons of longer wavelengths in front. This is why the signal appears first in the blue part of the spectra (one can imagine this as fast car (pump beam) overtaking the truck (probe beam) with the spectrum on its side, where the red part of the spectrum is closer the cabin of the truck and the blue part of the spectrum is towards the back of the truck). The effect is more pronounced in the blue/UV spectral region where the dependency of the refractive index of most of

the optical materials on the wavelength is stronger. The curve of time zero can

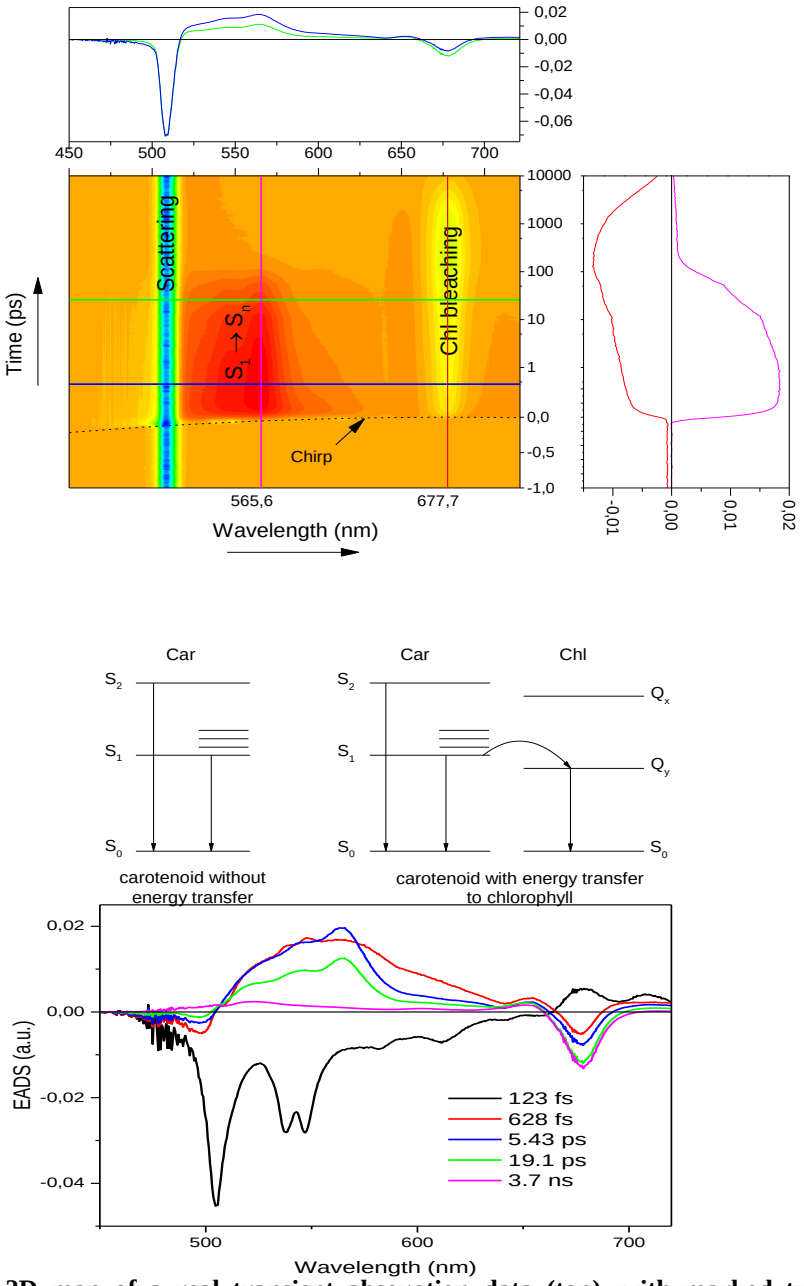

Figure 2-2: A 2D map of a real transient absorption data (top), with marked typical properties and kinetics and spectra above it and next to it. Kinetic scheme used for analyzing the data (middle). The result of fitting procedure (bottom).

be approximated by the polynomial (usually the order of the polynomial is less than 5) and corrected via this fit. The chirp is a problem only for the spectrally broad probe beam while the pump beam is not affected since it is spectrally narrow in our case. After the correction of data, we can proceed to actual fitting.

For a closer look at the obtained data, it is possible to plot only selected row of a data matrix to get a spectrum at a specific time (blue and green line in Figure 2-2) or to plot individual column to obtain the kinetic trace (red and magenta line in Figure 2-2). This allows us to see better information about some local trends (for example a single-wavelength decay analysis can be performed), yet it is not good enough to estimate the behavior of a complex system. The final goal is to obtain a simplified picture that represents the dataset. To achieve this, one needs to carry out a global fit,[16] in other words to expand the single-decay analysis to the whole dataset, by

$$\psi(t, \lambda_i) = \sum_{j=0}^{n} c_j(t)\epsilon_j(\lambda_i) \tag{2.5}$$

where $\epsilon_j(\lambda_i)$ and $c_j(t)$ are the extinction coefficient and concentration of absorbing species of component j, respectively. The later can be written as

$$c_j(t) = exp(-k_j t) = exp\left(-\frac{t}{\tau_j}\right) \tag{2.6}$$

k_j and τ_j being decay rate and lifetime, respectively.

At this moment, there comes an important user input in estimating the basic properties of the measured system, such as: how many states are involved, initial guess of the lifetimes of the individual states, scheme of the energy transfer, etc. Especially in the case of a new system, it is not easy to make all these decisions, but the knowledge of parts of the system (for example the lifetime of involved carotenoid in solution) and taking models of energy transfer from a simpler system typically help to solve the problem. The fitting model can have three basic forms, namely sequential, parallel, and compartmental (Figure 2-3).

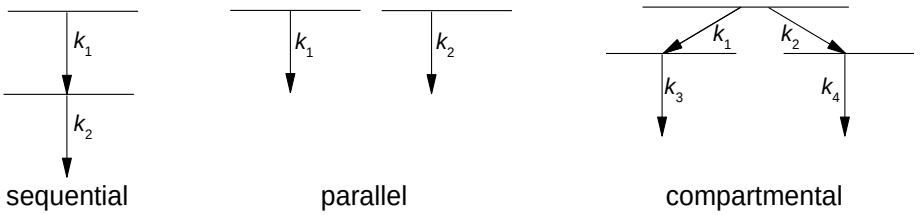

Figure 2-3: Possible kinetic schemes used for global (left and middle) and target (right) analysis.

In the sequential model, the population flows from the highest state to the lower states in an irreversible cascade way, which can be represented as

$$A \overset{\tau_1}{\rightarrow} B \overset{\tau_2}{\rightarrow} C \overset{\tau_3}{\rightarrow} D \ldots \tag{2.7}$$

Here the capital letters characterize the excited state species, while τ's represent lifetimes of the particular states. The fitting then produces so-called evolution-associated difference spectra (EADS).

The second possible model for data fitting is called parallel. It is used when there is an independent mono-exponential decay of each state and it results in decay associated difference spectra (DADS).

The last model, denoted as compartmental or target, is used to unravel and explain the systems, which are too complicated to be treated with the sequential or the parallel model. In an ideal case, it includes all possible states and all possible energy transfer channels, initially defined by the user. The result of fitting data by this approach is called species associated difference spectra (SADS)

Currently, there are many options for choosing software for data fitting. For the purpose of data fitting in the papers included in this thesis, the DAFit (Pascher Instruments), Glotaran (Vrije Universiteit Amsterdam), and CarpetView (Light Conversion), were used, together with some other scripts written by the author.

2.2.3 Z-SCAN

The knowledge of the two-photon cross-section is crucial for studying the excited states of carotenoids since the two-photon allowed S_0-S_1 transition. The z-scan technique can reveal the energy of the S_1 state and thus determine the excitation wavelength for two-photon experiments on carotenoids (Paper 1). The physical quantities describing a behavior of a material during the two-photon excitation are nonlinear refractive coefficient (n_2) and nonlinear absorption coefficient (β), from which the two-photon cross-section can be calculated.

Measuring of nonlinear refractive coefficient and nonlinear absorption coefficient can be done by various experiments, e.g. by nonlinear interferometry,[17,18] degenerate-four-wave mixing,[19] nearly degenerate three-wave mixing,[20] etc. These methods usually request a complex experimental apparatus, complicated analysis, or both mentioned. The z-scan technique, first introduced by Mansoor Sheik-Bahae and his colleagues in 1989,[21] significantly simplified this task. Although the z-scan technique combines setup simplicity (it is a single beam method in the most basic alternative) and quite easy data analysis (one can see the sign and approximately the magnitude of the nonhomogenity even without an analysis), it exhibits high precision and accuracy.[21,22]

An analysis of data obtained by the z-scan technique is based on studies investigating the propagation of intense laser beams inside nonlinear materials. The nonlinearities of any order can be considered, but only a cubic nonlinearity is discussed here. In this case, the index of refraction n and the absorption coefficient α are expressed as

$$n = n_0 + n_2 I \tag{2.8}$$

and

$$\alpha = \alpha_0 + \beta I \tag{2.9}$$

where n_0 is the linear index of refraction, α_0 is the linear absorption coefficient, and I is the irradiance of the laser beam within the sample.

2.2.3.1 Z-SCAN EXPERIMENTAL SETUP

There are two main arrangements of a z-scan setup – closed and open aperture. The closed aperture z-scan setup is shown in Figure 2-4 (top left). The incoming beam is split into reference and probe beams. The reference beam is directed to a photodiode (D1). This signal is used to reduce the noise caused by fluctuations of the laser and was first proposed by Ma et al. in 1991.[23] The second beam continues through a lens to the sample, which is placed on a translation stage and moved along the z-axis of a focused beam – thus the name z-scan. After passing the sample, the probe reaches the aperture where only part of the light is

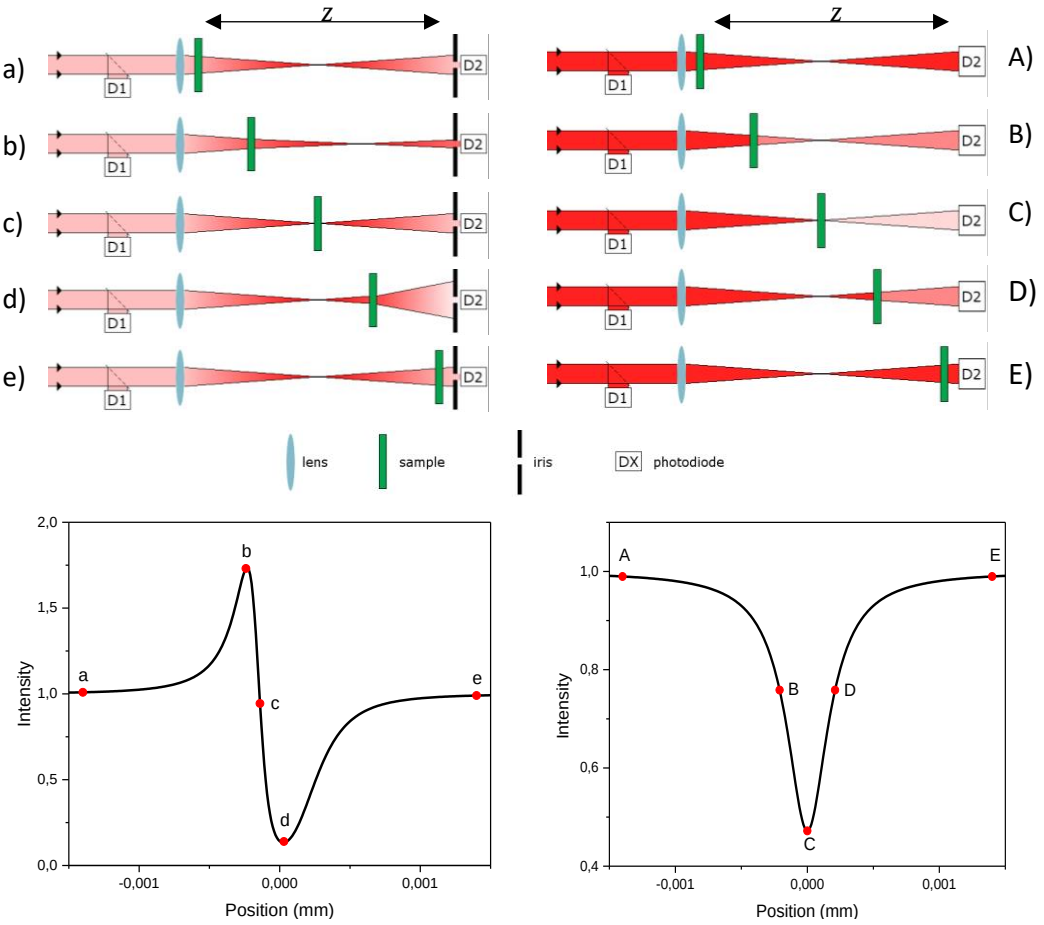

Figure 2-4: A scheme of z-scan closed (top left) and open (top right) aperture setup. Different positions of the sample are marked a) – e) and they corespond to the red marks on the bottom graphs, showing the typical curves for closed (left) and open (right) aperture measurement.

transmitted and measured by the photodiode D2. Dividing the intensities measured by the photodiodes D2 and D1 provides normalized energy transmitted through an aperture in the far-field as the function of the sample position (*z*).

The shape of the z-dependence can be described as follows (see Figure 2-4, left part, marked a-e): If a self-defocusing sample ($n_2 < 0$) is placed after the lens far from the focus, the intensity of light is too small and nonlinear refraction does not contribute to the signal. Moving the sample closer to the focus and thus increasing the intensity causes the sample to start to behave as a negative lens because of the nonlinear refraction. Prior to the focus, this negative lensing effect collimates the beam so more light passes through the aperture. This leads to the "peak" (Figure 2-4b) in the signal. The sample placed at the focus exhibits a minimal far-field pattern change and the signal is thus equal to approximately one. With a larger *z*, the negative lensing effect of the sample tends to strengthen diffraction and there is a "valley" (Figure 2-4d) in the graph as a result. The farther away from the sample, the less the irradiance is and the normalized transmittance returns to the original linear value. For the self-focusing sample ($n_2 > 0$) the positive lensing effect causes a lower transmittance when the sample is prior to the focus ("valley") and a higher transmittance for sample after the ("peak").

The setup of the open aperture is similar to the setup of the closed aperture, except there is no aperture in front of the photodiode D2 (Figure 2-4, right part). Since the whole beam passes to the detector, this setup loses sensitivity to nonlinear refraction, but it remains sensitive to the nonlinear absorption.

Despite the simplicity of the setup, one must be aware of mistakes made during the experiment, which can lead to incorrect conclusions.[24] The most common mistakes include the thermal lens effect,[22] using a thick sample, poor alignment of the aperture, high laser power, or a poor spatial profile of the beam.[24] Some of these imperfections can be later removed by using proper analysis.

Since the first application of closed and open z-scan apertures approximately thirty years ago, improvements of both the setups were published e.g. eclipsing,[25] two-color,[23,26] reflection,[27] or WLC z-scan.[28] In addition, the modified approaches and analyses were proposed for a case of not perfect Gaussian

beam.[29–31] I mention only the brief list of these improved methods because none of them was used during my experiments, yet I would consider the chapter incomplete without it.

2.2.3.2 ANALYSIS OF Z-SCAN DATA

First, it is convenient to introduce a few assumptions that will simplify further analysis. First, the beam is a TEM_{00} Gaussian beam which magnitude of the electric field can be written in a form of

$$|E(r,z,t)| = |E_0(t)|\frac{w_0}{w(z)}e^{-\frac{r^2}{w^2(z)}} \tag{2.10}$$

where $w(z)$ is the beam radius at z and can be expressed as $w(z) = w_0^2(1 + z^2/z_0^2)$, $z_0 = \frac{kw_0^2}{\lambda}$ is the Rayleigh length (diffraction length of the sample), with wave vector $k = 2\pi/\lambda$ and λ being the laser wavelength. E_0 expresses the amplitude of the electric field at the focus, w_0 denotes the waist radius, and r is radial distance from the center axis of the beam.

Second, we consider the sample "thin", introducing two rules: The sample length $L \ll z_0$, and $L \ll z_0/\Delta\varphi(0)$, for linear diffraction and for nonlinear refraction, respectively, $\Delta\varphi(0)$ being the phase change. In other words, the sample length is small enough so either diffraction or nonlinear refraction do not affect the beam diameter within the sample. The rules are often too strict and can be mitigated (for the first criterion it was showed that condition $L < z_0$ is sufficient,[32] and the second criterion is usually fulfilled since $\Delta\varphi(0)$ is small).

The quantity one can easily obtain from the normalized transmittance graph (Fig. 2-4a) is the difference between peak and valley, denoted as ΔT_{p-v}. For small phase distortion $|\Delta\varphi_0|$ and small apertures S, ΔT_{p-v} is almost linearly dependent on $|\Delta\varphi_0|$. This feature can be used for the first rough (but still quite accurate) estimation of n_2 via[21]

$$T_{p-v} \cong 0.406(1-S)^{0.27}|\Delta\varphi_0| \tag{2.11}$$

for $|\Delta\varphi_0| = kn_2IL_{eff} \leq \pi$, where I is the peak intensity, and the effective length of the sample can be expressed as $L_{eff} = [1 - e^{-\alpha_0 L}]/\alpha_0$.

For the open aperture, the quantity ΔT_{p-v} is defined as the difference between the maximum (since the transmittance is normalized, it is always 1) and the minimum of transmittance and it can be fit by

$$T_{p-v} \cong \left|1 - \frac{1}{Q_0} ln(1 + Q_0)\right| \tag{2.12}$$

where $Q_0 = \beta IL_{eff}$. Equation 2.12 is correct to all orders of I.[24]

The normalized z-scan transmittance of a closed aperture can be calculated as[32]

$$T(z) = \frac{\int_{-\infty}^{\infty} P_T\big(\Delta\varphi_0(t)\big)dt}{S\int_{-\infty}^{\infty} P_i(t)dt} \tag{2.13}$$

with power transmitted through aperture given by

$$P_T(\Delta\varphi_0(t)) = c\epsilon_0 n_0 \pi \int_0^{r_a} |E_a(r,t)|^2 r dr \tag{2.14}$$

and the instantaneous power

$$P_i(t) = \pi w_0^2 I(t)/2 \tag{2.15}$$

where ϵ_0 is the permittivity of vacuum, $E_a(r,t)$ is the electric field pattern, and $S = 1 - e^{-2r_a^2/w_a^2}$ is the aperture linear transmittance with r_a being aperture radius and w_a the beam radius at the aperture in the linear regime.

For a two-photon process, the open-aperture z-scan data can be fitted by[33]

$$T(z) = \frac{1}{\sqrt{\pi} q_0(z,0)} \int_{-\infty}^{\infty} ln\big[1 + q_0(z,0)e^{-\tau^2}\big]d\tau, \tag{2.16}$$

with $q_0 = \beta IL\big(1 + (z^2/z_0^2)\big)^{-1}$. By this fitting procedure, the nonlinear absorption coefficient β can be obtained and further used for determination of the two-photon cross-section, using[33,34]

$$\sigma_{2PA} = \frac{h\omega\beta}{2\pi N}, \tag{2.17}$$

usually quoted in the units of Goeppert-Mayer (GM), where 1 GM is 10^{-50} cm^4 s photon^{-1}. Measuring of σ_{2PA} at different wavelengths can help to reveal the energies and cross sections of dark states of carotenoids.

Despite the simplicity of the z-scan experimental setup, one always faces some difficulties. The problems related to the z-scan experiment can be divided into two main categories, namely those connected with sample preparation, and those associated with the beam quality.

During the preparation of a sample, which is in our case usually a carotenoid, the first problem arises when choosing a solvent. To populate directly the S_1 state by two-photon excitation the light with a wavelength between 1300 and 1500 nm is needed. But most of the typical solvents used for carotenoids absorb in this spectral region. The only possibility is to choose the small spectral windows where the solvent does not absorb or deal with the problem during the analysis. To the best of my knowledge, all the z-scan experiments, which studied carotenoids, were made in the spectral region outside NIR, thus not directly affecting the 0-0 transition of the S_1 state. After finding a proper solvent from the previous point of view, there comes a solubility requirement. The OD for the carotenoid z-scan experiment has to be high (the OD used in experiments reported earlier was around 20)[35]. The last problem associated with the sample is a cuvette that can give a false signal. Again, the false signal can be handled during analysis, or a closed-loop pump-driven wire-guided flow jet can be used instead of the cuvette.

The other issue that must be taken into account is the beam quality. The beam quality factor M^2 is usually used for quality assessment of the Gaussian beam. It represents the degree of variation of a beam from an ideal Gaussian beam. It is calculated as the ratio of the beam parameter product of the measured beam to a Gaussian beam with the same wavelength. This leads to a result that M^2 is exactly one for a single-mode TEM_{00} (Gaussian) laser beam. M^2 can be measured using e.g. a laser beam profiler or a knife-edge method.

In the knife-edge method the beam, focused by a lens, is progressively covered by a blade. The transmitted power is measured and the typical graph

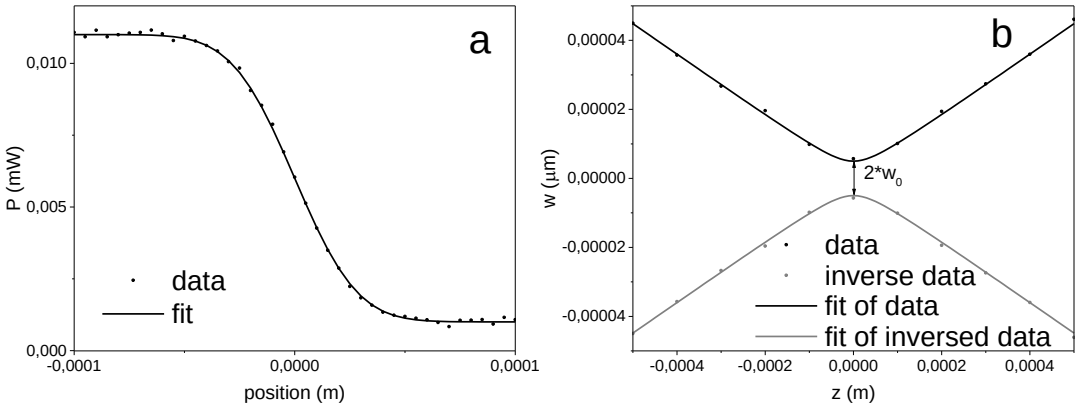

Figure 2-5: (a) The curve obtained by the knife-edge method measurement. (b) The radii of a Gaussian beam obtained by the knife-edge measurement at different possitions with the respect to the focus, showing the profile of the Gaussian beam.

based on this measurement is showed in Fig. 2-5a. The curve of power dependence on the position is defined by

$$P = P_0 + \frac{P_{max}}{2}\left(1 - erf\left[\frac{\sqrt{2}(x - x_0)}{w}\right]\right) \tag{2.18}$$

where P_0 is a background power, P_{max} is a maximal power, x_0 is a position of shift with the half of real power, and erf is a standard error function. The result of the fitting is a beam radius w. Figure 2-5b shows a graph of radii of a beam at different positions with the respect to the focus. The data can be fitted by a formula

$$w = w_0\left(1 + \frac{(z - z_1)^2(M^2\lambda)^2}{(w_0^2\pi)^2}\right) \tag{2.19}$$

where z_1 is a beam waist position, λ is the beam wavelength. After fitting, we get beam waist radius w_0 and beam quality parameter M^2.

The knife-edge measurement should be done in x and y direction to ensure the circularity of the Gaussian beam. For the z-scan measurement, the recommended value of a beam quality parameter is $M^2 < 1.1$.

The data measured on my own setup are shown in Figure 2-6. Even though we were able to measure the typical z-scan-shaped curves, we were not able to

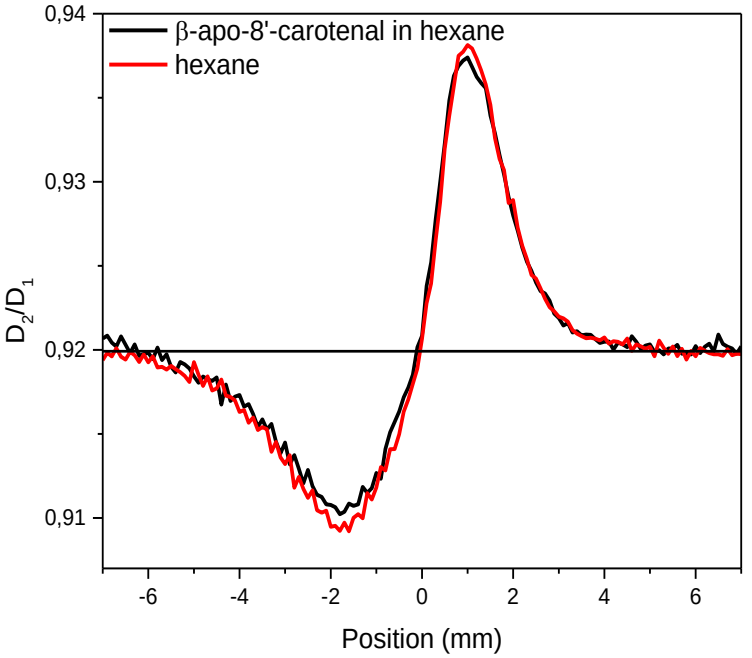

Figure 2-6: Examples of the closed-aperture z-scan traces measured for β-apo-8‘-carotenal in hexane and the solvent only at 800 nm.

get the valuable data for carotenoids. This was due to the fact that the data measured on the carotenoid solution were the same as the data measured on the solvent itself (the effect could be caused also by the cuvette). The beam quality, determined by the knife-edge method, has to be improved the in following experiments too. Nevertheless there is an promising outlook to perform the z-scan experiment in our lab and it is a great force to motivate us to solve the above mentioned problems and measure the two-photon cross-section for the NIR region.

REFERENCES

1. Z. Zhang, Y. Xiao, D. Li, C. Liu, Identification and quantification of all-trans-zeaxanthin and its cis-isomers during illumination in a model system, Int. J. Food Prop. 19 (2016) 1282–1291. https://doi.org/10.1080/10942912.2015.1072209.
2. P.O. Andersson, T. Gillbro, L. Ferguson, R.J. Cogdell, Absorption spectral shifts of carotenoids related to medium polarizability, Photochem. Photobiol. 54 (1991) 353–360. https://doi.org/10.1111/j.1751-1097.1991.tb02027.x.
3. T.W. Goodwin, The Biochemistry of the carotenoids - Volume I, Plants, Springer, Dordrecht, 1980. https://doi.org/10.1007/978-94-009-5860-9.
4. T. Polívka, V. Sundström, Ultrafast dynamics of carotenoid excited states-from solution to natural and artificial systems, Chem. Rev. 104 (2004) 2021–2071. https://doi.org/10.1021/cr020674n.
5. J.R. Lakowicz, Principles of fluorescence spectroscopy, 3rd edition, Springer, Berlin, Germany, 2006. https://doi.org/10.1117/1.2904580.
6. P. Tavan, K. Schulten, Electronic excitations in finite and infinite polyenes, Phys. Rev. B. 36 (1987) 4337–4358. https://doi.org/10.1103/PhysRevB.36.4337.
7. H. Staleva, J. Komenda, M.K. Shukla, V. Šlouf, R. Kaňa, T. Polívka, R. Sobotka, Mechanism of photoprotection in the cyanobacterial ancestor of plant antenna proteins, Nat. Chem. Biol. 11 (2015) 287–291. https://doi.org/10.1038/nchembio.1755.
8. T. Sashima, Y. Koyama, T. Yamada, H. Hashimoto, The $1B_u^+$, $1B_u^-$, and $2A_g$ energies of crystalline lycopene, β-carotene, and mini-9-β-carotene as determined by resonance-Raman excitation profiles: Dependence of the $1B_u^-$ state energy on the conjugation length, J. Phys. Chem. B. 104 (2000) 5011–5019. https://doi.org/10.1021/jp994185b.
9. K. Furuichi, T. Sashima, Y. Koyama, The first detection of the $3A_g^-$ state in carotenoids using resonance-Raman excitation profiles, Chem. Phys. Lett. 356 (2002) 547–555. https://doi.org/10.1016/S0009-2614(02)00412-8.
10. R. Fujii, T. Ishikawa, Y. Koyama, M. Taguchi, Y. Isobe, H. Nagae, Y. Watanabe, Fluorescence spectroscopy of all-trans-anhydrorhodovibrin and spirilloxanthin: Detection of the $1B_u^-$ fluorescence, J. Phys. Chem. A. 105 (2001) 5348–5355. https://doi.org/10.1021/jp010150b.
11. T. Sashima, H. Nagae, M. Kuki, Y. Koyama, A new singlet-excited state of all-trans-spheroidene as detected by resonance-Raman excitation profiles, Chem. Phys. Lett. 299 (1999) 187–194. https://doi.org/10.1016/S0009-2614(98)01278-0.
12. P.J. Walla, J. Yom, B.P. Krueger, G.R. Fleming, Two-photon excitation spectrum of light-harvesting complex II and fluorescence upconversion after one- and two-photon

excitation of the carotenoids, J. Phys. Chem. B. 104 (2000) 4799–4806. https://doi.org/10.1021/jp9943023.

13. P.J. Walla, P.A. Linden, C.P. Hsu, G.D. Scholes, G.R. Fleming, Femtosecond dynamics of the forbidden carotenoid S_1 state in light-harvesting complexes of purple bacteria observed after two-photon excitation, Proc. Natl. Acad. Sci. U. S. A. 97 (2000) 10808–10813. https://doi.org/10.1073/pnas.190230097.

14. P.A. Linden, J. Zimmermann, T. Brixner, N.E. Holt, H.M. Vaswani, R.G. Hiller, G.R. Fleming, Transient absorption study of peridinin and peridinin-chlorophyll a-protein after two-photon excitation, J. Phys. Chem. B. 108 (2004) 10340–10345. https://doi.org/10.1021/jp031331b.

15. A. Betke, H. Lokstein, Two-photon excitation spectroscopy of photosynthetic light-harvesting complexes and pigments, Faraday Discuss. 216 (2019) 494–506. https://doi.org/10.1039/c8fd00198g.

16. I.H.M. Van Stokkum, D.S. Larsen, R. Van Grondelle, Global and target analysis of time-resolved spectra, Biochim. Biophys. Acta - Bioenerg. 1657 (2004) 82–104. https://doi.org/10.1016/j.bbabio.2004.04.011.

17. M.J. Weber, D. Milam, W.L. Smith, Nonlinear refractive index of glasses and crystals, Opt. Eng. 17 (1978) 463–469. https://doi.org/10.1117/12.7972266.

18. M.J. Moran, C.Y. She, R.L. Carman, Interferometric measurements of the nonlinear refractive-index coefficient relative to CS_2 in laser-system-related materials, IEEE J. Quantum Electron. 11 (1975) 259–263. https://doi.org/10.1109/JQE.1975.1068611.

19. S.R. Friberg, P.W. Smith, Nonlinear optical glasses for ultrafast optical switches, IEEE J. Quantum Electron. 23 (1987) 2089–2094. https://doi.org/10.1109/JQE.1987.1073278.

20. R. Adair, L.L. Chase, S.A. Payne, Nonlinear refractive-index measurements of glasses using three-wave frequency mixing, in: 1987: pp. 875–881. https://doi.org/10.1364/JOSAB.4.000875.

21. M. Sheik-bahae, A.A. Said, E.W. Van Stryland, High-sensitivity, single-beam n_2 measurements, Opt. Lett. 14 (1989) 955–957. https://doi.org/10.1364/ol.14.000955.

22. R. de Nalda, R. del Coso, J. Requejo-Isidro, J. Olivares, A. Suarez-Garcia, J. Solis, C.N. Afonso, Limits to the determination of the nonlinear refractive index by the Z-scan method, J. Opt. Soc. Am. B. 19 (2002) 289–296. https://doi.org/10.1364/josab.19.000289.

23. H. Ma, A.S.L. Gomes, C.B. De Araujo, Measurements of nondegenerate optical nonlinearity using a two-color single beam method, Appl. Phys. Lett. 59 (1991) 2666–2668. https://doi.org/10.1063/1.105933.

24. P.B. Chapple, J. Staromlynska, J.A. Hermann, T.J. Mckay, R.G. Mcduff, Single-beam Z-scan: Measurement techniques and analysis, J. Nonlinear Opt. Phys. Mater. 6 (1997) 251–293. https://doi.org/10.1142/S0218863597000204.

25. T. Xia, D.J. Hagan, M. Sheik-Bahae, E.W. Van Stryland, Eclipsing Z-scan measurement of $\lambda/10^4$ wave-front distortion, Opt. Lett. 19 (1994) 317–319. https://doi.org/10.1364/ol.19.000317.

26. H. Ma, C.B. de Araújo, Two-color Z -scan technique with enhanced sensitivity , Appl. Phys. Lett. 66 (1995) 1581–1583. https://doi.org/10.1063/1.113858.

27. D. V. Petrov, A.S.L. Gomes, C.B. De Araújo, Reflection Z-scan technique for measurements of optical properties of surfaces, Appl. Phys. Lett. 65 (1994) 1067–1069. https://doi.org/10.1063/1.112175.

28. L. De Boni, A.A. Andrade, L. Misoguti, C.R. Mendonca, S.C. Zilio, Z-scan measurements using femtosecond continuum generation, Opt. Express. 12 (2004) 3921–3927. https://doi.org/10.1364/opex.12.003921.

29. S.M. Mian, B. Taheri, J.P. Wicksted, Effects of beam ellipticity on Z-scan measurements, J. Opt. Soc. Am. B. 13 (1996) 856–863. https://doi.org/10.1364/josab.13.000856.

30. Y.-L. Huang, C.-K. Sun, Z-scan measurement with an astigmatic Gaussian beam, J. Opt. Soc. Am. B. 17 (2000) 43–47. https://doi.org/10.1364/josab.17.000043.

31. G. Tsigaridas, I. Polyzos, P. Persephonis, V. Giannetas, A novel approach for analyzing open Z-scan experiments, Opt. Commun. 266 (2006) 284–289. https://doi.org/10.1016/j.optcom.2006.04.015.

32. M. Sheik-Bahae, A.A. Said, T.H. Wei, D.J. Hagan, E.W. Van Stryland, Sensitive measurement of optical nonlinearities using a single beam, IEEE J. Quantum Electron. 26 (1990) 760–769. https://doi.org/10.1109/3.53394.

33. M.G. Vivas, D.L. Silva, L. Misoguti, R. Zaleśny, W. Bartkowiak, C.R. Mendonca, Degenerate two-photon absorption in all-trans retinal: Nonlinear spectrum and theoretical calculations, J. Phys. Chem. A. 114 (2010) 3466–3470. https://doi.org/10.1021/jp910010g.

34. M.G. Vivas, C.R. Mendonca, Temperature effect on the two-photon absorption spectrum of all-trans-β-carotene, J. Phys. Chem. A. 116 (2012) 7033–7038. https://doi.org/10.1021/jp303789s.

35. A. Major, F. Yoshino, J.S. Aitchison, P.W.E. Smith, D. Zigmantas, V. Barzda, Picosecond z-scan measurements of the two-photon absorption in beta-carotene solution over the 590-790 nm wavelength range, Org. Photonic Mater. Devices VII. 5724 (2005) 269–276. https://doi.org/10.1117/12.590669.

RESEARCH SECTION

3 Time-resolved two-photon spectroscopy of carotenoids

This chapter is based on Paper I:

V. Šebelík, M. Fuciman, R. G. West, T. Polívka Time-resolved two-photon spectroscopy of carotenoids. Chem. Phys., 522 (2019), pp. 171–177, https://doi.org/10.1016/j.chemphys.2019.02.023

Abstract

We have developed an experimental set-up allowing to measure transient absorption spectra of carotenoids after two-photon excitation (2PE), thereby exciting the lowest excited state S_1 directly. We have compared 2PE and 1PE data of three carotenoids, lycopene, β-carotene, and neurosporene. Compared to 'standard' 1PE, the transient absorption spectra of all three carotenoids are broader after 2PE, suggesting larger conformational disorder induced by direct excitation of the S_1 state. Also, 2PE generates slightly longer S_1 lifetimes compared to 1PE, which is most likely due to increased magnitude of the S* signal after 2PE. The difference in the S* signal magnitude is explained by a different subsets of conformers excited by 1PE and 2PE.

3.1 INTRODUCTION

Carotenoids are natural pigments whose rich photophysics has initiated a number of experimental and theoretical studies of their excited states. Detailed knowledge of carotenoids excited-state dynamics is a prerequisite for understanding their important dual role in photosynthesis. In photosynthetic pigment-protein complexes, they can either serve as light-harvesting pigments transferring the absorbed energy to chlorophylls (Chl)[1-4] or, under the condition of excess light, they can dissipate the excess energy in the form of heat to prevent the damage of the photosynthetic apparatus.[3,5,6]

Excited states of carotenoids can be in the first approximation described by a three-level scheme, consisting of S_0, S_1 and S_2 states representing the ground state, the first excited state and the second excited state, respectively. Since the key discovery nearly 50 years ago,[7] it is known that the one-photon allowed HOMO-LUMO transition is associated with the S_0-S_2 transition, while the S_0-S_1 transition is one-photon forbidden. After population of the S_2 state, excited carotenoid undergoes fast relaxation to the S_1 state in 50 – 300 fs.[8] The S_1 state is, therefore, of crucial importance for understanding the excited-state processes in carotenoids, both in solution and in photosynthetic systems.

The properties of the carotenoid S_1 state has been studied intensively by various ultrafast spectroscopy techniques, providing information about both the S_1 state energy,[9-14] and lifetimes[15,16] and their relation to the structure of a particular carotenoid.[8,17,18] Yet, because of the forbidden nature of the $S_0 - S_1$ transition, the properties of the S_1 state are typically studied after population of the S_1 state from the S_2 state. In this approach, the S_1 state is always prepared as a hot state that cools down on the sub-picosecond time scale.[19,20] Further, other forbidden excited states, such as the B_u^- state, often referred to as an intermediate state in the S_2-S_1 relaxation process,[21] and intramolecular charge transfer (ICT) state, characteristic of keto-carotenoids,[22-24] can be populated during the relaxation from the S_2 state. This vastly complicates identification of the excited-state related solely to the S_1 state as the signals originating from different states often overlap.[23-25] Moreover, recent study of quenching processes in certain photosynthetic proteins suggested that relaxation from the S_2 state may result in

population of a different part of the S_1 potential surface than direct transition from the ground state.[5]

Another heavily discussed excited state is the S* state associated with a transient signal manifested as a blue shoulder of the main S_1-S_n peak in the transient absorption spectrum, and whose origin is still a subject of discussion.[26-28] The S* signal was first reported for long β-carotene analogs and assigned to a hot ground state;[29] later, however, it was assigned to a separate excited state.[30] The origin of the S* signal is still a matter of a considerable debate,[27,31] yet the latest results and models points to its origin in the hot ground state,[30,32] though in carotenoids with N<11 a contribution from a transition involving vibrational levels of the S_1 state is also expected.[31,33]

Thus, it is of interest to carry out experiments exciting the S_1 state directly, bypassing the relaxation processes potentially induced by the S_2-S_1 internal conversion. Due to the doubly-excited nature of the S_1 state,[21] the S_1-S_0 transition is allowed for two-photon processes. The pioneering two-photon excitation (2PE) experiment on carotenoids was conducted by Shreve et al.[34] on the diatom *Phaeodactylum tricornutum*, in which they monitored Chl emission after two-photon excitation of carotenoids. Further experiments detecting Chl fluorescence using 2PE were later carried out for carotenoids in other light-harvesting systems such as LH2,[35] LHCII,[36-38] or PCP.[9,39] These experiments identified the range of possible S_1 energies of carotenoids in light harvesting proteins as well as the carotenoid-(B)Chl energy transfer rate via the S_1 route by monitoring the up-converted (B)Chl emission in ultrafast fluorescence up-conversion experiments.

Ultrafast transient absorption experiments (pump-probe) with 2PE of carotenoids have also been reported. Buckup et al.[40] and Kosumi et al.[41] reported a 2PE transient absorption experiment on β-carotene in cyclohexane. In both these experiments, the S_1 state was excited with excess energy (2PE into higher vibrational levels of the S_1 state) and both studies addressed the vibrational relaxation in the S_1 state. Further, both studies identified long-lived signals associated with either carotenoid triplets or radicals that were likely generated by multi-photon processes exciting directly higher excited states. Besides β-carotene, 2PE experiment was also carried out for the keto-carotenoids fucoxanthin[42] and peridinin.[39] For fucoxanthin, Kosumi et al.[42] reported that 2PE

has ability to selectively excite either the S_1 or intramolecular charge transfer state of fucoxanthin.[42]

Earlier transient absorption studies on carotenoids in solution using 2PE mostly used excitation wavelengths in 1000-1300 nm range, thereby exciting the S_1 state with an excess energy. Here we use wavelengths corresponding to photon energies exciting either at or slightly below the expected energy of the 0-0 band of the S_0-S_1 transition. We compare ultrafast transient absorption data obtained after 1PE (via the S_2 state) and 2PE (S_1 state directly) of three typical carotenoids: β-carotene, lycopene, and neurosporene in *n*-hexane. We show that the spectroscopic properties of the S_1 state differ after 1PE and 2PE; the main difference is related to the magnitude of the S* signal that is enhanced after 2PE.

3.2 EXPERIMENTAL DETAILS

For generating excitation (pump) and probe pulses, Spitfire Ace regenerative amplifier system (Spectra Physics), seeded with Ti:sapphire oscillator (MaiTai SP, Spectra Physics) and pumped by Nd:YLF laser (Empower 30, Spectra Physics), was used. The Spitfire Ace produces 4 mJ pulses centered at 800 nm with a 1 kHz repetition rate and the pulse duration ~ 100 fs. The excitation wavelengths of 1400 nm and 1500 nm (for 2PE experiment), and 475, 480, and 510 nm (for 1PE experiment) were achieved through parametric amplification (Topas Prime, Light Conversion). In 2PE experiment, the pump beam was focused before the sample by a lens with focal length of 150 mm and its pump power was set between 5 and 8 mW, resulting in intensity of about 10^{17} photons/pulse cm^2. In the 1PE experiment, a 1000 mm focal length was used to focus the pump beam and the excitation intensity of pump pulses was ~ 2×10^{14} photons/pulse cm^2. The white light supercontinuum (WLC) was generated in a 2-mm CaF_2 plate by focusing a fraction of 800 nm beam from Spitfire Ace. The polarization between pump and probe beams was set parallel by Berek compensator. In order to minimize a noise the WLC was split to a reference and probe beam. The probe beam was focused to a sample with the spot size of approximately same size as the pump beam spot. Probe and reference beams were focused to the entrance slit of a spectrograph and dispersed onto a double CCD array. The solvent response was measured separately and subtracted from the

data. Measurements of lycopene with different intensities of pump beam showed power squared dependence, which confirms two-photon excitation. The obtained data were fitted using Glotaran global fitting analysis software (VU Amsterdam) under a sequential exponential decay scheme resulting in evolution-associated difference spectra (EADS) that correspond to the spectra of each spectral component in the sequential scheme.

β-carotene was purchased from Sigma-Aldrich (≥95 %, HPLC), lycopene (95 %, HPLC), and neurosporene (95 %, HPLC) were purchased from CaroteNature GmbH. All the samples were stored at -40°C in dark. The sample was dissolved in *n*-hexane to OD ~1.5/mm and maintained at room temperature during transient absorption measurements within a 2-mm quartz cuvette. The steady state absorption spectra were made before and after measurements to check for photodegradation.

3.3 RESULTS

Absorption spectra of the three studied carotenoids, lycopene, β-carotene, and neurosporene dissolved in *n*-hexane are shown in Fig. 3-1. They exhibit the characteristic vibrational structure of the S_0-S_2 transition, with the lowest energy peaks at 503, 478, and 470 nm for lycopene, β-carotene, and neurosporene. The vibrational bands of β-carotene are less resolved than those of lycopene and neurosporene due to extension of conjugation to the terminal rings of β-carotene that is known to increase the conformational disorder leading to a larger distribution of energies.[43] Even though the extension of conjugation to the terminal rings as well as the overall carotenoid structure, which in minimal energy takes a sigmoidal shape, breaks the ideal C_{2h} symmetry,[44] no signs of the S_0-S_1 transition are found in absorption spectrum. Based on earlier data relying on either a weak S_1 emission or measuring the energy of the S_1-S_2 transition,[12-14,45,46] the position of the 0-0 band of the S_0-S_1 transition of these three carotenoids should be in the spectral range 630-850 nm as also depicted in Fig. 3-1.

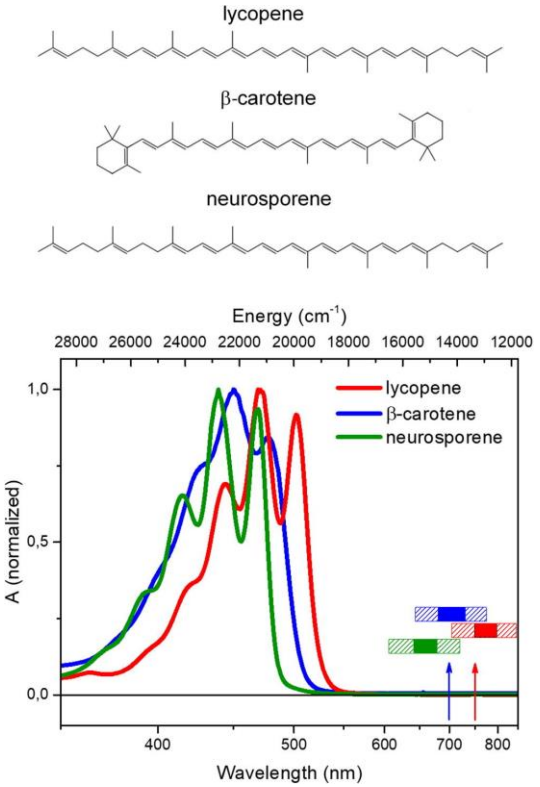

Figure 3-1: Molecular structures (top) and absorption spectra of lycopene, β-carotene, and neurosporene in *n*-hexane. Color boxes show assumed energies of S_1 states of these carotenoids. Solid boxes represents the range of 0-0 energies obtained from various experiments,[8] the extended area represents expected range of the absorption of the 0-0 band of the S_0-S_1 transition. Arrows represent two-photon energies used to excite neurosporene (blue) or lycopene and β-carotene (red) in the 2PE experiment.

Transient absorption spectra measured after exciting lycopene and β-carotene at 1500 nm and neurosporene at 1400 nm are shown in Fig. 3-2. Since there is no linear absorption in the spectral region of

excitation, and since the photon energies corresponding to these excitation wavelengths correspond to about half of the expected energy of the 0-0 band of the S_0-S_1 transition (Fig. 3-1), the data in Fig. 3-2 represent transient absorption spectra after two-photon excitation of the carotenoids. Further evidence is provided by the approximately quadratic dependence of the signal intensity on excitation intensity (Supporting Information, Fig. 3-S1). Based on the expected energies of the S_1 state (Fig. 3-1), the wavelengths selected for two-photon excitation hit the low-energy part of the 0-0 band of the S_0-S_1 transition of β-carotene and neurosporene, while lycopene should be excited slightly above the maximum of the 0-0 band. This differs from the earlier report on two-photon excitation of β-carotene,[41] where the authors used two-photon excitation wavelengths of about 1100 and 1300 nm, roughly corresponding to excitation of the 0-2 and 0-1 vibrational bands of the S_0-S_1 transition.[41]

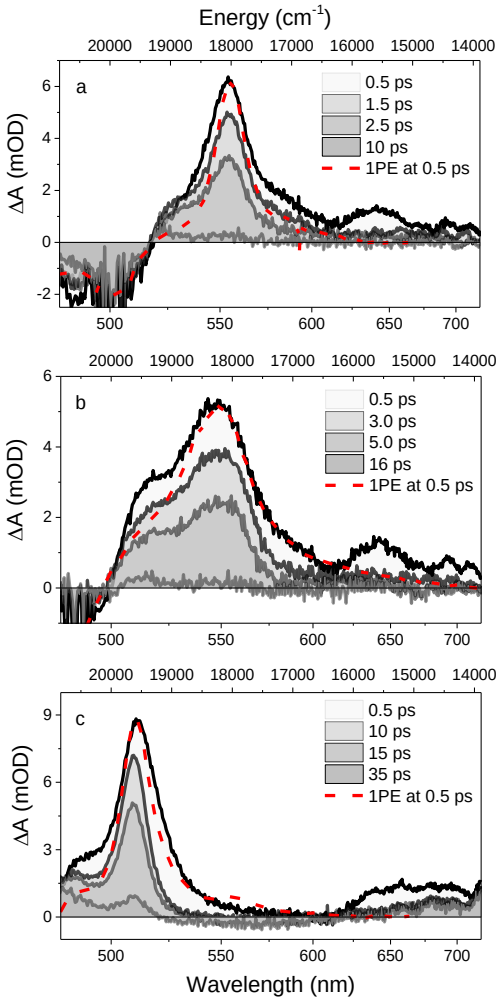

Figure 3-2: Transient absorption data after 2PE of lycopene (a), β-carotene (b), and neurosporene (c) at various delay times after excitation. Red dashed lines show transient absorption spectra at 0.5 ps after 1PE; in the 1PE experiment lycopene, β-carotene, and neurosporene were excited at 510 nm 480 nm, and 475 nm, respectively.

The overall shape of the 2PE transient absorption spectra is comparable to the S_1-S_n spectra obtained after 1PE of the S_2 state. The spectra are dominated by the strong S_1-S_n band peaking at 555 nm (lycopene), 550 nm

(β-carotene), and 512 nm (neurosporene), matching the S_1-S_n maxima obtained after 1PE, and proving that the S_1 state is populated via 2PE. However, the transient absorption spectra obtained after 1PE and 2PE also reveal differences that must be related to the different way of preparing the S_1 state in the 1PE and 2PE experiments.

Comparison of 1PE and 2PE transient absorption spectra measured at 0.5 ps (Fig. 3-2) shows that the 2PE produces spectra that are slightly broader than those obtained after one-photon excitation, possibly indicating larger conformational disorder in the S_1 state after 2PE. The main systematic difference is, however, the increased intensity on the blue part of the main S_1-S_n band. In all studied carotenoids there is a shoulder around 530 nm (lycopene), 520 nm (β-carotene), and 490 nm (neurosporene), which is known as the S* signal.[47] The S* signal is more pronounced in the 2PE experiment and this is valid for all three studied carotenoids. In the 1PE experiment on lycopene the S* signal is nearly absent, while the 2PE experiment generates a distinct band associated with the S* signal.

Besides the increased S* magnitude after two-photon excitation, another extra signal missing in a standard one-photon experiment occurs in the 600-700 nm spectral region. A clear spectral band in the 0.5 ps spectrum has obviously a different dynamics than the S_1 state as it is present solely within the first picosecond after excitation (see also the fitting results below). The only signals that were for carotenoids reported in this spectral region are either due to a transition from higher vibrational levels of the S_1 state[48] or due to an intramolecular charge transfer (ICT) state.[23] However, our choice of excitation wavelengths in 2PE experiment prevents population of higher vibrational levels of the S_1 state and the ICT state is observed exclusively in keto-carotenoids with conjugated C=O group. Thus, the origin of the 600-700 nm band in the 0.5 ps spectrum remains unknown. A possibility could be that we excite the elusive $1B_u^-$ state[11,47] via three-photon excitation, because the S_0-$1B_u^-$ transition is both one- and two-photon forbidden.[21] Then, the 600-700 nm band would be due to a transition from the $1B_u^-$ state decaying with 1-2 ps lifetime. This would mean that the $1B_u^-$ state is not populated during the S_2-S_1 relaxation as no such signals were ever observed in numerous 1PE experiments on various carotenoids. Further experiments are however needed to test this hypothesis.

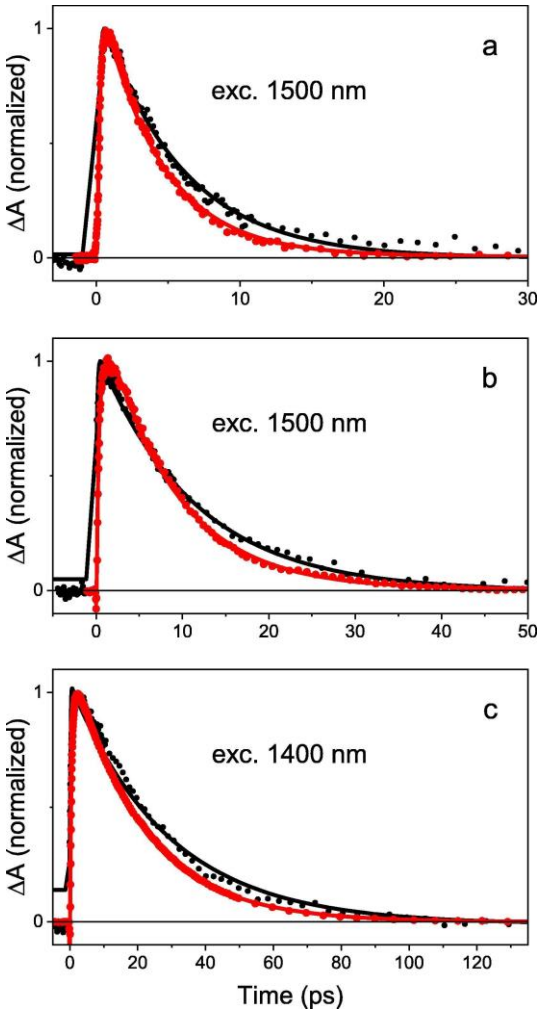

Figure 3-3: Normalized kinetics measured after 2PE at the maximum of the S_1-S_n transition (black) of lycopene (a), β-carotene (b), and neurosporene (c) compared with the 1PE kinetics (red). Solid lines represent the result of global fitting.

The differences between the 1PE and 2PE are further demonstrated in kinetics shown in Fig. 3-3. Due to strong coherent artifact around time zero originating from interaction of the intense near-IR pulses with solvent, the solvent contribution has been subtracted as shown in Supporting Information, Fig. 3-S2. The kinetics in Fig. 3-3 are measured at wavelengths corresponding to the maxima of the S_1-S_n band and for all three carotenoids, the decay of the S_1-S_n signal after the two-photon excitation is slightly slower than after one-photon excitation. This is further confirmed by global analysis of the spectro-temporal datasets obtained after two-photon excitation shown in Fig. 3-4. Since we excite the S_1 state directly, having discarded the very early dynamics due to coherent artifacts, already the first EADS is related to the S_1 state. However, it has a shape reminiscent of that typically assigned to a hot S1 state,[15] indicating that even direct S_1 excitation via 2PE process generates non-equilibrated S_1 state that relaxes on the time scale of 1-2 ps. This relaxation process is clearly identified by the change of spectral shape of the first (black) and second (red) EADS in Fig. 3-4. We note that our excitation wavelengths do not allow for excitation of higher vibrational states of the C-C or C=C stretching modes so this relaxation must be

related to relaxation of the low (<1000 cm^{-1}) frequency modes. The second EADS then corresponds to the relaxed S_1 state, which has a lifetime of 5.6, 11 and 29 ps for lycopene, β-carotene and neurosporene, respectively. These lifetimes are slightly longer than those obtained from 1PE experiments as also visually demonstrated by comparing the 1PE and 2PE kinetics in Fig. 3-3. Final EADS having lifetime longer than 1 ns has a shape characteristic of a triplet state, demonstrating we generate some fraction of the triplet state via 2PE in agreement with earlier observations.[41,49]

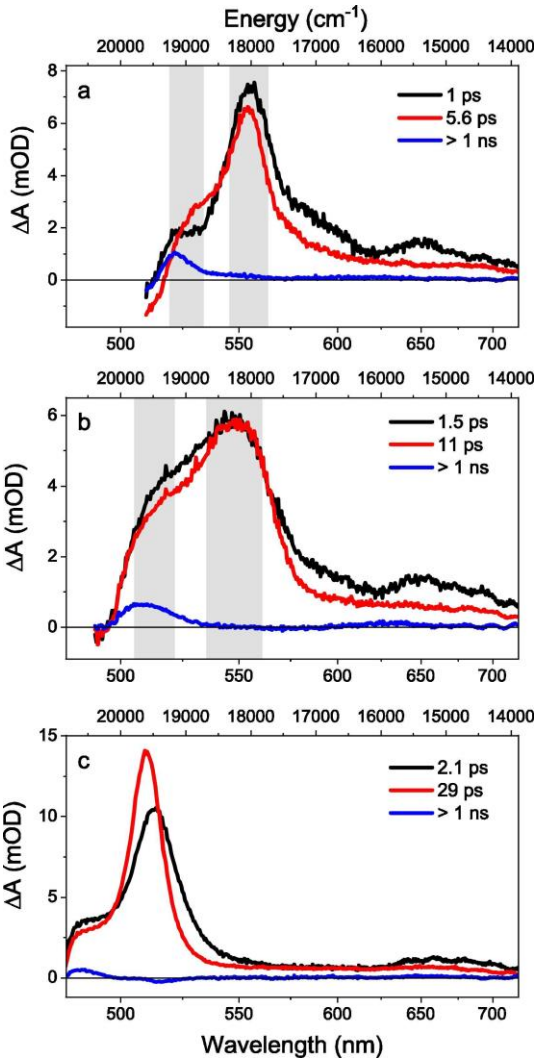

Figure 3-4: EADS obtained from global fitting of 2PE transient absorption data of lycopene (a), β-carotene (b), and neurosporene (c). The gray areas in (a) and (b) represent the wavelength ranges used for the ratio calculation shown in Fig. 3-6.

3.4 DISCUSSION

Our data show that the spectrum corresponding to the relaxed S_1 state produced via 2PE differs from that obtained via 1PE. This is demonstrated in Fig. 3-5 which compares EADS associated with the relaxed S_1 state obtained after 1PE and 2PE. The low energy side of the S_1-S_n band is essentially independent of the type of excitation, but the high-energy side exhibits significant increase of signal in the spectral region associated with the S* signal. The increase of the S* signal after 2PE correlates with carotenoid structure. It is rather negligible for neurosporene

(with the number of conjugated C=C bonds in the carotenoid structure N = 9) but as the conjugation length increases, the effect of 2PE on the magnitude of the S* signal becomes more pronounced. Obviously, it is not solely the conjugation length responsible for this effect as the largest change of the S* signal induced by 2PE is observed for β-carotene whose effective conjugation length is shorter than that of lycopene.[18] Thus, the extension of conjugation to the terminal rings (β - carotene) facilitates the effect of 2PE on magnitude of the S* signal. The structural effects promoting the increase of the S* signal after 2PE are in fact the same as those facilitating the appearance of the S* signal after standard 1PE. It is a well-established fact that the S* signal is readily observed in long carotenoids[30,32] and that extension of conjugation to terminal rings also enhances the S* signal.[50] Thus, our data shows that 2PE enhances the effect of these known structural factors, making the S* signal even stronger than after 1PE.

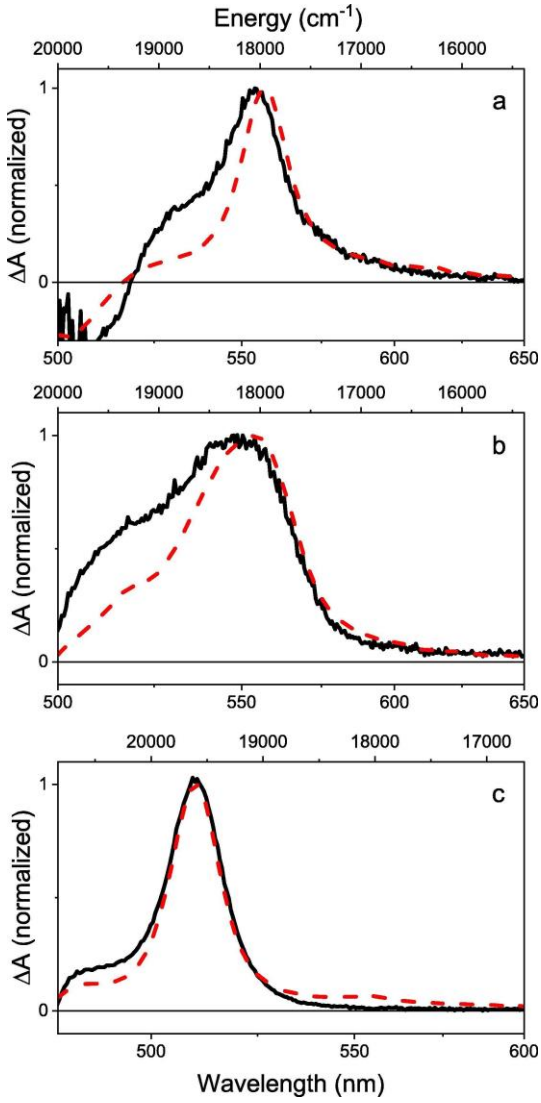

Figure 3-5: Comparison of the EADS corresponding to the S_1 spectrum obtained after 2PE (solid black line) and 1PE (dashed red line) for lycopene (a), β-carotene (b), and neurosporene (c).

The enhanced S* signal after 2PE is further accompanied by slight prolongation of the S_1 lifetime (Fig. 3-3). This is in line with the earlier report of the S_1 state of β-carotene populated via

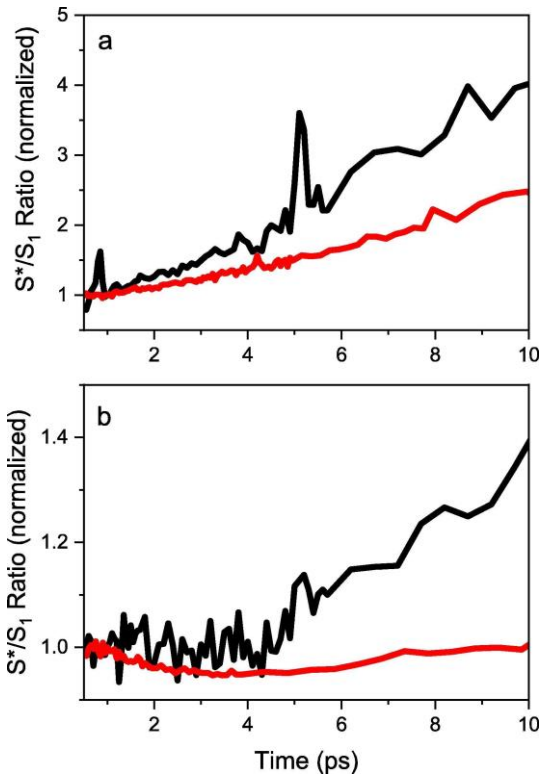

Figure 3-6: Time evolution of the ratio of S*/S1 signals calculated as integral in the spectral ranges depicted in Fig. 3-4 for lycopene (a), and β-carotene (b). The ratios are shown for 2PE (black) and 1PE (red). The ratios are normalized to the value at 1 ps.

energy transfer from chlorophyll, thus also directly from the ground state.[5] Similarly, as in the data reported here, β-carotene in Staleva et al.[5] also exhibits large magnitude of the S* signal than after 1PE excitation. However, similarity of the S_1-S_n spectra in the low energy part rules out the hypothesis that 2PE results in population of different energy minimum at the S_1 potential surface as suggested in Staleva et al.[5]

The origin of the prolonged S_1 state can be rather traced in overlap of the 'true' S_1 spectrum and the S* signal. It is known that the S* signal in long carotenoids decays longer than the S_1 state; the difference in S_1 and S* lifetimes is significant especially for carotenoids with N>12 such as rhodoxanthin[51] or spirilloxanthin.[30] For the carotenoids studied here, however, no differences in lifetimes measured at the S_1-S_n maximum and in the S* shoulder have been reported.[50] The global fitting of 2PE data shown in Fig. 3-4 did not find difference between the S_1 and S* lifetimes either, but if the difference is too small, the global fitting procedure may miss it. Therefore, in Fig. 3-6 we show the time dependence of the S*/S_1 amplitude ratio for lycopene and β-carotene (neurosporene was excluded as the S* signal is weak). The individual S* and S_1 amplitudes were for each time point obtained by integration of signal over the spectral ranges as indicated in Fig. 3-4. The ratio is normalized to the value at 1 ps to suppress influence of initial relaxation processes. For the same decay properties of the S_1 and S* signals there

should be no change in the ratio over the time scale of the S_1 lifetime. Yet, the data in Fig. 3-6 show that this is valid only for β-carotene after 1PE for which the ratio is nearly constant over the first 10 ps. In other cases (2PE β-carotene, 1PE and 2PE lycopene), the ratio increases with time signaling slower decay of the S* signal compared to the S_1 lifetime.

The question is whether the 2PE data can provide further information for the two decades long discussion about the origin of the S* signal. There has been a shift in the explanation of its origin from assigning it to a hot ground state[29] to an excited state associated with specific carotenoid conformation either in the ground[51,52] or excited[50] state, and back to the hot ground state.[26,53] The most recent model using the vibrational energy redistribution approach (VERA) suggests the S* signal originating from both vibrational properties of the S_1 state and from a hot ground state, the contribution of each depending on the conjugation length of the carotenoid. While for long carotenoids (N>12) the hot ground state contribution dominates, for the shorter ones, including β-carotene, the S* signal comes mostly from the S_1 state.[26,31] Similar conclusion was provided by Lenzer's group[28,53] who demonstrated by kinetic modelling that in the heavily congested region of the S* signal (overlapping contributions from the ground state bleaching, S_1-S_n excited state absorption, possible hot ground state absorption and even the triplet state absorption) it is possible to reproduce spectral and kinetic features of β-carotene or zeaxanthin using combination of hot S_1 and hot ground state contributions to the S* signal.[28]

In both these models the S* signal in the first 10 ps for carotenoids with N~11 is due to a transition from the relaxed S_1 state to the 0-1 vibrational band of the upper S_n state, while the hot ground state contribution to the S* signal becomes important only at later (>20 ps) times.[28] This is most likely also the case here, explaining the presence of the strong S* signal already 0.5 ps after excitation when hot ground state cannot be significantly populated yet. The model using VERA explains the magnitude of the S* shoulder in β-carotene by shift between minima of the S_1 and S_n potential surfaces.[31] Thus, within the frame of this model the larger magnitude of the S* signal after 2PE is due to a different shift of the S_1 and S_n potential surfaces. It results in a slight variation of the Franck-Condon factors for the vibronic transitions between the S_1 and S_n states,

enhancing the amplitude of the 0-1 vibronic transition between the S_1 and S_n states responsible for the S* signal at delay times <10 ps. The reason why this happens after 2PE is the inhomogeneous ground state model suggested earlier.[51,52] The excited volume of the sample contains a certain conformational distribution and 2PE preferentially excites molecules with specific conformation exhibiting stronger S* signal due to the S_1-S_n 0-1 vibronic transition. Our data, therefore, provides support for the inhomogeneous ground state model.

Yet, the data presented in Fig. 3-6 show that the S_1-S_n 0-1 vibronic transition cannot be the sole origin of the S* signal. If it were, the kinetics measured in the maximum of the S_1-S_n transition and the spectral region of the S* signal must decay with the same lifetime, which is not the case. The difference in lifetimes is small and hard to be picked up in global analysis, but it is detectable. This means that hot ground state also contributes to the S* signal, even though the contribution is rather minor as also showed by Ehlers et al.[28] for zeaxanthin. Note that for β-carotene the expected absorption from the hot ground state should be in the spectral range 510-525 nm, while the 0-1 vibronic band of the S_1-S_n transition falls to essentially identical spectral region. This makes the signals nearly impossible to separate resulting in seemingly contradictive explanations of the S* signals in the literature. Both contributions were initially suggested as the sole origin of the S* signal in β-carotene: either the 0-1 vibronic band of the S_1-S_n transition[33] or the hot ground state.[53] Only merging these two models[26,28,31] provided correct explanation of the S* signal and our 2PE data reported here support this combined model explaining the S* signal. The 2PE data further add the necessity of the inhomogeneous ground state model to explain differences between the 1PE and 2PE measurements.

Finally, we note that we observe only small amplitude long-lived signals attributable to a triplet state. This is in contrast to 2PE experiments on β-carotene reported by Kosumi et al.[41] This is most likely due to different excitation wavelengths we used in this study, because Kosumi et al.[49] have shown that the long-lived signals are predominantly due to a β-carotene triplet state generated via four-photon excitation. Our choice of excitation wavelengths and intensities minimizes the contribution from the presumed four-photon absorption resulting in minor contribution of the long-lived signals to our data.

Acknowledgement. Financial support for this research was provided by the grant 16-10417S from the Czech Science Foundation, and the grant 021/2017/P from the Grant Agency of the University of South Bohemia.

3.5 SUPPORTING INFORMATION

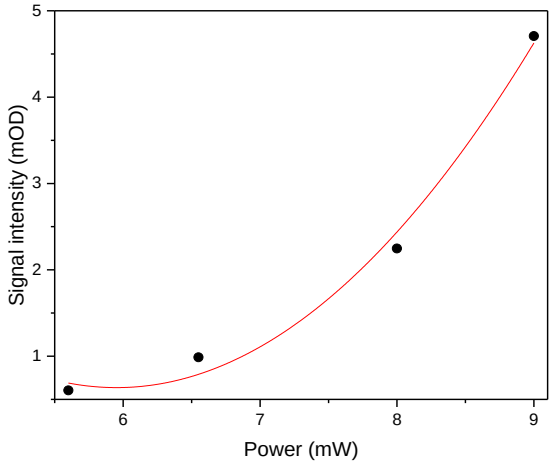

Figure 3-S1: Power dependence of the 2PE signal. The data points corresponds to the S_1-S_n signal at 2 ps for each excitation power. The red line shows results of fitting the data to second order polynomial function.

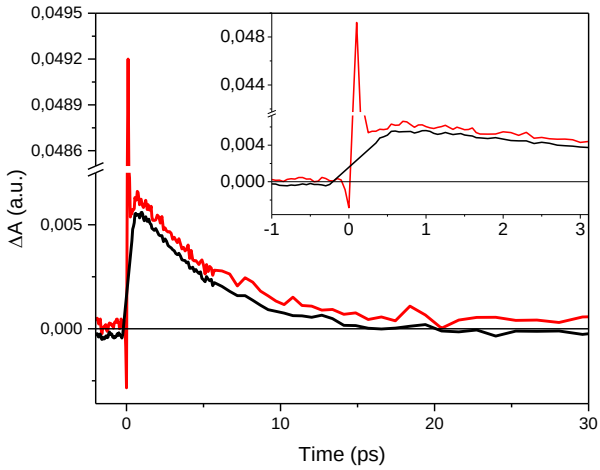

Figure 3-S2: Comparison of the 2PE raw data (red) and data obtained after subtraction of strong coherent artifacts around time zero (black).

REFERENCES

1. T. Mirkovic, E. E. Ostroumov, J. M. Anna, R. van Grondelle, Govindjee, G. D. Scholes Light absorption and energy transfer in the antenna complexes of photosynthetic organisms Chem. Rev., 117 (2017), pp. 249-293, 10.1021/acs.chemrev.6b00002

2. G. D. Scholes, G. R. Fleming, A. Olaya-Castro, R. van Grondelle Lessons from nature about solar light harvesting Nat. Chem., 3 (2011), pp. 763–774, 10.1038/nchem.1145

3. R. Croce, H. van Amerongen Natural strategies for photosynthetic light harvesting. Nat. Chem. Biol., 10 (2014), pp. 492–501, 10.1038/nchembio.1555

4. T. Polívka, H. A. Frank Molecular factors controlling photosynthetic light harvesting by carotenoids Acc. Chem. Res., 43 (2010), pp. 1125–1134, 10.1021/ar100030m

5. H. Staleva, J. Komenda, M. K. Shukla, V. Šlouf, R. Kaňa, T. Polívka, R. Sobotka Mechanism of photoprotection in the cyanobacterial ancestor of plant antenna proteins Nat. Chem. Biol., 11 (2015), pp. 287-291, 10.1038/nchembio.1755

6. K. K. Niyogi, T. B. Truong Evolution of flexible non-photochemical quenching mechanisms that regulate light harvesting in oxygenic photosynthesis Current Opinion in Plant Biology, 16 (2013), pp. 307-314, 10.1016/j.pbi.2013.03.011

7. K. Schulten, M. Karplus On the origin of a low-lying forbidden transition in polyenes and related molecules Chem. Phys. Lett., 14 (1972), pp. 305-309, 10.1016/0009-2614(72)80120-9

8. T. Polívka, V. Sundström Ultrafast dynamics of carotenoid excited states−from solution to natural and artificial systems Chem. Rev., 104 (2004), pp. 2021-2071, 10.1021/cr020674n

9. S. Shima, R. P. Ilagan, N. Gillespie, B. J. Sommer, R. G. Hiller, F. P. Sharples, H. A. Frank, R. R. Birge Two-photon and fluorescence spectroscopy and the effect of environment on the photochemical properties of peridinin in solution and in the peridinin-chlorophyll-protein from *Amphidinium carterae* J. Phys. Chem. A, 107 (2003), pp. 8052-8066, 10.1021/jp022648z

10. K. Furuichi, T. Sashima, Y. Koyama The first detection of the $3A_g^-$ state in carotenoids using resonance-Raman excitation profiles Chem. Phys. Lett., 356 (2002), pp. 547-555, 10.1016/S0009-2614(02)00412-8

11. T. Sashima, Y. Koyama, T. Yamada, H. Hashimoto The $1B_u^+$, $1B_u^-$, and $2A_g^-$ energies of crystalline lycopene, β-carotene, and mini-9-β-carotene as determined by resonance-Raman excitation profiles: Dependence of the $1B_u^-$ state energy on the conjugation length J. Phys. Chem. B, 104 (2000), pp. 5011–5019, 10.1021/jp994185b

12. R. Fujii, K. Onaka, M. Kuki, Y. Koyama, Y. Watanabe The $2A_g^-$ energies of all-trans-neurosporene and spheroidene as determined by fluorescence spectroscopy Chem. Phys. Lett., 288 (1998), pp. 847-853, 10.1016/S0009-2614(98)00376-5

13. R. Fujii, T. Ishikawa, Y. Koyama, M. Taguchi, Y. Isobe, H. Nagae, Y. Watanabe Fluorescence spectroscopy of all-trans-anhydrorhodovibrin and spirilloxanthin: Detection of the $1B_u^-$ fluorescence J. Phys. Chem. A, 105 (2001), pp. 5348–5355, 10.1021/jp010150b

14. T. Polívka, J. L. Herek, D. Zigmantas, H.-E. Åkerlund, V. Sundström Direct observation of the (forbidden) S_1 state in carotenoids Proc. Natl. Acad. Sci. U.S.A., 96 (1999), pp. 4914-4917, https://doi.org/10.1073/pnas.96.9.4914

15. H. H. Billsten, D. Zigmantas, V. Sundström, T. Polívka Dynamics of vibrational relaxation in the S_1 state of carotenoids having 11 conjugated C=C bonds, Chem. Phys. Lett., 355 (2002), pp. 465-470, https://doi.org/10.1016/S0009-2614(02)00268-3

16. H. H. Billsten, P. Bhosale, A. Yemelyanov, P. S. Bernstein, T. Polívka Photophysical properties of xanthophylls in carotenoproteins from human retina Photochemistry and Photobiology, 78 (2003), pp. 138–145, https://doi.org/10.1562/0031-8655(2003)0780138PPOXIC2.0.CO2

17. R. Fujii, T. Inaba, Y. Watanabe, Y. Koyama, J.-P. Zhang Two different pathways of internal conversion in carotenoids depending on the length of the conjugated chain Chem. Phys. Lett, 369 (2003), pp. 165-172, 10.1016/S0009-2614(02)01999-1

18. M. Fuciman, G. Keşan, A. M. LaFountain, H. A. Frank, T. Polívka Tuning the spectroscopic properties of aryl carotenoids by slight changes in structure J. Phys. Chem. B, 119 (2015), pp. 1457–1467, 10.1021/jp512354r

19. N. Macpherson, T. Gillbro Solvent dependence of the ultrafast S_2–S_1 internal conversion rate of β-carotene J. Phys. Chem. A, 102 (1998), pp. 5049–5058, 10.1021/jp980979z

20. D. Kosumi, M. Fujiwara, R. Fujii, R. J. Cogdell, H. Hashimoto, M. Yoshizawa The dependence of the ultrafast relaxation kinetics of the S_2 and S_1 states in β-carotene homologs and lycopene on conjugation length studied by femtosecond time-resolved absorption and Kerr-gate fluorescence spectroscopies J. Chem. Phys., 130 (2009), pp. 214506, 10.1063/1.3147008

21. P. Tavan, K. Schulten Electronic excitations in finite and infinite polyenes. Phys. Rev. B, (1987), pp. 4337-4358, https://doi.org/10.1103/PhysRevB.36.4337

22. H. A. Frank, J. A. Bautista, J. Josue, Z. Pendon, R. G. Hiller, F. P. Sharples, D. Gosztola, M. R. Wasielewski Effect of the solvent environment on the spectroscopic properties and dynamics of the lowest excited states of carotenoids J. Phys. Chem. B, 104 (2000), pp. 4569–4577, 10.1021/jp000079u

23. D. Zigmantas, T. Polívka, R. G. Hiller, A. Yartsev, V. Sundström Spectroscopic and dynamic properties of the peridinin lowest singlet excited states J. Phys. Chem. A, 105 (2001), pp. 10296–10306, 10.1021/jp010022n

24. N. L. Wagner, J. A. Greco, M. M. Enriquez, H. A. Frank, R. R. Birge The nature of the intramolecular charge transfer state in peridinin Biophys. J., 104 (2013), pp. 1314–1325, 10.1016/j.bpj.2013.01.045

25. J. A. Bautista, R. E. Connors, B. B. Raju, R. G. Hiller, F. P. Sharples, D. Gosztola, M. R. Wasielewski, H. A. Frank Excited state properties of peridinin: observation of a solvent dependence of the lowest excited singlet state lifetime and spectral behavior unique among carotenoids. J. Phys. Chem. B, 103 (1999), pp. 8751–8758, 10.1021/jp9916135

26. V. Balevičius Jr., D. Abramavicius, T. Polívka, A. G. Pour, J. Hauer A unified picture of S* in carotenoids J. Phys. Chem. Lett., 7 (2016), pp. 3347-3352, 10.1021/acs.jpclett.6b01455

27. F. Ehlers, M. Scholz, J. Schimpfhauser, J. Bienert, K. Oum, T. Lenzer Collisional relaxation of apocarotenals: identifying the S* state with vibrationally excited molecules in the ground electronic state S_0* Phys. Chem. Chem. Phys., 17 (2015), pp. 10478-10488, 10.1039/C4CP05600K

28. F. Ehlers, M. Scholz, K. Oum, T. Lenzer Excited-state dynamics of 3,3′-dihydroxyisorenieratene and (3R,3′R)-zeaxanthin: Observation of vibrationally hot S_0 species Arch. Biochem. Biophys., 646 (2018), pp. 137-144, 10.1016/j.abb.2018.03.035

29. P. O. Andersson, T. Gillbro Photophysics and dynamics of the lowest excited singlet state in long substituted polyenes with implications to the very long-chain limit J. Chem. Phys., 103 (1995), pp. 2509-2519, 10.1063/1.469672

30. C. C. Gradinaru, J. T. M. Kennis, E. Papagiannakis, I. H. M. van Stokkum, R. J. Cogdell, G. R. Fleming, R. A. Niederman,, R. van Grondelle An unusual pathway of excitation energy deactivation in carotenoids: Singlet-to-triplet conversion on an ultrafast timescale in a photosynthetic antenna Proc. Natl. Acad. Sci. U.S.A, 98 (2001), pp. 2364-2369, https://doi.org/10.1073/pnas.051501298

31. V. Balevičius Jr., A. G. Pour, J. Savolainen, C. N. Lincoln, V. Lukeš, E. Riedle, L. Valkunas, D. Abramaviciusa, J. Hauer Vibronic energy relaxation approach highlighting deactivation pathways in carotenoids Phys. Chem. Chem. Phys., 17 (2015), pp. 19491-19499, 10.1039/C5CP00856E

32. W. Wohlleben, T. Buckup, H. Hashimoto, R. J. Cogdell, J. L. Herek, M. Motzkus Pump−deplete−probe spectroscopy and the puzzle of carotenoid dark states J. Phys. Chem. B, 180 (2004), pp. 3320–3325, 10.1021/jp036145k

33. E. E. Ostroumov, M. G. Müller, M. Reus, A. R. Holzwarth On the nature of the “dark S*” excited state of β-carotene J. Phys. Chem. A, 115 (2011), pp. 3698–3712, 10.1021/jp105385c

34. P. Shreve, J. K. Trautman, T. G. Owens, A. C. Albrecht Two-photon excitation spectroscopy of thylakoid membranes from *Phaeodactylum tricornutum*: Evidence for an in vivo two-photon-allowed carotenoid state Chem. Phys. Lett., 170 (1990), pp. 51-56, 10.1016/0009-2614(90)87088-9

35. P. Krueger, J. Yom, P. J. Walla, G. R. Fleming Observation of the S_1 state of spheroidene in LH2 by two-photon fluorescence excitation. Chem. Phys. Lett., 310 (1999), pp. 57-64, 10.1016/S0009-2614(99)00729-0

36. P. J. Walla, P. A. Linden, Ch.-P. Hsu, G. D. Scholes, G. R. Fleming Femtosecond dynamics of the forbidden carotenoid S_1 state in light-harvesting complexes of purple bacteria observed after two-photon excitation Proc. Natl. Acad. Sci. U.S.A., 97 (2000a), pp. 10808-10813, 10.1073/pnas.190230097

37. P. J. Walla, J. Yom, B. P. Krueger, G. R. Fleming Two-photon excitation spectrum of light-harvesting complex II and fluorescence upconversion after one- and two-photon excitation of the carotenoids J. Phys. Chem. B, 104 (2000b), pp. 4799-4806, 10.1021/jp9943023

38. P. J. Walla, P. A. Linden, K. Ohta, G. R. Fleming Excited-state kinetics of the carotenoid S_1 state in LHC II and two-photon excitation spectra of lutein and β-carotene in solution: Efficient CarS_1→Chl electronic energy transfer via hot S_1 states? J. Phys. Chem. A, 106 (2002), pp. 1909-1916, 10.1021/jp011495x

39. J. Zimmermann, P. A. Linden, H. M. Vaswani, R. G. Hiller, G. R. Fleming Two-photon excitation study of peridinin in benzene and in the peridinin chlorophyll a-protein (PCP) J. Phys. Chem. B, 106 (2002), pp. 9418-9423, 10.1021/jp020565c

40. T. Buckup, A. Weigel, J. Hauer, M. Motzkus Ultrafast multiphoton transient absorption of β-carotene Chem. Phys., 373 (2010), pp. 38-44, 10.1016/j.chemphys.2009.12.020

41. D. Kosumi, K. Abe, H. Karasawa, M. Fujiwara, R. J. Cogdell, H. Hashimoto, M. Yoshizawa Ultrafast relaxation kinetics of the dark S_1 state in all-trans-β-carotene explored by one- and two-photon pump–probe spectroscopy. Chem. Phys., 373 (2010), pp. 33-37, 10.1016/j.chemphys.2009.12.013

42. D. Kosumi, T. Kusumoto, R. Fujii, M. Sugisaki, Y. Iinuma, N. Oka, Y. Takaesu, T. Taira, M. Iha, H. A. Frank, H. Hashimoto One- and two-photon pump-probe optical spectroscopic measurments reveal the S_1 and intramolecular charge transfer states are distinct in fucoxanthin. Chem. Phys. Lett. 483 (2009), 95-100, 10.1016/j.cplett.2009.10.077

43. R. L. Christensen, M. Goyette, L. Gallagher, J. Duncan, B. DeCoster, J. Lugtenburg, F. J. Jansen, I. van der Hoef S_1 and S_2 states of apo- and diapocarotenes J. Phys. Chem. A, 103 (1999), pp. 2399–2407, 10.1021/jp983946s

44. L. Fiedor, Heriyanto, J. Fiedor, M. Pilch Effects of molecular symmetry on the electronic transition in carotenoids J. Phys. Chem. Lett., 7 (2016), pp. 1821-1829, 10.1021/acs.jpclett.6b00637

45. H. H. Billsten, J. L. Herek, G. Garcia-Asua, L. Hashøj, T. Polívka, C. N. Hunter, V. Sundström Dynamics of energy transfer from lycopene to bacteriochlorophyll in genetically-modified LH2 complexes of *Rhodobacter sphaeroides* Biochemistry, 41 (2002), pp. 4127–4136, 10.1021/bi011741v

46. K. Onaka, R. Fujii, H. Nagae, M. Kuki, Y. Koyama, Y. Watanabe The state energy and the displacements of the potential minima of the $2A_g^-$ state in all-trans-β-carotene as determined by fluorescence spectroscopy Chem. Phys. Lett., 315 (1999), pp. 75-81, 10.1016/S0009-2614(99)01212-9

47. T. Polívka, V. Sundström Dark excited states of carotenoids: Consensus and controversy Chem. Phys. Lett., 477 (2009), pp. 1-11, 10.1016/j.cplett.2009.06.011

48. D. Niedzwiedzki, J. F. Koscielecki, H. Cong, J. O. Sullivan, G. N. Gibson, R. R. Birge, H. A. Frank Ultrafast dynamics and excited state spectra of open-chain carotenoids at room and low temperatures J. Phys. Chem. B, 111 (2007), pp. 5984-5998, 10.1021/jp070500f

49. D. Kosumi, M. Fujiwara, H. Hashimoto, M. Yoshizawa Ultrafast nonlinear optical responses induced by multiphoton excitation in all-trans-β-carotene: Nonresonant excitation to the optically allowed S_2 state Journal of the Physical Society of Japan, 78 (2009), pp. 104715-104715, 10.1143/jpsj.78.104715

50. D. M. Niedzwiedzki, J. O. Sullivan, T. Polívka, R. R. Birge, H. A. Frank Femtosecond time-resolved transient absorption spectroscopy of xanthophylls J. Phys. Chem. B, 110 (2006), pp. 22872–22885, 10.1021/jp0622738

51. P. Chábera, M. Fuciman, P. Hříbek, T. Polívka Effect of carotenoid structure on excited-state dynamics of carbonyl carotenoids Phys. Chem. Chem. Phys., 11 (2009), pp. 8795-8803, 10.1039/B909924G

52. V. Lukeš, N. Christensson, F. Milota, H. F. Kauffmann, J. Hauer Electronic ground state conformers of β-carotene and their role in ultrafast spectroscopy Chem. Phys. Lett., 506 (2011), pp. 122-127, 10.1016/j.cplett.2011.02.060

53. T. Lenzer, F. Ehlers, M. Scholz, R. Oswald, K. Oum Assignment of carotene S* state features to the vibrationally hot ground electronic state Phys. Chem. Chem. Phys., 12 (2010), pp. 8832-8839, 10.1039/B925071A

4 Spectroscopy and excited state dynamics of nearly infinite polyenes

This chapter is based on Paper II:

V. Šebelík, M. Kloz, M. Rebarz, M. Přeček, E.-H. Kang, T.-L. Choi, R. L. Christensen, T. Polívka Spectroscopy and excited state dynamics of nearly infinite polyenes.

Abstract

Steady-state and transient absorption spectra with <50 fs time resolution were obtained for two conjugated polymers, both with >200 conjugated double bonds (*N*), constrained in planar, stable, polyene frameworks. Solutions of the polymers exhibit the same $S_2 \rightarrow S_1 \rightarrow S^* \rightarrow S_0$ decay pathway observed for the N = 11-19 polyene oligomers and for zeaxanthin homologues with N = 11-23. Comparisons with the excited state dynamics of polydiactylene and a much longer, more disordered polyene polymer (Poly(DEDPM)) show that the S_2, S_1, and S* lifetimes of the four polymers are almost identical. The S* signals in the polymers are assigned to absorption from vibrationally excited ground states. In spite of significant heterogeneities and variations in conjugation lengths in these long polyenes, their $S_0 \rightarrow S_2$ absorptions are vibronically-resolved in room temperature solutions with electronic origins at ≈600 nm. The limiting wavelength for the $S_0 \rightarrow S_2$ transitions is consistent with the persistence of bond length alternation in the electronic ground states and a HOMO-LUMO band gap in polyenes with $N > 200$. The coincidence of the well-resolved $S_0 \rightarrow S_2$ electronic origins and the convergence of the excited state lifetimes in the four polymers point to a common, "nearly infinite" polyene limit.

This chapter is a manuscript prepared for submission. The full version is archived by the Faculty of Science, University of South Bohemia in České Budějovice.

5 Energy transfer pathways in the CAC light-harvesting complex of *Rhodomonas salina*

This chapter is based on Paper III:

V. Šebelík, R. G. West, E. Kuthanová Trsková, R. Kaňa, T. Polívka Energy transfer pathways in the CAC light-harvesting complex of *Rhodomonas salina*. *BBA-Bioenergetics, in press.*

Abstract

Photosynthetic organisms had to evolve diverse mechanisms of light-harvesting to supply photosynthetic apparatus with enough energy. *Cryptophytes* represent one of the groups of photosynthetic organisms combining external and internal antenna systems. They contain one type of immobile phycobiliprotein located at the lumenal side of the thylakoid membrane, together with membrane-bound chlorophyll a/c antenna (CAC). Here we employ femtosecond transient absorption spectroscopy to study energy transfer pathways in the the CAC proteins of cryptophyte *Rhodomonas salina*. The major CAC carotenoid, alloxanthin, is a cryptophyte-specific carotenoid, and it is the only naturally-occurring carotenoid with two triple bonds in its structure. In order to explore the energy transfer pathways within the CAC complex, three excitation wavelengths (505, 590, and 640 nm) were chosen to excite pigments in the CAC antenna. The excitation of Chl-c at either 590 or 640 nm proves efficient energy transfer between Chl-c and Chl-a. The excitation of alloxanthin at 505 nm shows an active pathway from the S_2 state with efficiency around 50%, feeding both Chl-a and Chl-c with approximately 1:1 branching ratio, yet, the S_1-route is rather inefficient. The 57 ps energy transfer time to Chl-a gives ~25% efficiency of the S_1 channel. The low efficiency of the S_1 route renders the overall carotenoid-Chl energy transfer efficiency low, pointing to the regulatory role of alloxanthin in the CAC antenna.

This chapter is a manuscript prepared for submission. The full version is archived by the Faculty of Science, University of South Bohemia in České Budějovice

6 Equilibration dependence of fucoxanthin S_1 and ICT signatures on polarity, proticity, and temperature by multi-pulse femtosecond absorption spectroscopy

This chapter is based on Paper IV:

R. G. West, M. Fuciman, H. Staleva-Musto, V. Šebelík, D. Bína, M. Durchan, V. Kuznetsova, T. Polívka Equilibration dependence of fucoxanthin S_1 and ICT signatures on polarity, proticity, and temperature by multi-pulse femtosecond absorption spectroscopy. J. Phys. Chem. B 122 (2018), pp. 7264–7276, https://doi.org/10.1021/acs.jpcb.8b04217

Abstract

To demonstrate the value of the multi-pulse method in revealing the nature of coupling between excited states and explore the environmental dependencies of S_1 and ICT state equilibration, we performed ultrafast transient absorption pump-dump-probe and pump-repump-probe spectroscopies on fucoxanthin in various solvent conditions. The effects of polarity, proticity, and temperature were tested in solvents methanol at 293 and 190 K, acetonitrile, and isopropanol. We show that manipulation of the kinetic traces can produce one trace reflecting the equilibration kinetics of the states which reveals that lower polarity, proticity, and temperature delays S_1/ICT equilibration. Based upon a two-state model representing the S_1 and ICT states on the same S_1/ICT potential energy surface, we were able to show that the kinetics are strictly dependent on the initial relative populations of the states as well as the decay of the ICT state to the ground state. Informed by global analysis, a systematic method for target analysis based upon this model allowed us to quantify the population transfer rates throughout the life of the S_1/ICT state as well as separate the S_1 and ICT spectral signatures. The results are consistent with the concept that the S_1 and ICT states are part of one potential energy surface.

6.1 INTRODUCTION

The carotenoids' various roles in the scheme of photosynthesis are well understood, but the diverse methods and mechanisms by which they perform their duty in host organisms, especially in light-harvesting[1-3] and photoprotection,[4,5] still provide a flourishing field of study. All carotenoids share a conjugated polyene backbone scheme, and their spectroscopic properties that are directly related to diverse functions. These functions are determined, in part, by the number of conjugate C=C bonds,[6] *N*, which is well understood by the theory of the electronic energetic structure for polyenes.[7] Specifically, carotenoid photophysics has attracted much attention particularly due to its dark excited states. Due to strong correlations among the conjugated π-electrons, the lowest excited state has a significant doubly-excited character, rendering the transition between the ground (S_0) and the lowest excited singlet state (S_1) forbidden for single-photon processes.[7] Nonetheless, the S_1 state has been shown to play the key role both in light-harvesting, serving as energy donor in a number of antenna proteins,[1] and in photoprotection, where it acts as a quencher of excited chlorophyll in some systems.[8-11]

The spectroscopic properties of both the strongly absorbing (S_2) state and the dark S_1 state are primarily determined by *N*, but significant tuning can be achieved by structural groups attached to the conjugated backbone as well as the environment which interacts with these groups. Such tuning is especially pronounced for carotenoids containing a conjugated keto group which are often referred to as carbonyl carotenoids.[12,13] Spectroscopic properties of carbonyl carotenoids depend on solvent polarity, which is related to an intramolecular charge transfer (ICT) state induced by the conjugated keto group.[13,14] With increasing polarity the typical signatures of the ICT state become more pronounced: the broad stimulated ICT emission found in the near-IR region (900-1000 nm) and a corresponding ICT excited state absorption in the 600-750 nm spectral region appear in transient absorption spectra. The appearance of these features correlates with shortening of the S_1 lifetime.[13,14]

Interestingly, however, the lifetimes of the S_1 and ICT bands in transient absorption spectra are typically indistinguishable in global analysis schemes,

leading to the concept of a coupled S_1/ICT state.[14,15] Since the first reported polarity-dependent behavior in peridinin,[12] the coupled behavior has been reported for a number of carbonyl carotenoids.[13,14,16-18] Although the conditions for which the ICT characteristics arise are known,[19-22] the observed behavior of the alleged ICT state has led to various, if not incongruent, conclusions about its nature and relation to the S_1 state.[23-27] In recent years, the ICT state has been considered to be 1) strongly coupled to the S_1 state and visualized as a potential minimum at S_1/ICT potential energy surface whereby the states are coherently mixed,[15,28] 2) a distinct electronic state,[12,24,25,29] or 3) even the S_1 state itself, albeit with enhanced charge transfer character.[30]

Due to its abundance in nature and the functional role of its ICT state in energy transfer within photosynthetic antenna proteins,[18,31,32] research has often centered on the characteristics of the carbonyl carotenoid fucoxanthin. In solution, fucoxanthin has well-resolved S_1-associated (~525 nm) and ICT-associated (600 and 640 nm) spectral bands in transient absorption spectra,[13] and the S_1/ICT lifetime spans the 20-60 ps range in various solvents,[13,19,23] making it a suitable candidate for systematic studies of polarity-dependent behavior. Moreover, contrary to other carbonyl carotenoids, fucoxanthin's properties also significantly depend on solvent proticity as evidenced by the S_1/ICT lifetimes in methanol (20 ps) and acetonitrile (30 ps).[33] Yet, despite numerous studies on polarity-dependent excited-state dynamics of fucoxanthin in solution,[33-38] the precise relation between the S_1 and ICT states has remained unclear. Even though a small difference between kinetics measured at the maxima of the S_1-associated and ICT-associated transitions were reported,[34,38] they are likely due to different fucoxanthin conformers whose ICT states have slightly different degrees of charge transfer character.[38]

A significant step forward in understanding the relation between the S_1 and ICT states was reported in a recent study by Redeckas, et. al.,[39] who employed pump-dump-probe spectroscopy to fucoxanthin in methanol. In this experiment, adding a second excitation pulse to the standard pump-probe scheme allows selective manipulation of excited-state populations, making it possible to monitor excited-state dynamics hidden in the standard pump-probe experiment (PP).[15,25,39-42] The second excitation pulse was tuned to 960 nm, matching the

maximum of the ICT stimulated emission, therefore, selectively dumping a fraction of ICT population back to the ground state. This manipulation of the ICT population of fucoxanthin in methanol, demonstrated that prematurely removing some of the population of the ICT state does not instantaneously, nor equally, affect the population of the S_1 state. Instead, the ICT dumping leads to distortion of equilibrium between the S_1 and ICT states which is restored in less than 5 ps.[39] Thus, the S_1 and ICT states are two strongly-interacting states in equilibrium. It must be noted that similar experiment was carried out more than a decade ago by Papagiannakis et al.[15] for peridinin in methanol, but fixed wavelength of the dump pulse (800 nm) limited selectivity of the ICT dumping in that experiment.

The study presented here seeks to explore further this interaction between the S_1 and ICT states of fucoxanthin. We expand the experiments to other solvents and temperatures to explore polarity, proticity, and temperature dependence of the S_1/ICT state equilibration. By fitting and modeling the pump-dump-probe data, we show that the equilibration between the S_1 and ICT states is the key process leading to the identical lifetimes of the S_1-associated and ICT-associated bands measured in pump-probe experiments. In addition, we find that equilibration is the controlling factor for the observed polarity, proticity, and temperature dependence of the S_1/ICT lifetime of fucoxanthin in pump-probe experiments. In addition to experiments using the dumping of the ICT state, for fucoxanthin in methanol we also apply repumping of the ICT and S_1 states by tuning the second excitation pulse into the S_1-like or ICT-like excited state absorption bands.

6.2 MATERIALS AND METHODS

6.2.1 Sample preparation

Analytical standard, all-trans fucoxanthin was obtained from Sigma-Aldrich and dissolved in methanol, acetonitrile, and isopropanol to absorbance of 0.4 for 2 mm path length at 490 nm. This allowed for fucoxanthin to be tested in various environments: polar aprotic and two protic solvents of different polarity. The samples were maintained at room temperature during the measurements and stirred with a magnetic stir bar within a 2 mm path length quartz cuvette.

Fucoxanthin in methanol, however, was also measured at 190 K in a plastic cuvette. Insignificant changes in the steady-state spectra before and after the measurement affirmed the invariability of the sample throughout the experiments.

6.2.2 Spectroscopy

The source of ultrafast pulses for time-resolved measurements was a chirped-pulse regenerative amplification system (Spectra Physics, Spitfire Ace) seeded by a mode-locked Ti:sapphire oscillator (MaiTai) and pumped by a Nd-YLF Q-switched laser (Empower). The system was configured to produce 100 fs, 4.2 mJ pulses centered at 800 nm at a repetition rate of 1 kHz. Beam splitters directed the pulses through optical parametric amplifiers (TOPAS Prime and TOPAS, Light Conversion) for tuning the pump and dump/repump pulses, respectively, as well as a 3 mm sapphire plate for producing a broadband, supercontinuum probe pulse which was then focused to a 100 μm spot size at the sample space.

For room temperature measurements, pump pulses were tuned to a central wavelength of 490 nm, resonant with the 0-0 transition to the S_2 state, and focused to an approximately 200 μm spot size with a 70 nJ/pulse. The dump pulse was tuned to 950 nm and focused to an approximately 350 μm spot size at 380 nJ/pulse. With a delay line, the dump pulse was set to arrive at the sample space about 1.7 ps after the excitation pulse. Repump pulses had similar focusing and timing as the dump pulse configuration and were tuned to 535 nm and 640 nm for respective S_1 and ICT repumping. For the repump measurements, pump power was about 25 nJ/pulse and repump power was adjusted to no greater than 200 nJ/pulse. For the measurement at 190 K, the focusing of all pulses remained the same as above though the pump wavelength was set to 510 nm and the dump wavelength remained at 950 nm; their respective energies were about 30 nJ/pulse and 360 nJ/pulse.

The supercontinuum produced by the sapphire plate was divided by a 50/50 beam splitter into a reference and probe beams which passed through the sample space; both were simultaneously directed onto the entrance slit of a 600-groove grating spectrograph equipped with a double linear CCD detection system (Pascher Instruments). To ensure the accuracy and quality of the difference in

absorption measurements (ΔA) the pump, dump, and probe pulses incident in the sample space were selectively staggered by choppers placed in the pump and dump beam paths, set at 500 Hz (pump) and 250 Hz (dump, repump), respectively. The configuration allowed for observation of the pulses' influence on the sample within three regimes: pump-probe (PP), dump-probe (DP), and pump-dump-probe (PDP').

6.2.3 Data analysis

The data-collection system produces one data set for each pulse regime mentioned above, including a fourth data set with the dump-probe (DP) data subtracted from pump-dump-probe data (PDP = PDP' – DP). This pump-dump-probe (PDP) data set is the data set featured in the graphs and analysis below. All global and target analyses were performed in data analysis software (CarpetView, Light Conversion) which allows simultaneous fitting of PP and PDP data sets.

For evaluation of PP data, a sequential scheme was considered for the global analysis to obtain the Evolution-Associated Difference Spectra (EADS). Global analysis using a parallel scheme was also performed on the double-difference data set (PP-PDP) to obtain the Decay-Associated Difference Spectra (DADS) to elucidate the immediate effect of the dump pulse on the system. To explore the equilibrium dynamics of the system perturbed by the dump pulse, both PP and PDP data were chirp-corrected and truncated from 1.0 ps after excitation for target analysis, and a simple two-state connectivity scheme was applied.

For a more rigorous analysis of S_1 and ICT state kinetics, as described in the discussion section, a simple, two-state model was analytically defined and applied to the target analyses of S_1-associated and ICT-associated species, informed by global analyses.

6.3 RESULTS

The absorption spectrum of fucoxanthin in the three solvents used in this study is shown in Fig. 6-1. At room temperature (Fig. 6-1a), negligible shift in the vibronic bands was observed among the three solvents, and the typical broadening of the vibronic spectral structure in more polar solvents is apparent. Upon lowering temperature to 190 K (Fig. 6-1b), the absorption spectrum of fucoxanthin in methanol broadens, indicating that polarity-related features are enhanced at low temperature. The excitation wavelength was chosen such that mostly the 0-0 transition to the S_2 state was excited in order that any dynamics within the vibrational manifold of the S_2 state would not complicate the dynamics.

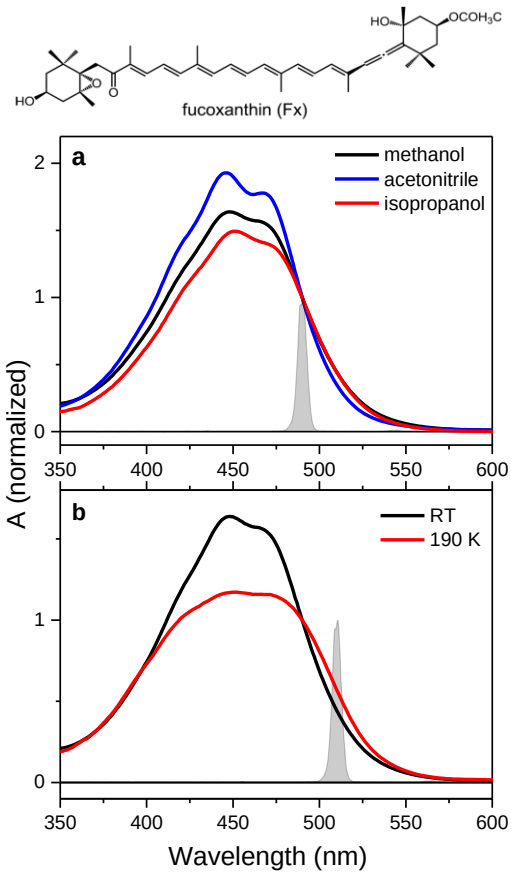

Figure 6-1: Molecular structure of fucoxanthin and absorption spectrum of fucoxanthin in various solvents at room temperature (a), and in methanol at room temperature and 190 K (b). Spectra are normalized to the value at 490 nm, the pump wavelength at room temperature which was tuned to select only the 0-0 vibrational transition. Spectral profile of excitation pulses at 490 nm (room temperature) and 190 K (510 nm) are also shown. Molecular structure of fucoxanthin is also shown.

Transient absorption spectra measured after excitation of fucoxanthin in acetonitrile at 490 nm in both PP and PDP regime are shown in Fig. 6-2a. Further, Fig. 6-2b demonstrates the effect of the dump pulse by showing the PP-PDP double difference spectra at selected times after applying the dump pulse. The transient absorption spectra of fucoxanthin in polar acetonitrile exhibit two positive features corresponding to the S_1-S_n transition, peaking at 535

nm and ICT-S_N transition in the 600-670 nm spectral region. When comparing the PP data set with the PDP data set, it is clear that within less than 1 ps after the dump, the dumping of the ICT state (640 nm band) appears to cause a comparable population drop also in the S_1 state (535 nm band), from which it does not recover throughout the decay lifetime (Fig. 6-2a). However, within picoseconds after the dump, the true nature of the relative effect on both states is clarified when the PDP spectra are subtracted from the PP spectra as in the double-difference spectra in Fig. 6-2b. These spectra more clearly reveal the equilibrium process between the two states. In the first moments after dumping, the ICT band indicates a greater population displacement in proportion to the S_1 state as indicated by the double-difference spectrum at 0.7 ps after the dump. Over time, however, the ratio of the effect of the dump in the ICT band in relation to the S_1 band is decreased as shown by double-difference spectra at later times.

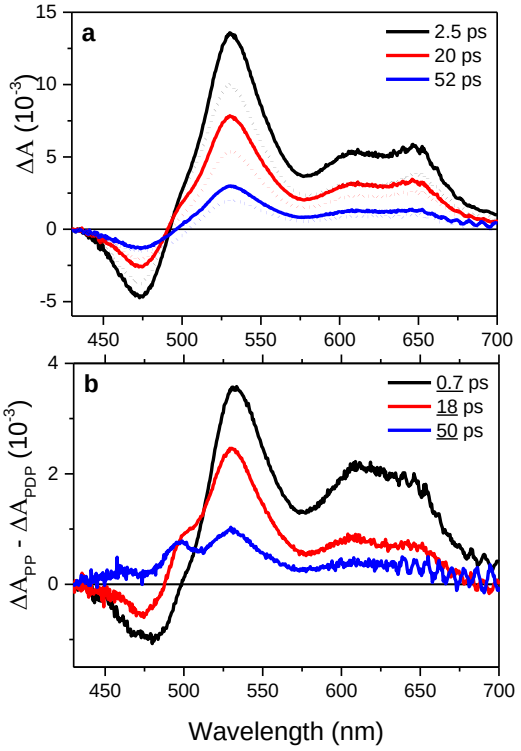

Figure 6-2: (a) PP (solid) and PDP (dotted) spectra of fucoxanthin in acetonitrile at various times after excitation. (b) The double-difference spectrum (PP – PDP) of fucoxanthin in acetonitrile. The underlined values indicate delay after the dump pulse.

Fig. 6-3 compares the PP and PDP data sets of fucoxanthin in methanol, but also includes the effect of temperature on the transient spectra. At room temperature, the overall behavior is comparable to that observed in acetonitrile. At low temperature (190 K), however, there is a red shift of the entire spectrum: the S_1-S_n band has a maximum at 543 nm at 190 K and the same shift from room temperature of ~8 nm occurs also for the ICT bands. As for absorption spectrum

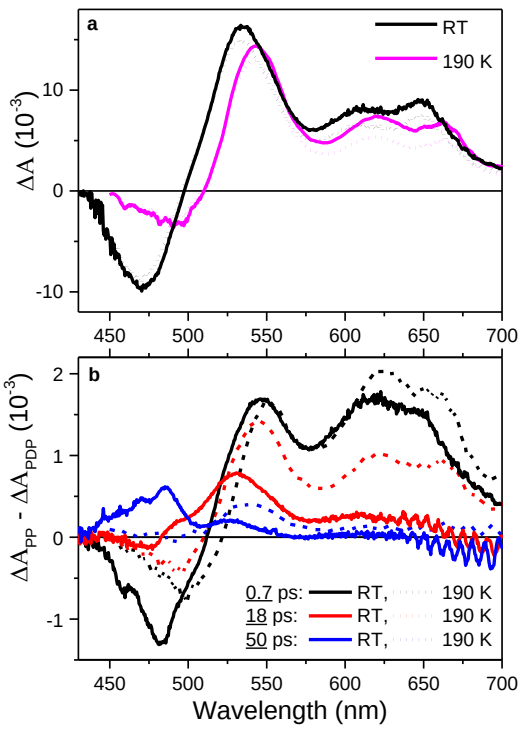

Figure 6-3: (a) Excited state spectra at 2.5 ps after excitation comparing fucoxanthin in methanol at room temperature (RT) and 190 K. The spectra of the pump-dump-probe regime is indicated by the dotted lines. (b) The double difference spectra (PP – PDP) demonstrating only the effect of the dump on fucoxanthin in methanol at three different times after the dump. The underlined values indicate delay after the dump pulse.

in Fig. 6-1, no narrowing of the transient spectral bands is observed upon cooling to 190 K. Evidence of S_1/ICT coupling by ICT state dumping is still evident at 190 K. This is shown by the reduction of the S_1 state signal at 2.5 ps after excitation in Fig. 6-3a, and an equilibration process similar to the room temperature measurement is also observed in the double-difference spectrum in Fig. 6-3b implying that an equilibration process is still present even at low temperature. The PP and PDP data sets measured for fucoxanthin in isopropanol again give qualitatively similar behavior, as observed in acetonitrile and methanol, shown in the Supporting Information (Fig. 6-S1).

Despite a number of reports on excited-state dynamics of fucoxanthin,[21,22,34,37,38,43] it has never been measured at low temperature. Therefore, we show the results of global fitting the PP data on fucoxanthin in methanol at 190 K in Fig. 6-4 to provide basic characterization of excited-state processes at low temperature. As for the room temperature data (Fig. 6-S2), four decay components are needed for a reasonable fit. Besides the first EADS which characterizes the decay of the

initially excited S_2 state, all other decay components are slower at 190 K. Vibrational decay of the S_1/ICT state is about twice slower (470 fs) at 190 K, and the same is observed for the two components characterizing the decay of the S_1/ICT state that yield 13 and 47 ps at 190 K. This is again slower than 8 and 20 ps obtained at room temperature. We note that two S_1/ICT decay components are needed to fit transient data of fucoxanthin exclusively in methanol, most likely due to multiple fucoxanthin conformations occurring in this solvent.[33,34,38,44] Interestingly, at 190 K the slow, 47 ps S_1/ICT decay component has significantly reduced ICT bands and blue-shifted bleaching (Fig. 6-4), suggesting that cooling the sample separates the different conformations better than at room temperature. The presence of different conformations is also the reason why there is no narrowing of the spectral bands upon cooling. EADS resulting from global fitting the data measured at room temperature in all three solvents are shown in Supporting Information (Fig. 6-S2). All time constants obtained from global fitting are summarized in Table 6-1.

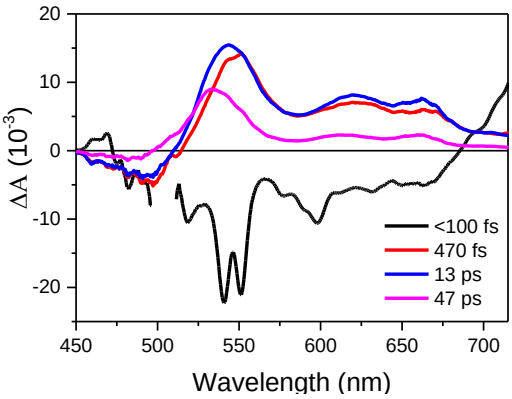

Figure 6-4: EADS of fucoxanthin in methanol at 190 K.

Table 6- 1: The decay rates for fucoxanthin in all solvent environments obtained from the EADS in order of appearance in the decay dynamics.

Rates^{-1} (ps)	methanol		acetonitrile	isopropanol
EADS	RT	190 K		
k_1^{-1}	0.10	<0.10	0.10	0.12
k_2^{-1}	0.19	0.47	0.34	0.28
k_3^{-1}	7.8	13	33	51
k_4^{-1}	19	47	--	--

Kinetics about the minimum of the bleaching (Fig. 6-5a) and in the S_1 (Fig. 6-5b) and ICT (Fig. 6-5c) band maxima for all solvents demonstrate the different lifetimes of the S_1/ICT state in different solvents: 19 ps, 33 ps and 51 ps in methanol, acetonitrile and isopropanol (Table 6-1) as reported earlier.[13,19,33] Application of the dump immediately removes some of the ICT state population, subsequently decreases the S_1 band, and returns a certain population to the ground state as indicated by the reduction of ground state bleaching. However, by comparison of the PDP traces in Figs. 6-5b and 6-5c, different dynamics within the S_1 and ICT bands following the dump pulse are obvious. This difference reflects the equilibration between the S_1 and ICT states after selectively perturbing the ICT population by the 950 nm pulse.[39] The dump pulse also repumps a very small S_1 population, most likely through the S_1-S_2 transition,[19] similar to that seen in our PDP study of fucoxanthin in FCP,[45] indicated by the notch in the S_1-associated dump traces in Fig. 6-5b. Oddly, the decay of the bleach of fucoxanthin at 490 nm in methanol seems unaffected by temperature. However, the EADS shown in Fig. 6-4 explain this, because the bleaching band associated with the longer, 47 ps component has negligible amplitude at 490 nm. The effect of the lower temperature on dynamics of fucoxanthin in methanol is clearly seen by comparing the kinetic traces to those at room temperature as in Fig. 6-5e-f. Normalized to the time just before dumping, the traces show how decay at 190 K is slower for the S_1 and ICT bands, but the effect of the dump is comparable.

To gain further insight into the excited-state dynamics, we have also carried out experiments with repumping the S_1 and ICT transition by tuning the second excitation (repump) pulse to 535 and 640 nm. The repump pulse was applied at 1.7 and 2 ps for repumping the ICT and S_1 population, respectively. The effect of selective repumping on the S_1 and ICT bands of fucoxanthin in acetonitrile at room temperature is shown in Fig. 6-6. Regardless of which state is selected for

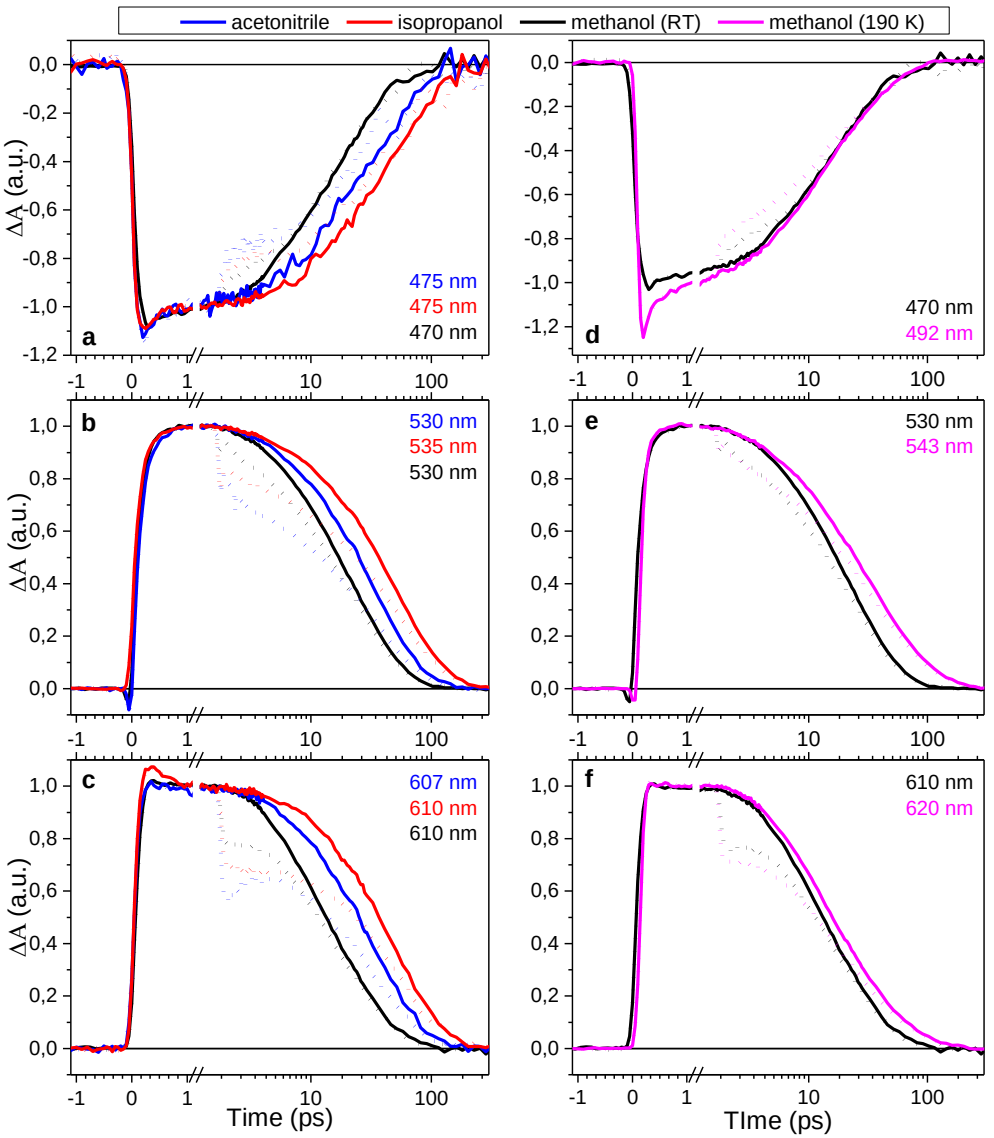

Figure 6-5: Kinetic traces of ground state bleaching minimum (a,d), S_1 state maximum (b,d), and ICT state maximum (c,f) bands of fucoxanthin in three solvents: methanol at room temperature (black) and methanol at 190 K (magenta), acetonitrile (blue), and 2-propanol (red). Pump-probe traces are indicated by the solid lines and the pump-dump-probe traces are dotted. The numbers indicate the wavelength of the traces, ordered according to the legend. All traces are normalized to the signal magnitude just before the dump.

repumping, the effect of a loss of population in the coupled state is immediately

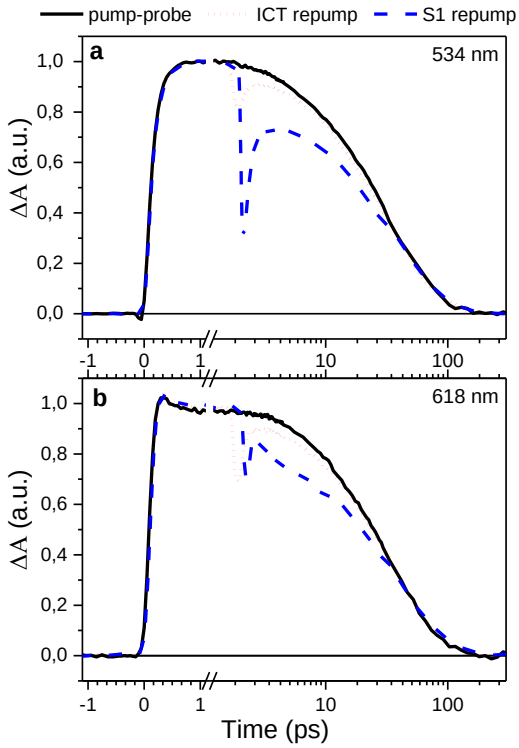

Figure 6-6: Kinetic traces of S_1 and ICT band repumping compared to pump-probe traces in (a) the S_1-associated band and (b) the ICT-associated band of fucoxanthin in acetonitrile (see Fig. 6-S3 for methanol).

seen. The population recovers quickly and dynamics of this fast recovery monitors return of the repumped population back to its initial state. Interestingly, while the repumped ICT population returns almost immediately, a slower component of the recovery is observed after S_1 repumping (Fig. 6-6). The same behavior is seen in methanol (Fig. 6-S3).

When simply looking at the traces of populations affected by the dump or repump pulse it is clear that the perturbation does affect the S_1 and ICT bands of the spectrum individually, and the system tends to return, or equilibrate, to the condition of an unperturbed system, regardless of the environment. However, the exact characteristics of the equilibration after perturbation are more easily examined when the kinetics of the S_1 and ICT traces are compared with respect to one another. One way to do this is to observe how the kinetic of the ratio of the S_1-associated ESA band to the ICT-associated band behaves.[38,45] In this way, the perturbation is seen clearly affecting the S_1:ICT ratio, setting the system into an imbalanced condition from which the system equilibrates toward the usually unperturbed trajectory (Fig. 6-7a). Further still, in order to clearly see how much the perturbation specifically affects the equilibration among these two states, the kinetic of the S_1:ICT ratio itself may be compared in the unperturbed and perturbed conditions—that is, for example, taking the ratio of the perturbed S_1:ICT ratio to that of the unperturbed S_1:ICT ratio, denoted here as $(S_1{:}\,ICT)_{PDP}{:}\,(S_1{:}\,ICT)_{PP}$. The traces of this ratio of ratios, as seen in Fig. 6-7b,

elucidate the pure dynamics of equilibration of fucoxanthin in various environments. The value of this manipulation of the kinetic traces is substantiated by the opposite effect of repumping the S_1 state where the imbalance is deviated in the opposite direction of the ICT dump or repump as in Fig. 6-7c (Fig. 6-S4 for methanol).

The pure equilibration dynamics shown in Fig. 6-7 reveal an interesting behavior. Clearly, though polarity of the environment is a factor determining the rate of the $S_1 \rightleftharpoons$ICT equilibration, in that the less polar isopropanol takes longer to equilibrate than methanol by a certain degree, it is not the only controlling factor. As for the S_1/ICT lifetime of fucoxanthin, the equilibration is also affected by solvent proticity because in aprotic acetonitrile, the equilibration rate is notably faster than in protic methanol even though both solvents have comparable polarity. Interestingly, however, the effect of proticity on equilibration dynamics is opposite than on the S_1/ICT lifetime: while equilibration is faster in aprotic acetonitrile, the S_1/ICT lifetime is slower in acetonitrile than in methanol (Table 6-1). Lowering the temperature of the methanol, as generally expected, slows the rate of equilibration, similar to the

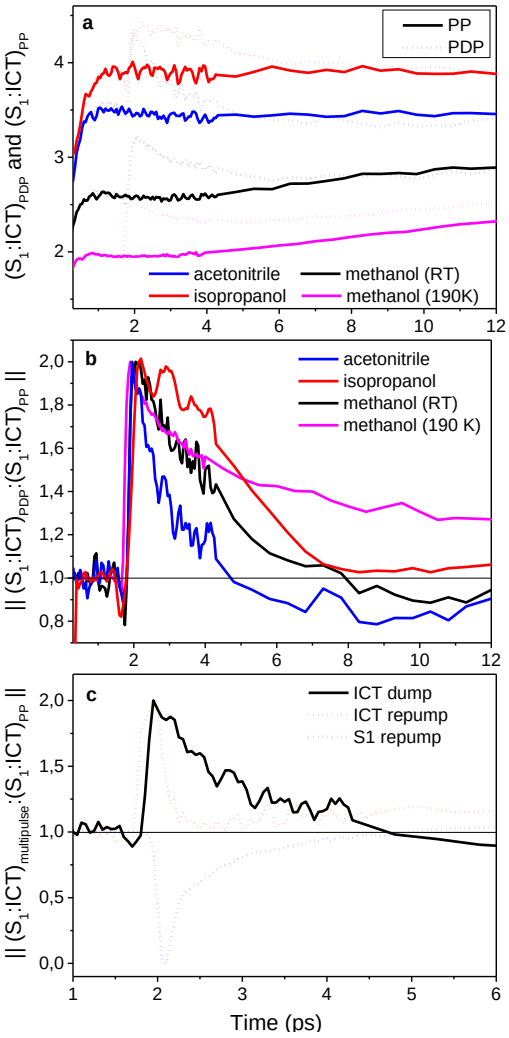

Figure 6-7: (a) The S_1-associated to ICT-associated band traces (S_1:ICT) in the PDP regime and the PP regime (PDP:PP). (b) The ratio of the S_1-associated to ICT-associated band traces (S_1:ICT) in the PDP regime to that of the PP regime (PDP:PP)—that is (S_1:ICT)PDP:(S_1:ICT)PP. (c) The same manipulation of the traces for the S_1 repump and the ICT repump in acetonitrile, compared to PDP (same graph for methanol in Supp. Fig. **6-**4). The magnitude of all traces are normalized to maximum.

behavior of Fucoxanthin-Chlorophyll *a* Protein (FCP) at 77 K, as reported in our previous study.[45]

As the ratio of perturbed and unperturbed S_1:ICT ratios reveals the nature of the equilibration in time, the Decay Associated Difference Spectra (DADS) of the data from unperturbed minus the perturbed systems reveal the spectrum of the equilibration. DADS provide valuable information regarding immediate, parallel processes induced by the dump such as the equilibration rate k_{eq}. Therefore, we fit globally the double-difference data (PP – PDP) obtained from experiments with dumping of the ICT state at 950 nm. These data contain solely information about the dynamics induced by the dump pulse, therefore fully and uniquely describing the equilibrium rate as well as the S_1/ICT decay rate. The S_1/ICT decay rate must appear in the double difference data because the 950 nm dump pulse sends a fraction of excited state population to the ground state. This missing fraction appears in the PP-PDP dataset as a kinetic process with the S_1/ICT decay lifetime.

The DADS obtained from the global fitting of the PP-PDP dataset of fucoxanthin in acetonitrile are shown in Fig. 6-8 (Fig. 6-S5 for remaining solvents). The black DADS has a lifetime of 120 fs and is most likely associated with a fraction of the S_1 population that is repumped by the 950 nm pulse via the S_1-S_2 transition. Its lifetime thus reflects the S_2 relaxation. The red DADS has a lifetime of 1.3 ps and clearly reflects the equilibration component as it demonstrates the imbalance between the S_1 and ICT bands, which is recovered at rate k_{eq}. More importantly, the last component takes the same shape and has the same lifetime of 33 ps as the PP EADS, corresponding to

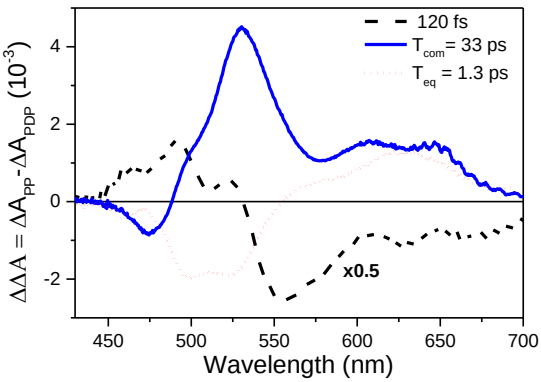

Figure 6-8: DADS of the double-difference spectrum (PP-PDP) of fucoxanthin in acetonitrile (results for other solvents in Fig. 6-S5). The amplitude of the fast component was reduced by half.

the S_1/ICT lifetime. This decay rate we will further denote as the common decay rate k_{com}.

The general shape of the DADS is maintained for isopropanol, with, as expected, longer rates of 8.3 ps (equilibration) and 51 ps (common rate) (Fig. 6-S5). In methanol at both 293 and 190 K, the components have similar trends but appear much more complex. The intermediate EADS components of 7.8 ps (293 K) and 13 ps (190 K), respectively, cannot be obtained in DADS of PP - PDP. This underlines the complexity of the excited-state dynamics of fucoxanthin in methanol and identifies limits of using EADS for such systems, as discussed recently.[38] The absence of the intermediate decay component in the double-difference DADS also suggests that the 'true' common S_1/ICT lifetime of fucoxanthin in methanol is rather associated with the slowest EADS having time constants of 19 ps (293 K) and 41 ps (190 K). The common and equilibration rates from global analyses are summarized in the first two lines of Table 6-2.

Table 6-2: Rates and initial S_1 to ICT initial population ratios determined by global and target analysis of data sets truncated from 1 ps. Common and equilibrium rates for the target analyses, k_{com} and k_{eq}, were calculated using the four individual rates extracted from target analysis.

Rates^{-1} (ps)	methanol		acetonitrile	isopropanol
global analysis	RT	190 K		
k_{com}^{-1}	19	41	33	51
k_{eq}^{-1}	3.5	12	1.3	8.3
target analysis				
k_{com}^{-1}	18	49	33	53
k_{eq}^{-1}	3.2	13	1	11
$k_{S_1 \rightarrow ICT}^{-1}$	6	60	2.0	33
$k_{ICT \rightarrow S_1}^{-1}$	10	40	2.0	25
$k_{S_1 \rightarrow S_0}^{-1}$	60	84	60	60
$k_{ICT \rightarrow S_0}^{-1}$	12	22	22	45
$\left(n_{S_1}/n_{ICT}\right)_0$	0.8	1.0	1.0	0.6

6.4 DISCUSSION

The data presented in the previous section demonstrate that the S_1 and ICT states can be selectively affected by the dump or repump pulse. As reported earlier for fucoxanthin in methanol,[39] the selective perturbation of the ICT population results in an imbalance of the equilibration between the ICT and S_1 states which eventually restores the original distribution of excited state population between the S_1 and ICT parts of the S_1/ICT potential energy surface. We also showed that by appropriate data treatment we can extract not only the common lifetime of the coupled S_1/ICT state, which is readily obtained from standard PP experiment, but also the $S_1 \rightleftharpoons$ICT equilibration time from the DADS of the double-difference data set (PP – PDP). Both these rates, $k_{com}$and k_{eq}, exhibit dependence on solvent polarity and proticity as well as the temperature.

Since direct application of global and/or target analyses to the collected datasets did not provide a unique solution, we make use of the knowledge of $k_{com}$and k_{eq} obtained from the fitting and focus first on modeling the equilibrium kinetics of the S_1/ICT state in terms of population dynamics of a two-state system to reveal the properties of this elusive state in the simplest way. By this basic two-state model, depicted in Fig. 6-9, we have also simplified our inquiry of the

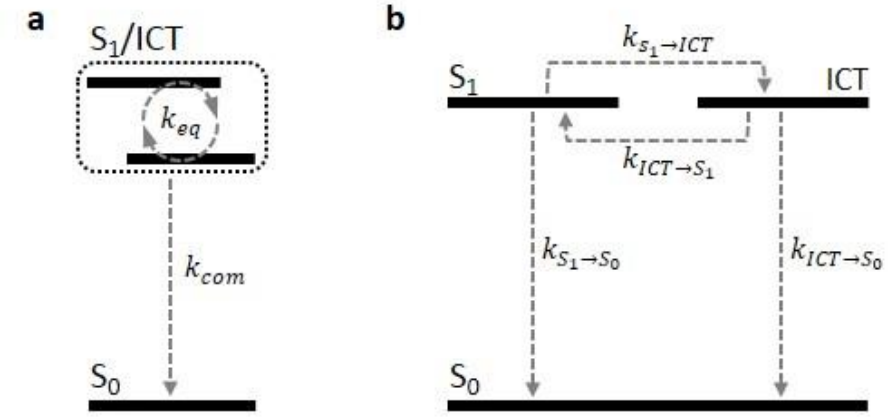

Figure 6-9: Diagram related to global and target analyses models of a two-state system of an excited carbonyl carotenoids from 1 ps after the dump, after all dynamics of higher states have taken place.

nature of the ICT state and have gained insight into what are reasonable rate parameters related to the S_1/ICT relaxation dynamics. Since the relaxation processes preceding the population of the $S_1 \rightleftharpoons$ICT state are mostly over within the first picosecond after excitation (the S_2 decay, vibrational cooling of hot S_1 and ICT states),[15,34,46] we begin our analyses at a time when a two-state model would be the most relevant: less than a picosecond before the dump pulse, 1.0 ps after excitation of fucoxanthin into the S_2 state. We note that the ground state intermediate (GSI) seen in some other studies,[14,39,42] upon dumping the ICT state, is ignored in this model. Its spectral influence has been seen as a relatively small peak shifted to the blue of the maximum S_1-S_N peak absorption wavelength. Nonetheless, we have found the two-state model to be fully sufficient to match the $S_1 \rightleftharpoons$ICT equilibration kinetics without consideration of the GSI. Also, our model does not account for repumping due to any resonance with the S_1-S_2 transition caused by the 950 nm pulse, which is seen in the S_1-associated band. Nonetheless, such transitions are quickly recovered as the dynamics targeted in our modeling are an order of magnitude slower. It is also important to note that though we have named these two states "S_1" and "ICT" in our model, we only imply their associations with the S_1 and ICT parts of one potential energy surface and how they appear to be equilibrating. By monitoring the absorption response, they represent individual concentrations, or species, of the sample undergoing disparate, yet interrelated, dynamics.

Global analyses of pump-probe studies cannot resolve the equilibration rate k_{eq} of the S_1/ICT coupled state; therefore, S_1 and ICT are seen as a single, common, decaying state at a rate k_{com} as depicted in Fig. 6-9. The imbalance caused by prematurely dumping the ICT state allows for the S_1 and ICT states to be observed acting separately, requiring four rates: the rates of transfer between the equilibrating states $k_{S1\rightarrow ICT}$ and $k_{ICT\rightarrow S1}$ as well as the decay of these individual states to a lower state, the S_0 state, $k_{S1\rightarrow S0}$ and $k_{ICT\rightarrow S0}$ (Fig. 6-9b). All four of these rates affect the common decay and equilibrium dynamics. However, as the following paragraphs describe, if the rate $k_{S1\rightarrow S0}$ is considered constant, regardless of solvent polarity at room temperature, only $k_{ICT\rightarrow S0}$ is required as the unknown rate parameter to describe the two-state system's evolution beyond 1 ps.

In this model, we treat the S_1, ICT, and S_0 states as separate species represented by a set of populations, or concentrations, $\{n_\ell\}$ of the sample undergoing interconversion processes determined by a set of real, positive rates, or decay parameters, $\{k_{i\to j} > 0 \mid i,j \in \ell\}$. The model of unperturbed relaxation, therefore, is described by these rate equations:

$$\begin{aligned}\frac{dn_{S1}}{dt} &= k_{ICT\to S1}n_{ICT} - k_{S1\to ICT}n_{S1} - k_{S1\to S0}n_{S1},\\ \frac{dn_{ICT}}{dt} &= k_{S1\to ICT}n_{S1} - k_{ICT\to S1}n_{ICT} - k_{ICT\to S0}n_{ICT}.\end{aligned} \tag{6.1}$$

If the system is briefly perturbed by a dump, the second rate equation can be modified with the addition of a transient Gaussian-shaped dump term $-\exp\{-2.77[(t-t_D)/\Delta\lambda]^2\}\,k_D n_{ICT}$ where t_D is the timing of the arrival of the dump pulse, $\Delta\lambda$ is the pulse width, and k_D is the rate at which the dump transfers population from the ICT to the S_0 state.[47,48] This expression is good for fitting the PDP data set; nonetheless, in this model, a dump can effectually be expressed as a change in initial conditions to Eqns. (6.1).

Nonetheless, Eqns. (6.1) represent the intrinsic behavior of the S_1 and ICT - associated populations in some decay trajectory, and they have analytical solutions with eigenvalues which are the common decay and equilibration rates:

$$k_{eq,com} = \frac{1}{2}\left\{K_{sum} \pm \sqrt{{K_{sum}}^2 - 4[K_{S1}K_{ICT} - k_{S1\to ICT}k_{ICT\to S1}]}\right\} \tag{6.2}$$

where

$$K_{sum} = k_{S1\to ICT} + k_{ICT\to S1} + k_{S1\to S0} + k_{ICT\to S0}\,,$$

the total S_1-associated species decay rate $K_{S1} = k_{S1\to ICT} + k_{S1\to S0}$ and the total ICT-associated species decay rate $K_{ICT} = k_{ICT\to S1} + k_{ICT\to S0}$. The common decay rate k_{com} takes the negative sign before the discriminant in Eq. 6.2, while

the equilibration rate k_{eq} takes the positive sign in Eqn. (6.2). Note also that from Eq. 6.2 we can directly obtain $K_{sum} = k_{com} + k_{eq}$, implying that the sum of the individual rates in the target model should equal the sum of the associated rates from global analysis.

Already, it is clear there exists a range of reasonable decay rates among the states restricted by the common decay rate k_{com} which can be determined by sequential global analysis (EADS) of the S_1/ICT state in the pump-probe (PP) regime. In the PDP regime, the dump pulse removes populations previously destined to decay to the ground state and induces an imbalance to be naturally recovered, revealing the equilibration rate. These parallel processes are best analyzed globally by the Decay-Associate Difference Spectra (DADS) of the double-difference (PP - PDP) data set. The DADS, as seen in Fig. 6-8 for acetonitrile (Fig. 6-S5 for other solvents), gives k_{eq} in addition to k_{com}, when k_{com} is fixed to the singlet state decay value found in the EADS (Fig. 6-S2).

Therefore, if k_{eq} and k_{com} are known from global analyses, then the rates of transfer between the states may be expressed as dependent parameters

$$k_{S1\rightarrow ICT} = \frac{k_{ICT\rightarrow S0}^2 - K_{sum}k_{ICT\rightarrow S0} + k_{com}k_{eq}}{k_{S1\rightarrow S0} - k_{ICT\rightarrow S0}} \quad (6.3a)$$

and

$$k_{ICT\rightarrow S1} = \frac{k_{S1\rightarrow S0}^2 - K_{sum}k_{S1\rightarrow S0} + k_{com}k_{eq}}{k_{ICT\rightarrow S0} - k_{S1\rightarrow S0}}. \quad (6.3b)$$

In many studies on the effect of solvent polarity on carbonyl carotenoids, it has been found that the ICT character becomes more pronounced in polar solvents,[13,14] whereas, in non-polar *n*-hexane, the ICT character of fucoxanthin is almost non-existent, and the lowest single excited state has been found to decay at a rate of $(60\ ps)^{-1}$ [19]. Therefore, if this is assumed to be the intrinsic rate $k_{S1\rightarrow S0}$ at room temperature, regardless of solvent polarity, the only independent rate parameter in the model would be $k_{ICT\rightarrow S0}$, and its range of possible values is limited by the model.

Other factors limiting the range of possible decay parameters are the initial conditions to Eqns. (6.1): the initial concentrations of the S_1 and ICT states.

Although an estimate of initial populations of the S_1 and ICT states are indeterminable without knowledge of their extinction coefficients, the ratio of their initial populations at the moment of dumping, $(n_{S1}/n_{ICT})_0$, is determinable by the model. Further still, the relative magnitude between $k_{S1\rightarrow ICT}$ and $k_{ICT\rightarrow S1}$ is also dependent on whether this ratio is greater or less than unity. Because it is not intrinsically known which rate is faster, target analyses of a two-state system may reveal more than one reasonable solution where $(n_{S1}/n_{ICT})_0$ is either equal to or greater than or less than unity. To gain insight into which solution is proper, the fit traces should ideally, by use of a scaling factor proportional to $(\varepsilon_{S1}/\varepsilon_{ICT})$, match closely the population ratio $n_{S1}/n_{ICT}\ (t)$ at all times. In other words, the ratio of the S_1-associated band to the ICT-associated band of the model $(S_1{:}ICT)_{model}$ should ideally, with a scaling coefficient, match the data $(S_1{:}ICT)_{data}$ in both pump probe and pump-dump-probe regimes shown in Fig. 6-7a. Certainly, special care should be taken as the spectral bands usually associated with the S_1 and ICT states contain dynamics of a mixture of populations. Therefore, the fitting algorithm for the model must include considerations for a mixture of signatures in these bands to properly match the data.

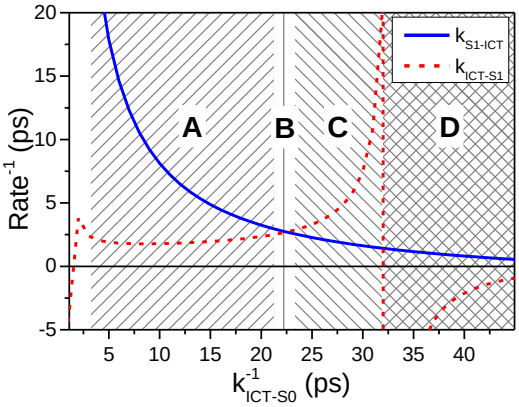

Figure 6-10: The possible values for the inter-S_1↔ICT energy transfer rates $k_{S1\rightarrow ICT}$) and $k_{ICT\rightarrow S1}$ as a function of ICT-ground state transfer rate $k_{ICT\rightarrow S0}$ under the two-state model according to the common and equilibrium rates of fucoxanthin in acetonitrile (results for other solvents in Fig. 6-S6). A, B, C, and D demarcate regions of non-convergence or convergence to different results in target analysis.

Before determining the remaining individual rates in the scheme in Fig. 6-9b, we must understand what limits the model intrinsically imply regarding these rates so that we may direct our fitting. As described above, according to the model and rates made available by global analyses, there are basically only two unknowns in the model: the ICT to ground-state decay rate, $k_{ICT\rightarrow S0}$, and the initial population ratio, $(n_{S1}/n_{ICT})_0$. There is a limitation to the possible values of $k_{ICT\rightarrow S0}$. In

acetonitrile, for example, according to the model it must be that $k_{ICT\to S_0} < (32\,ps)^{-1}$since $k_{ICT\to S1}$ is negative for all $k_{ICT\to S0} > (32\,ps)^{-1}$. This requirement is clearly seen when considering both S_1↔ICT rates, described by Eqns. 6.3a and 6.3b, as a function of $k_{ICT\to S0}$. The possible values are presented in Fig. 6-10 for acetonitrile (Fig. 6-S6 for the remaining solvents). If we assume, as in earlier reports[24,38] $k_{S_1\to ICT}$ be faster than $k_{ICT\to S_1}$, then the possible values are limited $(21ps)^{-1} < k_{ICT\to S_0} < (32\,ps)^{-1}$. Beyond this restriction, convergences may be found in all three allowed regions labeled A, B, and C; whereby, these regions differ in the relative magnitudes of the S_1↔ICT transfer rates $k_{S1\to ICT}$ and $k_{ICT\to S1}$. Therefore, we sought a fit, which produced distinct S_1 and ICT spectra having a spectral profile expected for these states, in one of these regions where the solutions of target analysis (1) produced rates in close agreement with global analyses, (2) the ratio $(S_1{:}ICT)_{model}$ of the fit traces more closely matched the empirical ratio $(S_1{:}ICT)_{data}$.

When applying these requirements to fucoxanthin in acetonitrile, the solution converges such that the ICT decay rate to the ground state is close to the lower limit of the range mentioned above: near 21 ps. Therefore, as seen in Fig. 6-10, the rates of S_1↔ICT population transfer converges to very similar rates as in region B. If the rate $k_{ICT\to S0}$ is applied as an initial condition in region D, that is $k_{ICT\to S0} > (32\,ps)^{-1}$, target analysis gives nonsensical solutions with rates in several μs^{-1} or even negative rates. This analysis provides the upper bound for $k_{ICT\to S_0}$ in all solvents, and according to Eqns. 6.3a and 6.3b this boundary remains even though $k_{S1\to S0}$ may change, as long as k_{com} and k_{eq} are described. For isopropanol, the limit for $k_{ICT\to S_0}$ is $(50\text{ ps})^{-1}$, and for methanol $(20\text{ ps})^{-1}$ and $(40\text{ ps})^{-1}$ for 293 and 190 K, respectively (Fig. 6-S6). These limits coincide with the common decay rates in these solvents.

In regard to the initial ratio of S_1 and ICT state populations, in acetonitrile, for example, the target analysis converges to reasonable results where $(n_{S1}/n_{ICT})_0 = 1$ and the S_1↔ICT rates are found in region B (see Fig. 6-10). This is demonstrated in Fig 6-S7 showing fits of the data (S_1:ICT) ratios in both pump probe and pump-dump-probe regimes. It clearly shows that while the equilibration rate (right column in Fig. 6-S7) does not depend on the initial

n_{S1}/n_{ICT} ratio, the (S_1:ICT) ratios in PP regime can be fitted only for $n_{S1}/n_{ICT} \sim 1$. The data shown in Fig. 6-S7 also imply that at the time of the dumping the S_1/ICT state of fucoxanthin in acetonitrile is equilibrated.

As for the other solvents, however, a solutions did not even converge to region B. The fitting shows that if the condition $k_{S1\rightarrow ICT} > k_{ICT\rightarrow S1}$ is expected, then it must be that $(n_{S1}/n_{ICT})_0 < 1$ in order for the solution to converge and produce distinct S_1 and ICT spectral amplitudes. This places reasonable convergence in regions A and C for isopropanol and methanol at both temperatures, respectively. Nonetheless, we found that often target analyses can converge in region A for the opposite case that $(n_{S1}/n_{ICT})_0 > 1$ as long as the associated condition $k_{S1\rightarrow ICT} > k_{ICT\rightarrow S1}$ is held. In fact, the spectra of the species in both conditions may be practically indistinguishable. However, when the ratio of the S_1-associated and ICT-associated bands (S_1:ICT) is considered (Fig. 6-7a; Fig. 6-S7, Fig. 6-S8) the model clearly fits better the conditions of region C. This implies that if it is desired that $k_{S1\rightarrow ICT} > k_{ICT\rightarrow S1}$, since the ICT state is generally considered to be lower in energy than the S_1 state due to its low energy stimulated emission,[19] the absolute rate from the S_2 state to ICT must be faster than to S_1.

Having knowledge of which values are more acceptable, we applied them as initial parameters in our target analyses, fixing $k_{S1\rightarrow S0}$ for all room temperature studies. For methanol at 190 K, we investigated also likely values for the rate $k_{S1\rightarrow S0}$ as an independent parameter because this rate should slow upon cooling.[23] The data sets for target analysis were chirp-corrected and truncated at 1 ps, just less than a picosecond before the dump. The parameter values and spectra resulting from target analyses are shown compared to results from global analyses in Fig. 6-11 and Table 6-2. This figure represents the individual components of the coupled S_1/ICT state underlying the common decay observed in transient absorption studies of carbonyl carotenoids as their sums closely match the spectral forms of the global analyses. Generally, values for the common decay rates reverse-calculated with the analysis results closely matched the values obtained by global analysis, again confirming the functionality of the two-state model. The equilibration rate values are less accurate, yet they follow the same general order already observed in Fig. 6-7b: acetonitrile equilibrates the fastest, and methanol at 190 K is the slowest; whereby, the 190 K model

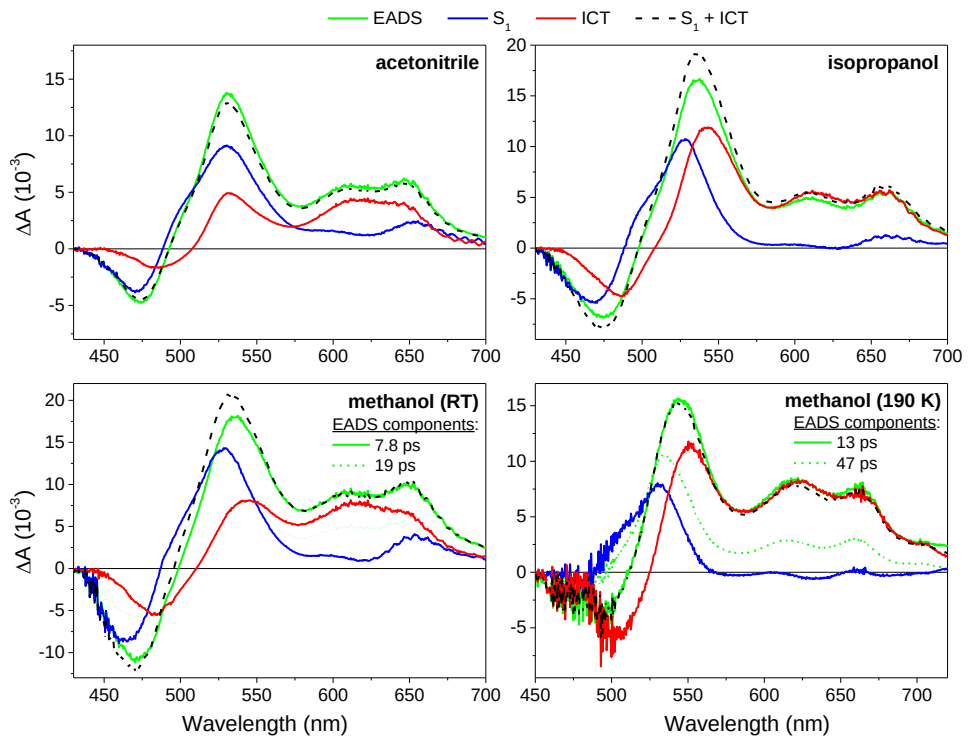

Figure 6-11: Comparison between a global sequential decay model (EADS, gray) and a two-compartment model (target analysis) representing the S_1 (blue) and ICT (red) related species, with their sum (dashed line), in all solvents and methanol at room temperature and 190 K.

converged such that the rate from S_1 to ICT was faster than the reverse path. Thus a reasonable convergence was found in region A.

Therefore, our approach allowed to discriminate feasible fitting solutions from a landscape of many possible models. The population transfer rates (Table 6-2) we have obtained for fucoxanthin in methanol qualitatively matches those reported by Redeckas et al.[39] Even the actual values differ slightly, the overall trend (e.g. $k_{S1\rightarrow ICT} > k_{ICT\rightarrow S1}$) is reproduced. Also, the S_1-like peak in the ICT spectra (Fig. 6-11) is somehow stronger in our target analysis compared to Redeckas et. al.[39] This high-energy, ICT-related peak is found shifting to the red as the equilibration rate decreases and the polarity of the solvent increases (Fig. 6-11). This strong mixing of the S_1 characteristics into the ICT spectrum could be related to absence of hot states in our model which can still have some

influence at the time of dumping, 1.7 ps after excitation. Also it must be noted that fucoxanthin in methanol displays more complicated dynamics compared to the other two solvents, an observation most likely resulting from existence of multiple species having different degree of charge transfer.[38,44]

Our extension of the PDP study of fucoxanthin to other solvents provided some new, interesting observations. First, the $k_{S1\rightarrow ICT}$ and $k_{ICT\rightarrow S1}$ rates characterizing the S_1-ICT equilibration become slower upon cooling the sample to 190 K, suggesting a presence of a barrier separating the S_1 and ICT parts of the S_1/ICT potential surface. Second, both these equilibration rates become faster with increasing polarity, which translates into decreasing the barrier between the S_1 and ICT parts of the S_1/ICT potential surface, confirming the hypothesis proposed a more than a decade ago.[23] Third, it is obvious that the difference in common S_1/ICT lifetimes measured in two solvents with nearly identical polarity, methanol and acetonitrile, results from different ICT-S_0 coupling as the ICT-S_0 rate is about twice slower in acetonitrile. On the other hand, the S_1-ICT equilibration rates are notably faster in acetonitrile, indicating that hydrogen bonding available in protic methanol likely increases the barrier between the S_1 and ICT parts of the S_1/ICT potential surface.

Further information about excited state dynamics is provided by experiments using repumping of either S_1 or ICT populations. The effect of repumping, shown in Fig. 6-7c for fucoxanthin in acetonitrile and in Fig. 6-S4 for fucoxanthin in methanol, reveals differences between behavior of S_1 and ICT populations. Repumping the ICT state results in return of the re-excited molecules back to equilibrium within less than ~300 fs (Fig. 6-7c), as the dynamics return to a fairly unperturbed trajectory, signaling that essentially all repumped ICT population returns back to its original location, the ICT part of the S_1/ICT potential surface. Repumping the S_1 population, however, results in more complicated population dynamics (Fig. 6-7c): it contains a fast recovery, which accounts for about half of the magnitude, again signaling a quick return of the re-excited population back to the S_1 potential minimum, but there is also a slower part. This slower part matches the S_1-ICT equilibration dynamics, implying that the re-excited S_1 population returns to both S_1 and ICT states. Qualitatively, the same behavior is observed for repumping the fucoxanthin in methanol (Fig. 6-S4) though the effect

of the repump subsides to a different equilibrium ratio, suggesting some loss of the repumped population, most likely due to formation of fucoxanthin radical from the upper excited state as reported earlier.[15,40]

Finally, we can hypothesize how the observed excited state behavior may relate to function of fucoxanthin (and possibly other carbonyl carotenoids) in light-harvesting antennae. We showed that hydrogen bonding with the polar methanol slows fucoxanthin's equilibration rate and the $S_1 \leftrightarrow$ICT rates as a result. Thus, hydrogen bonding in the polar environment of light-harvesting antennae would be conceivably more advantageous for energy transfer to chlorophyll. If indeed this is the case, the advantage of using keto carotenoids in light harvesting antennae could also be the possibility of tuning the S_1/ICT equilibration by hydrogen bonding.

In our study of FCP,[45] we claimed to observe fast and slow-decaying fucoxanthin species and that only the S_1 part of the S_1/ICT potential energy surface of the slow species transfers energy to chlorophyll with a lifetime of 1.9 ps. How the preferred donor states are selected we cannot hypothesize; however, it is certain that if one state is a donor to chlorophyll, the advantage of having equilibrating states is that the other state may support the donor state by population transfer. Longer equilibration would generally be more advantageous such that energy transfer to the acceptor is preferred. With exception of acetonitrile, this study indicates the $S_1 \leftrightarrow$ICT transfer rates are slower than energy transfer rates determined for PCP and FCP. Though fucoxanthin in the less polar isopropanol demonstrates the longest equilibration time, its ICT character is slightly mitigated compared to that in methanol, as is its dipole strength. In this less polar hydrogen bonding condition, energy transfer via the S_1 state may be conceivably preferred in FCP.

6.5 CONCLUSIONS

The systematic analysis in this ultrafast multi-pulse study, aimed at the equilibration of the S_1/ICT state in fucoxanthin in solution, utilized the results of global analysis (EADS of PP data and DADS of PP-PDP data) to properly inform target analysis of the S_1 and ICT states as separate species. Truncated at the time where S_1-ICT coupling and decay is most relevant, target analysis of pump-dump

probe data reveals a tight restriction on the possible parameters for target analysis. Building a simple, two-state model with decay to the ground state allows that the description of population transfer to solely depend on the ICT state decay rate $k_{ICT \rightarrow S0}$ and initial S_1 and ICT state population ratio $(n_{S1}/n_{ICT})_0$. In addition to this analysis we manipulated the modeled kinetic traces to achieve an effective equilibrium trace $(S_1{:}ICT)_{PDP}{:}(S_1{:}ICT)_{PP}$ which reveals the dependence of the equilibration on polarity, proticity, and temperature.

When comparing the two protic solvents, methanol and isopropanol, the highly polar methanol exhibits a relative shortening of the S_1/ICT equilibration in fucoxanthin at room temperature but similar dynamics at 190 K. If the S_1 and ICT states are considered to be two parts of one potential energy surface separated by a barrier and measured by their equilibration lifetime, lower polarity, proticity, and temperature increases this barrier. Target analysis affirms this trend and quantifies the relative rates population transfer between the S_1 and ICT states such that population transfer from S_1 to ICT is preferred in polar environments and with hydrogen bonding. This conclusion is congruent with previous studies indicating that the S_1 and ICT states are best modeled as parts of the same potential energy surface.[23,24,26]

The results demonstrate a strong dependence on hydrogen bonding; whereby, the rate of equilibration among the S_1 and ICT states is prolonged. This implies a possible advantage in hydrogen bonding for antenna-bound carotenoids in that energy transfer to chlorophyll may be preferred to internal conversion such as equilibration. If this is the case, a primary donating state, S_1 for example, may be supported by the secondary or non-donating state in equilibrium. Hydrogen bonding in a highly polar environment creates a distinct advantage in that the charge transfer character will be enhanced.

Acknowledgment. The research was funded from the Czech Science Foundation grant 16-10417S, and by the institutional support RVO:60077344.

6.6 SUPPORTING INFORMATION

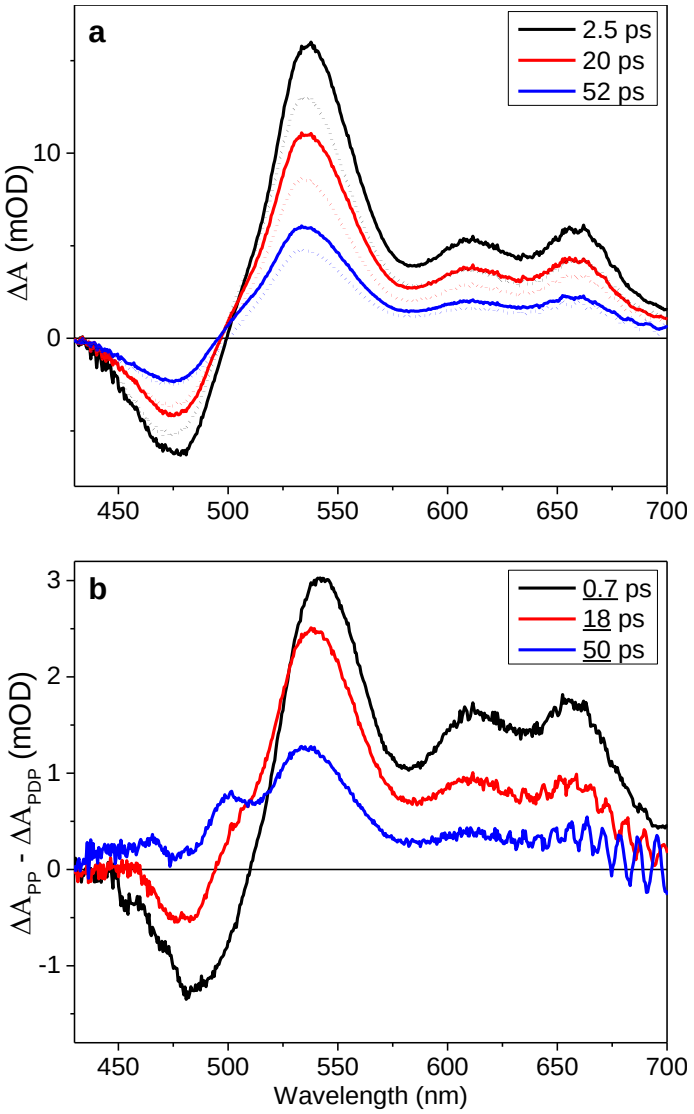

Figure 6-S1: (a) PP (solid) and PDP (dotted) spectra of fucoxanthin in isopropanol at various times after excitation. (b) The double-difference spectrum (PP – PDP) of fucoxanthin in isopropanol. The underlined values indicate the delay time after the dump pulse.

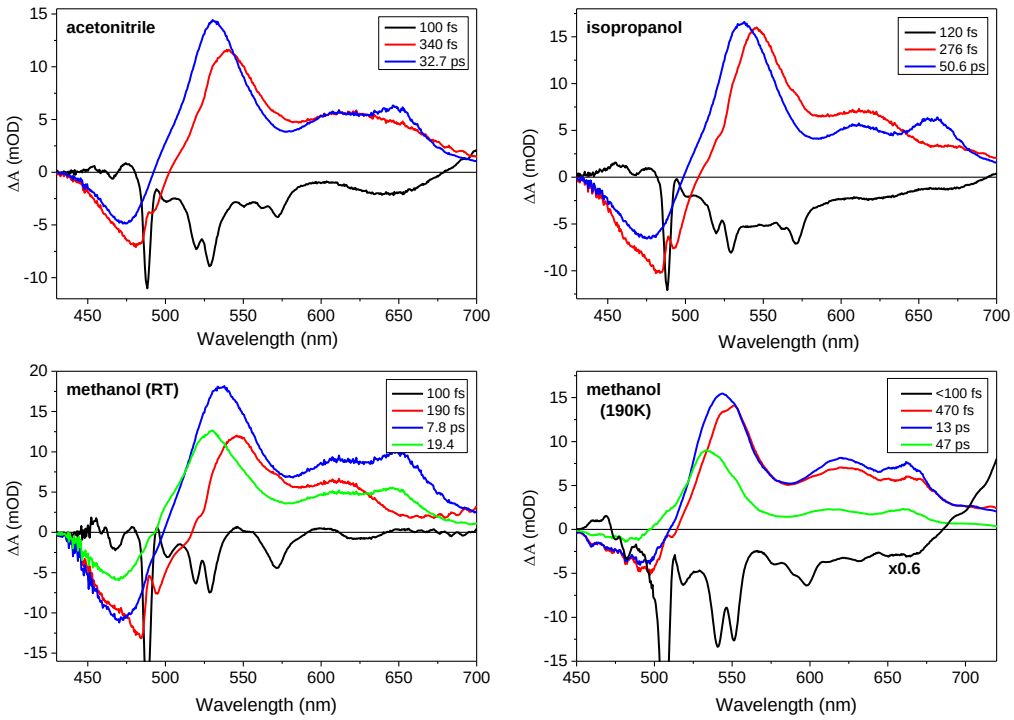

Figure 6-S2: EADS obtained from global fitting the data measured for fucoxanthin in all solvents.

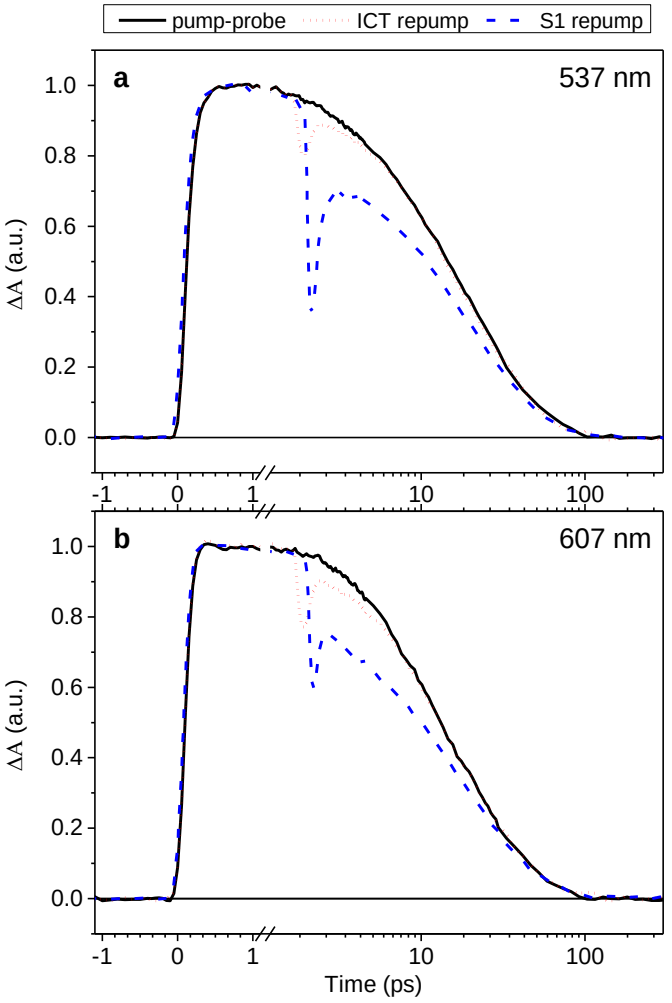

Figure 6-S3: Kinetic traces measured after repumping of either S_1 (blue) or ICT (red) state compared to PP traces (black) in (a) the S_1-associated band and (b) the ICT-associated band of fucoxanthin in methanol.

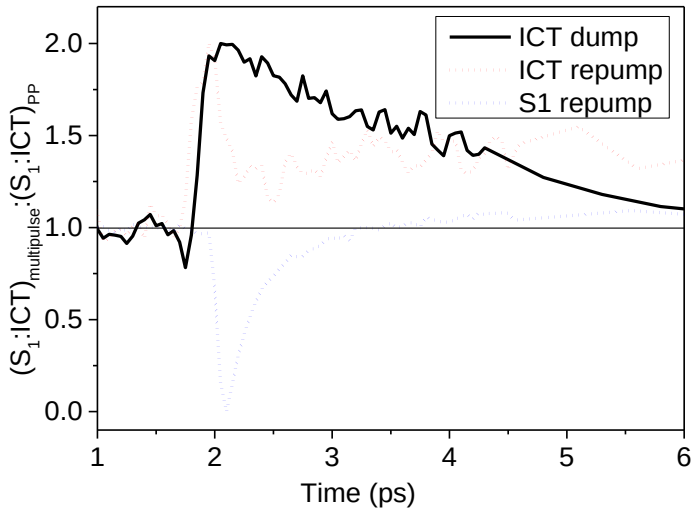

Figure 6-S4: Equlibration dynamics following repumping either the S_1 (blue) or ICT (red) state monitored as amplitude ratio of the S_1-associated and ICT-associated signal normalized to the same signal measured in the PP regime, that is the (S_1:ICT)PrPP:(S_1:ICT)PP ratio. The equilibration dynamics after dumping the ICT state (black) is shown for comparison.

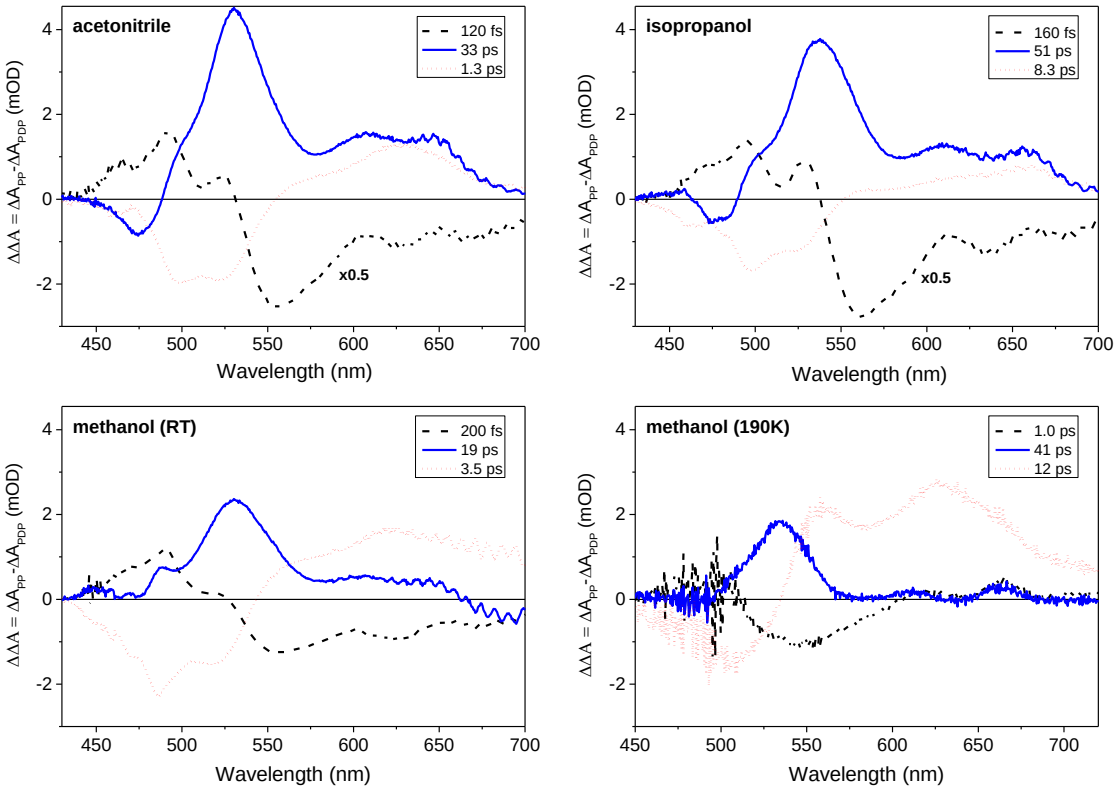

Figure 6-S5: DADS of the double-difference spectrum (PP-PDP) of fucoxanthin in all solvents. The amplitude of the fastest component was reduced by half in each case.

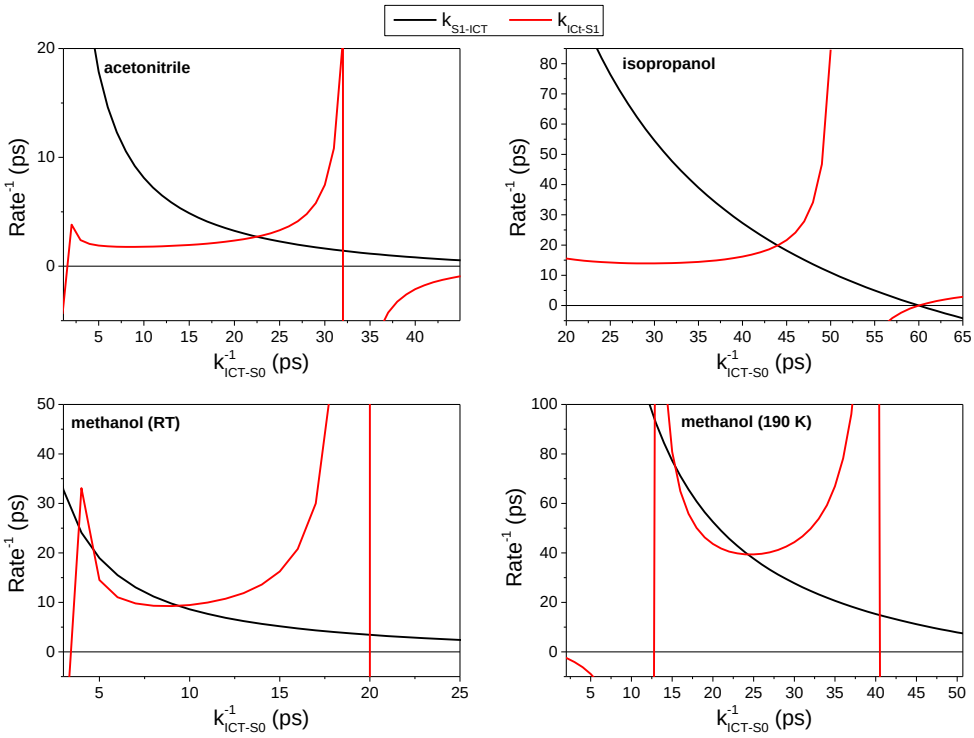

Figure 6-S6: The possible values for the inter-S_1-ICT energy transfer rates $k_{S1\rightarrow ICT}$ and $k_{ICT\rightarrow S1}$ as a function of ICT-S_0 transfer rate $k_{ICT\rightarrow S0}$ under the two-state model according to the common and equilibrium rates of fucoxanthin in all solvent environments. Curves in methanol at both temperatures are associated with the longer common decay components as found in the EADS.

$(n_{s_1}/n_{ICT})_0$	(S_1/ICT)	(S_1/ICT)$_{PDP}$/ (S_1/ICT)$_{PP}$

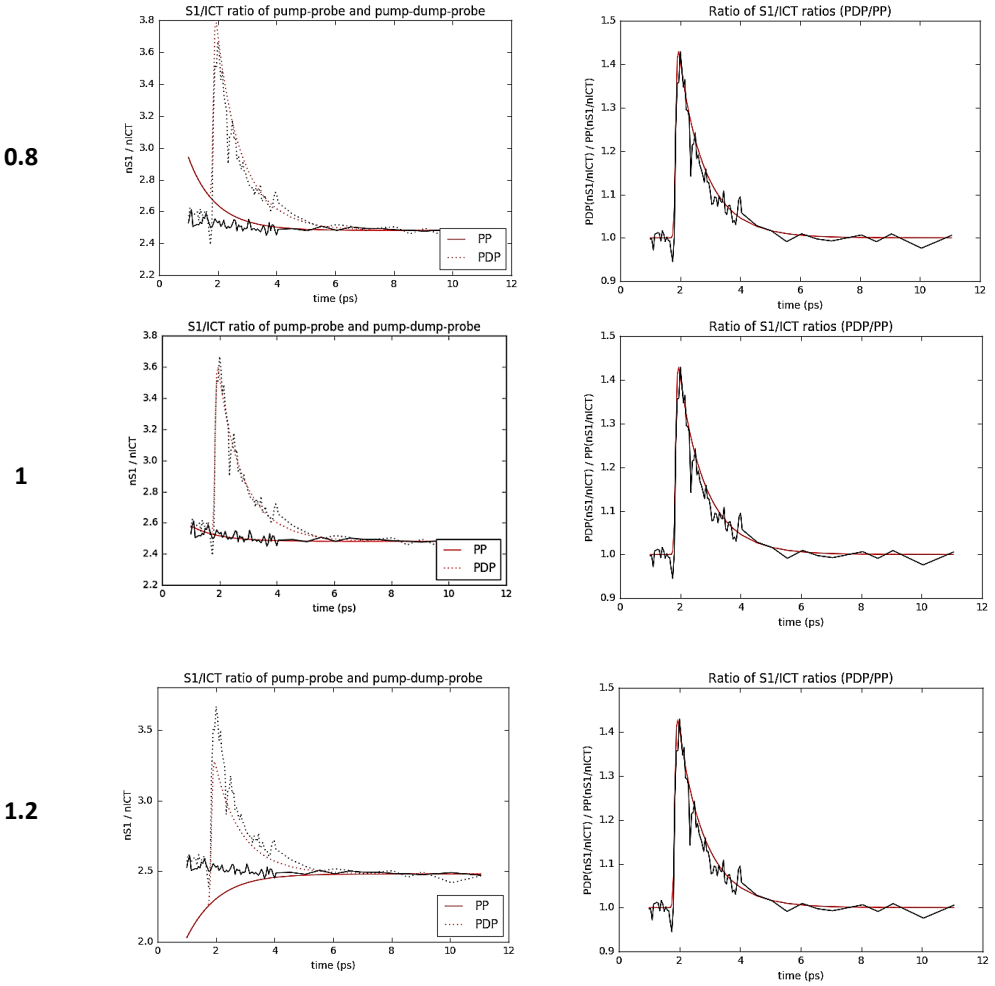

Figure 6-S7: Influence of the initial (at the time of the dumping) population ratio $(n_{S1}/n_{ICT})_0$ on fitting the S_1:ICT ratios of fucoxanthin in acetonitrile.

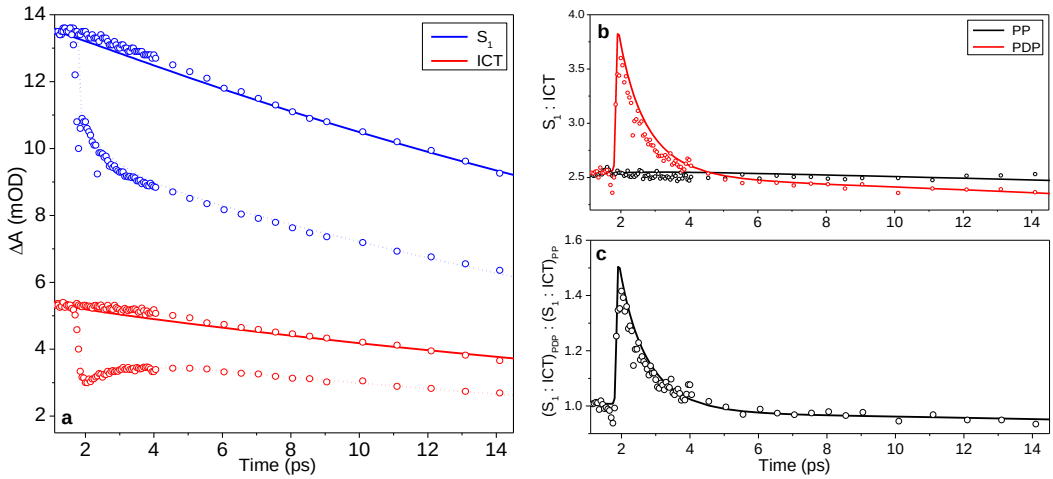

Figure 6-S8: Fits resulting from the two-level model of the coupled S_1 and ICT states for fucoxanthin in acetonitrile. As kinetic signatures of these states and the ground state overlap, the proper amount of S_0 bleaching and excite state absorption (ESA) signal had to be determined in order to match the contributions at 535 nm (61% S_1 ESA, 13% S_0 bleaching, 26% ICT ESA) and 610 nm (91% ICT ESA, 9% S_1 ESA). The dump pulse width is 70 fs, and the rate of dumping is $(120\ fs)^{-1}$. (a) Fits associated with undumped (solid) and dumped (dotted) populations of the S_1 (535 nm) and ICT (610 nm) states. (b) The ratio of the S_1 band to the ICT band (535:610 nm) for undumped (solid) and dumped (dotted) populations. (c) The effect of the dump demonstrated in the ratio of the dumped S_1:ICT ratio (dotted line in b) to the undumped S_1:ICT ratio (solid line in b).

REFERENCES

1. T. Polívka, H. A. Frank Molecular factors controlling photosynthetic light harvesting by carotenoids Acc. Chem. Res., 43 (2010), pp. 1125-1134
2. R. Croce, H. van Amerongen Natural strategies for photosynthetic light harvesting Nat. Chem. Biol., 10 (2014), pp. 492–501
3. T. Mirkovic, E. E. Ostroumov, J. M. Anna, R. van Grondelle, Govindjee, G. D. Scholes Light absorption and energy transfer in the antenna complexes of photosynthetic organisms Chem. Rev., 117 (2017), pp. 249-293
4. P. Jahns, A. R. Holzwarth The role of the xanthophyll cycle and of lutein in photoprotection of photosystem II Biochim. Biophys. Acta - Bioenerg., 1817 (2012), pp. 182–193
5. C. D. P. Duffy, A. V. Ruban Dissipative pathways in the photosystem-II antenna in plants J. Photochem. Photobiol. B Biol., 152 (2015), pp. 215–226
6. T. Polívka, V. Sundström Ultrafast dynamics of carotenoid excited states-from solution to natural and artificial systems Chem. Rev., 104 (2004), pp. 2021–2071
7. P. Tavan, K. Schulten Electronic excitations in finite and infinite polyenes Phys. Rev. B 36 (1987), pp. 4337–4358
8. N. E. Holt, D. Zigmantas, L. Valkunas, X. P. Li, K. K. Niyogi, G. R. Fleming Carotenoid cation formation and the regulation of photosynthetic light harvesting Science, 307 (2005), pp. 433-436
9. A. V. Ruban, R. Berera, C. Ilioaia, I. H. M. van Stokkum, J. T. M. Kennis, A. A. Pascal, H. van Amerongen, B. Robert, P. Horton, R. van Grondelle Identification of a mechanism of photoprotective energy dissipation in higher plants Nature, 450 (2007), pp. 575–578
10. S. Bode, C. C. Quentmeier, P. N. Liao, N. Hafi, T. Barros, L. Wilk, F. Bittner, P. J. Walla On the regulation of photosynthesis by excitonic interactions between carotenoids and chlorophylls Proc. Natl. Acad. Sci. USA, 106 (2009), pp. 12311-12316
11. H. Staleva, J. Komenda, M. K. Shukla, V. Šlouf, R. Kaňa, T. Polívka, R. Sobotka Mechanism of photoprotection in the cyanobacterial ancestor of plant antenna proteins Nat. Chem. Biol., 11 (2015), pp. 287-291
12. J. A. Bautista, R. E. Connors, B. B. Raju, R. G. Hiller, F. P. Sharples, D. Gosztola, M. R. Wasielewski, H. A. Frank Excited state properties of peridinin: observation of a solvent

dependence of the lowest excited singlet state lifetime and spectral behavior unique among carotenoids J. Phys. Chem. B, 103 (1999), pp. 8751–8758

13. H. A. Frank, J. A. Bautista, J. Josue, Z. Pendon, R. G. Hiller, F. P. Sharples, D. Gosztola, M. R. Wasielewski Effect of the solvent environment on the spectroscopic properties and dynamics of the lowest excited states of carotenoids J. Phys. Chem. B, 104 (2000), pp. 4569–4577
14. D. Zigmantas, T. Polívka, R. G. Hiller, A. Yartsev, V. Sundström Spectroscopic and dynamic properties of the peridinin lowest singlet excited states *J. Phys. Chem. A, 105 (***2001)**, pp. 10296-10306
15. E. Papagiannakis, M. Vengris, D. S. Larsen, I. H. M. van Stokkum, R. G. Hiller, R. van Grondelle Use of ultrafast dispersed pump-dump-probe and pump-repump-probe spectroscopies to explore the light-induced dynamics of peridinin in solution J. Phys. Chem. B, 110 (2006), pp. 512–521
16. S. Stalke, D. Wild, T. Lenzer, M. Kopczynski, P. W. Lohse, K. Oum Solvent-dependent ultrafast internal conversion dynamics of n'-apo-β-carotenoic-n'-acids (n = 8, 10, 12) Phys. Chem. Chem. Phys., 10 (2008), pp. 2180–2188
17. D. M. Niedzwiedzki, N. Chatterjee, M. M. Enriquez, T. Kajikawa, S. Hasegawa, S. Katsumura, H. A. Frank spectroscopic investigation of peridinin analogues having different-electron conjugated chain lengths: exploring the nature of the intramolecular charge transfer state J. Phys. Chem. B, 113 (2009), pp. 13604–13612
18. D. Kosumi, M. Kita, R. Fujii, M. Sugisaki, N. Oka, Y. Takaesu, T. Taira, M. Iha, H. Hashimoto Excitation energy-transfer dynamics of brown algal photosynthetic antennas J. Phys. Chem. Lett., 3 (2012), pp. 2659-2664
19. D. Zigmantas, R. G. Hiller, F. P. Sharples, H. A. Frank, V. Sundström, T. Polívka Effect of a conjugated carbonyl group on the photophysical properties of carotenoids Phys. Chem. Chem. Phys., 6 (2004), pp. 3009–3016
20. M. M. Enriquez, S. Hananoki, S. Hasegawa, T. Kajikawa, S. Katsumura, N. L. Wagner, R. R. Birge, H. A. Frank Effect of molecular symmetry on the spectra and dynamics of the intramolecular charge transfer (ICT) state of peridinin J. Phys. Chem. B, 116 (2012), pp. 10748–10756

21. D. Kosumi, T. Kajikawa, S. Okumura, M. Sugisaki, K. Sakaguchi, S. Katsumura, H. Hashimoto Elucidation and control of an intramolecular charge transfer property of fucoxanthin by a modification of its polyene chain length J. Phys. Chem. Lett., 5 (2014), pp. 792–797
22. H. Staleva-Musto, V. Kuznetsova, R. G. West, G. Keşan, B. Minofar, M. Fuciman, D. Bína, R. Litvín, T. Polívka Nonconjugated acyloxy group deactivates the intramolecular charge-transfer state in the carotenoid fucoxanthin. J. Phys. Chem. B, 122 (2018), pp. 2922–2930
23. D. Zigmantas, R. G. Hiller, A. Yartsev, V. Sundström Dynamics of excited states of the carotenoid peridinin in polar solvents : dependence on excitation wavelength, viscosity, and temperature J. Phys. Chem. B, 107 (2003), pp. 5339–5348
24. H. M. Vaswani, C.-P. Hsu, M. Head-Gordon, G. R. Fleming Quantum chemical evidence for an intramolecular charge-transfer state in the carotenoid peridinin of peridinin−chlorophyll−protein J. Phys. Chem. B, 107 (2003), pp. 7940–7946
25. E. Papagiannakis, D. S. Larsen, I. H. M. van Stokkum, M. Vengris, R. G. Hiller, R. van Grondelle Resolving the excited state equilibrium of peridinin in solution Biochemistry, 43 (2004), pp. 15303–15309
26. N. L. Wagner, J. A. Greco, M. M. Enriquez, H. A. Frank, R. R. Birge The nature of the intramolecular charge transfer state in peridinin Biophys. J., 104 (2013), pp. 1314–1325
27. D. Carbonera, M. Di Valentin, R. Spezia, A. Mezzetti The unique photophysical properties of the peridinin-chlorophyll- a -protein Curr. Protein Pept. Sci., 15 (2014), pp. 332–350
28. P. A. Linden, J. Zimmermann, T. Brixner, N. E. Holt, H. M. Vaswani, R. G. Hiller, G. R. Fleming Transient absorption study of peridinin and peridinin−chlorophyll a−protein after two-photon excitation J. Phys. Chem. B, 108 (2004), pp. 10340–10345
29. C. Bonetti, M. T. A. Alexandre, I. H. M. van Stokkum, R. G. Hiller, M. L. Groot, R. van Grondelle, J. T. M. Kennis Identification of excited-state energy transfer and relaxation pathways in the peridinin-chlorophyll complex: an ultrafast mid-infrared study Phys. Chem. Chem. Phys., 12 (2010), pp. 9256–9266
30. S. Shima, R. P. Ilagan, N. Gillespie, B. J. Sommer, R. G. Hiller, F. P. Sharples, H. A. Frank, R. R. Birge Two-photon and fluorescence spectroscopy and the effect of environment on the photochemical properties of peridinin in solution and in the peridinin-chlorophyll-protein from *Amphidinium carterae* J. Phys. Chem. A, 107 (2003), pp. 8052–8066

31. E. Papagiannakis, I. H. M. Van Stokkum, H. Fey, C. Büchel, R. Van Grondelle Spectroscopic characterization of the excitation energy transfer in the fucoxanthin-chlorophyll protein of diatoms Photosynth. Res., 86 (2005), pp. 241–250
32. N. Gildenhoff, S. Amarie, K. Gundermann, A. Beer, C. Büchel, J. Wachtveitl Oligomerization and pigmentation dependent excitation energy transfer in fucoxanthin-chlorophyll proteins Biochim. Biophys. Acta – Bioenerg., 1797 (2010), pp. 543–549
33. G. Keşan, M. Durchan, J. Tichý, B. Minofar, V. Kuznetsova, M. Fuciman, V. Šlouf, C. Parlak, T. Polívka Different response of carbonyl carotenoids to solvent proticity helps to estimate structure of the unknown carotenoid from *Chromera velia* J. Phys. Chem. B, 119 (2015), pp. 12653–12663
34. D. Kosumi, T. Kusumoto, R. Fujii, M. Sugisaki, Y. Iinuma, N. Oka, Y. Takaesu, T. Taira, M. Iha, H. A. Frank Ultrafast excited state dynamics of fucoxanthin: excitation energy dependent intramolecular charge transfer dynamics Phys. Chem. Chem. Phys., 13 (2011), pp. 10762
35. D. Kosumi, R. Fujii, M. Sugisaki, N. Oka, M. Iha, H. Hashimoto characterization of the intramolecular transfer state of marine carotenoid fucoxanthin by femtosecond pump-probe spectroscopy Photosynth. Res., 121 (2014), pp. 61–68
36. D. Kosumi, T. Kajikawa, S. Okumura, M. Sugisaki, K. Sakaguchi, S. Katsumura, H. Hashimoto Elucidation and control of an intramolecular charge transfer property of fucoxanthin by a modification of its polyene chain length J. Phys. Chem. Lett., 5 (2014), pp. 792-797
37. D. Kosumi, T. Kajikawa, K. Yano, S. Okumura, M. Sugisaki, K. Sakaguchi, S. Katsumura, H. Hashimoto Roles of allene-group in an intramolecular charge transfer character of a short fucoxanthin homolog as revealed by femtosecond pump-probe spectroscopy Chem. Phys. Lett., 602 (2014), pp. 75-79
38. V. Kuznetsova, P. Chábera, R. Litvín, T. Polívka, M. Fuciman Effect of isomerization on excited-state dynamics of carotenoid fucoxanthin J. Phys. Chem. B, 121 (2017), pp. 4438–4447
39. K. Redeckas, V. Voiciuk, M. Vengris Investigation of the S_1/ICT equilibrium in fucoxanthin by ultrafast pump–dump–probe and femtosecond stimulated raman scattering spectroscopy Photosynth. Res., 128 (2016), pp. 169-181

40. D. S. Larsen, E. Papagiannakis, I. H. M. van Stokkum, M. Vengris, J. T. M Kennis, R. van Grondelle Excited state dynamics of β-carotene explored with dispersed multi-pulse transient absorption Chem. Phys. Lett., 381 (2003), pp. 733–742
41. M. Vengris, I. H. M. van Stokkum, X. He, A. F. Bell, P. J. Tonge, R. van Grondelle, D. S. Larsen Ultrafast excited and ground-state dynamics of the green fluorescent protein chromophore in solution J. Phys. Chem. A, 108 (2004), pp. 4587–4598
42. K. Redeckas, V. Voiciuk, D. Zigmantas, R. G. Hiller, M. Vengris Unveiling the excited state energy transfer pathways in peridinin-chlorophyll a-protein by ultrafast multi-pulse transient absorption spectroscopy Biochim. Biophys. Acta - Bioenerg., 1858 (2017), pp. 297–307
43. D. Kosumi, T. Kusumoto, R. Fujii, M. Sugisaki, Y. Iinuma, N. Oka, Y. Takaesu, T. Taira, M. Iha, H. A. Frank One- and two-photon pump-probe optical spectroscopic measurements reveal the S_1 and intramolecular charge transfer states are distinct in fucoxanthin Chem. Phys. Lett., 483 (2009), pp. 95–100
44. D. Kosumi, R. Fujii, M. Sugisaki, N. Oka, M. Iha, H. Hashimoto Characterization of the intramolecular transfer state of marine carotenoid fucoxanthin by femtosecond pump-probe spectroscopy Photosynth. Res., 121 (2014), pp. 61–68
45. R. G. West, D. Bína, M. Fuciman, V. Kuznetsova, R. Litvín, T. Polívka Ultrafast multi-pulse transient absorption spectroscopy of fucoxanthin chlorophyll a protein from *Phaeodactylum tricornutum* Biochim. Biophys. Acta - Bioenerg., 1859 (2018), pp. 357–365
46. D. Zigmantas, R. G. Hiller, V. Sundstrom, T. Polivka Carotenoid to chlorophyll energy transfer in the peridinin-chlorophyll-a-protein complex involves an intramolecular charge transfer state Proc. Natl. Acad. Sci. U. S. A., 99 (2002), pp. 16760–16765
47. P. Changenet-Barret, C. T. Choma, E. F. Gooding, W. F. DeGrado, R. M. Hochstrasser Ultrafast dielectric response of proteins from dynamics stokes shifting of coumarin in calmodulin J. Phys. Chem. B, 104 (2000), pp. 9322–9329
48. S. L. Logunov, V. V. Volkov, M. Braun, M. A. El-Sayed The relaxation dynamics of the excited electronic states of retinal in bacteriorhodopsin by two-pump-probe femtosecond studies Proc. Natl. Acad. Sci. U. S. A., 98 (2001), pp. 8475–8479

SUMMARY AND CONCLUSIONS

The main purpose of this thesis was to reveal some of the secrets of the optically hidden (sometimes called also dark) life of carotenoids. It has been done with the help of lesser-used methods (Paper 1 and 4) as well as some more „exotic“ carotenoids and polyenes (Paper 2 and 3). Some questions have been clarified, some new ones have arisen. In the following summary, I repeat the most important once again, and at the same time, for some experiments, I present steps that could help in further research, eventually. These include the experiments I would like to do later myself.

In Paper 1, the two-photon excitation (2PE) was used to study the S_1 state of three carotenoids; lycopene, β-carotene, and neurosporene. This approach makes it possible to investigate the S_1 state without additional dynamics associated with S_2-S_1 relaxation typically observed after one-photon excitation (1PE), as it is populated directly and not from higher energy levels. The major consequence of 2PE was an increased magnitude of the S* signal, compared to the standard 1PE experiment. This was explained by different subsets of conformers excited by 1PE and 2PE. The next step in studying the S_1 state directly is the z-scan study of carotenoids in NIR. Using this approach the two-photon cross-section of carotenoid's S_1 state can be determined and thus the excitation wavelength in a 2PE experiment can be selected with a better precision. Further, the natural systems and possibly carotenoidless mutants should be compared by 2PE transient absorption spectroscopy. This would reveal the real cause of the fluorescence observed after the 2PE of light-harvesting complexes during the historically first experiments dealing with the topic.

Paper 2 deals with two polyenes with an extreme conjugation length, which are of the interest while studying photophysics of carotenoids, since polyenes often replace carotenoids in theoretical studies. The steady state absorption spectra of both polyenes show well-resolved vibrational bands, despite the complexity of the polymers. This indicates narrow distributions of polyene

conjugation lengths and conformations as well as a well-defined configuration of the conjugated chains. Another similarity to carotenoids is the energy separation of the 0-0 and 0-1 vibrational bands, which is ca 1200 cm^{-1}. The values of 0-0 energy of the S_0-S_2 transition observed for the polyenes, 17210 cm^{-1} and 17030 cm^{-1} are also not far from the values calculated for hypothetical carotenoids having the same conjugation length. In contrast to the well-resolved vibrational bands observed in the steady state absorption spectrum, the excited state absorption bands are very broad, showing a higher conformational disorder of the excited states compared to the ground state. The observation of the S* signal on the blue shoulder of S_1-S_n transition is also consistent with the experiment previously done on carotenoids, indicating the increase of the S* signal with increasing the length of the conjugated system. Despite the larger complexity of their structure, the studied polyenes showed a lot in common, thus allowing naturally extend the earlier studies of long carotenoids.

In the Paper 3 we studied the CAC antennae of the cryptophyte *Rhodomonas salina*. It contains alloxanthin, a unique carotenoid possessing two triple bonds. The question was how this carotenoid contributes to light harvesting and non-photochemical quenching. We conducted three separate pump-probe experiments with excitation wavelengths falling into the absorption bands of either alloxanthin, Chl a, or Chl c. These experiments proved the energy transfer from alloxanthin to Chl's after 505 nm excitation, while there was only Chl c to Chl a energy transfer on a time scale of a few picoseconds when using 590 or 640 nm excitation wavelength, rejecting the possible role of the alloxanthin S_1 state in light-harvesting.

In the last Paper of this thesis, Paper IV, it was shown the ICT state of the carotenoid fucoxanthin behaves differently at different conditions. The response of the ICT state behavior to temperature, polarity, and proticity was studied. The multipulse method used in this paper, pump-dump-probe, is able to follow the evolution of ICT state population better than a traditional pump-probe spectroscopy. With a help of a sophisticated analysis we report that the potential barrier of the ICT state increases with higher temperature, polarity, and proticity, leading to longer equilibration lifetimes.

Despite the great progress in the carotenoid (and other conjugated systems) research in the last few decades, many problems remain unresolved, especially those related to photophysics of dark excited states and their roles in the light-harvesting and photoprotective function in photosynthetic organisms. To uncover the unknown, we need to perform more experiments, create new setups, improve the current ones, and search for new directions of research. In the future, the result of ongoing studies may help to produce the energy in a "cleaner" way and help humans to protect our one and only planet. This thesis is a small piece of a mosaic that will help us to make step forward in our understanding of the nature.

sebelik00@gmail.com

Excited state processes in linear conjugated systems
Ph.D. Thesis Series, 2020, No. 16

Printed in the Czech Republic by Typodesign
Edition of 20 copies

University of South Bohemia in České Budějovice
Faculty of Science
Branišovská 1760
CZ-37005 České Budějovice, Czech Republic

Phone: +420 387 776 201
www.prf.jcu.cz, e-mail: sekret-fpr@prf.jcu.cz